ABSTRACT

SAKON, JOHN JOSEPH. Detecting the Conformation of Individual Proteins in Live Cells using Single Molecule Fluorescence Resonance Energy Transfer. (Under the direction of Dr. Keith R. Weninger.)

Single molecule fluorescence resonance energy transfer (smFRET) is a technique capable of measuring dynamic information of single molecules at the nanoscale. This makes it ideal for individuating biological events at this scale, such as the conformations and binding states of proteins. While this technique has been used extensively *in vitro*, smFRET of individual proteins has not been achieved within the biologically applicable yet optically noisy environment of a cell. I combined smFRET with single particle tracking in live cells using site-specifically labeled SNARE proteins to image their dynamic folding into complexes at the cellular membrane. By microinjecting dilute solutions of this recombinant, fluorescently-labeled protein I was able to localize these individual folding events over time and determine transient states that could not be measured with bulk fluorescence methods. This novel technique is broadly applicable to cellular interactions at the nanoscale and provides *in vivo* dynamic information unavailable through any other means. I prove the efficacy of this technique with multiple findings significant to SNARE biology.

Detecting the Conformation of Individual Proteins in Live Cells using Single Molecule Fluorescence Resonance Energy Transfer

by
John Joseph Sakon

A dissertation submitted to the Graduate Faculty of
North Carolina State University
in partial fulfillment of the
requirements for the Degree of
Doctor of Philosophy

Physics

Raleigh, North Carolina

2010

APPROVED BY:

Keith Weninger Chair	Robert Riehn
James Knopp	Jason Bochinski

BIOGRAPHY

I was born in Farmington, CT in 1983 and grew up mostly in Avon, CT. My grade schools go something like Roaring Brook Elementary, Avon Middle and Avon High School. I think I wanted to be a baseball player most of that time.

Even though it was only third on my list, I was fortunate enough to be placed in Dr. Dennis Manos' freshman seminar entitled "The Shape of Things," in which we learned how the physical world shapes everything around us. My final paper for this class was called "The possibility, requirements and structure of extraterrestrial life," and detailed the constraints the universe imposes on the formation of life. The substance of this class and Dr. Manos' breadth of scientific knowledge inspired me to start taking classes in physics, and for a few years I found myself spending long nights in the Small Hall physics library (much to my chagrin). Back when I was calculating how far projectiles would land no one warned me physics was going to be hard.

At some point I learned of summer research programs called REUs and applied to 12 throughout the country. The one that let me in—likely due to the inclusion of my final paper from "The Shape of Things"—was at the Arkansas-Oklahoma Center for Space and Planetary Sciences. The program focused on studying Mars. I was assigned to the microbiology lab of Dr. Robert Burnap, who guided me through my baby steps in biological research with the help of then graduate student Dr. Brad Postier. Under the tutelage of Dr. Burnap as well as program directors Drs. Derek Sears and Richard Marston during consecutive summers in Oklahoma I developed a strong interest in scientific research and even managed to publish a paper in astrobiology.

I used my newly learnt biological skills in my senior physics research project at William and Mary. There I worked on conditions for optoporation—the opening of cells with pulses of laser—during my senior year and the following summer under Drs. William Cooke, Margaret Saha and Eric Bradley at the College.

With a continued interest in biophysics (and because Grant was applying to graduate school), I applied to a number of physics programs near William and Mary. Upon visiting NC State I was worried that no one did biophysics outside of their hard drives until my last visit to Dr. Keith Weninger's lab. After attending a semester's worth of lab meetings I was able to join the lab in January of 2006. During my time in Dr. Weninger's lab I've worked with nanocrystalline diamonds, DNA, proteins, viruses and even synaptic vesicles.

Finally, the confluence of my research on SNARE proteins, work with George Augustine's lab at Duke, a book by Eric Kandel and many episodes of Radiolab have piqued my interest in neuroscience. In some sense I have gone from the most basic life to the most advanced, as I endeavor to study the biological underpinnings of memory.

-John J. Sakon, November 2010

ACKNOWLEDGEMENTS

To my advisor, Keith Weninger: thank you for being as understanding a professor as humanly possible. I never got the feeling I was wasting your time (even when I probably was) and your tireless effort to teach prepared me as a scientist more than I could have hoped for.

To my parents, John and Linda Sakon: thank you for all your help throughout the years. I feel privileged to make it to this point and wouldn't be where I am without your support and encouragement.

To my teachers: thank you for making my education never seem like a secondary concern.

To my friends: I couldn't have done this without you. I stepped foot in North Carolina with one friend and feel gifted to have made it this far with so many strong relationships. And to my high school and college friends: I owe my success in NC to your influence. Also to Baker: thanks for being on GChat that one time and giving me that word, which is in here somewhere even though I seem to have forgotten what it was.

TABLE OF CONTENTS

LIST OF TABLES……vii
LIST OF FIGURES……viii
LIST OF ABBREVIATIONS……x

Chapter 1. Introduction to Method and Biological System of Study……1
1.1. Overview: Methods.....1
1.1.1 Single Molecule Measurements.....2
1.1.2 Fluorescence Resonance Energy Transfer (FRET).....3
1.1.3 Single Molecule Fluorescence Microscopy and FRET.....6
1.1.4 Total Internal Reflection Fluorescence Microscopy.....7
1.2 Overview: Significance of Technique……...9
1.2.1 Protein folding……10
1.2.2 Importance of live cell work……...11
1.2.3 What smFRET can achieve in a live cell……12
1.2.4 Difficulties of smFRET *in vivo*……13
1.3. Overview: Biological System of Study……...14
1.3.1 SNARE proteins……16
1.3.2 SNARE folding……18
1.3.3 Open questions concerning SNAREs……18

Chapter 2. Strategies for implementing smFRET *in vivo*……...20
2.1. Overview: Design of biological constructs……...20
2.1.1 Strategic mutations and dye-labeling……25
2.1.2 SN25CC and SN25NC……26
2.1.3 SN29NN……...29
2.1.4 SNAP-25 control constructs……32
2.1.5 Synaptobrevin control constructs……33
2.2. Overview: TIRFM alignment……34
2.2.1 Custom built alignment of TIRFM……34
2.2.2 Imaging with near TIRFM……36
2.3. Overview: Imaging and microinjection……36
2.3.1 Experimental setup……37
2.3.2 Backgrounds of glass coverslips ……39
2.3.3 Microinjection……...43
2.4. Overview: Cell culture and media additives……48
2.4.1 Cell types and culture……48
2.4.2 Imaging in cultured cells……52
2.4.3 Improving dye properties with media additives……54
2.5. Step by step process of data acquisition……58

Chapter 3. Results and Discussion……...63
3.1. Overview: Data Analysis……...63
3.1.1 Data extraction……..…...……64
3.1.2 %highFRET……...64
3.2. Overview: Proof of method and data accumulation……..…....65
3.2.1 Examples of data traces……..…...……65
3.2.2 Histogram of FRET values……..…...……68
3.2.3 Histograms of %highFRET……..…...……..…71
3.3. Overview: Controls……..…...……72
3.3.1 *In vitro* work on FRET constructs……..…...……..73
3.3.2 Mutated construct eliminates high FRET signal……..…...73
3.3.3 Imaging singly-labeled SNAP-25……..…...……..……74
3.3.4 Imaging low FRET synaptobrevin construct……..…....…80
3.3.5 Ensuring microinjection and laser do not influence biological signal…….83
3.4. Overview: Advanced Single Molecule Data Analysis……...…84
3.4.1 Localizing smFRET events within cells……...…84
3.4.2 Tracking individual molecules……..…...……85
3.4.3 Differentiating biological events by binding times……...…87
3.5. Overview: Implications for SNARE biology……..…...……..89
3.5.1 Instant SNAP-25 and SNAP-29 complex formation in multiple cell types displays the promiscuity of SNAREs……..…….……..89
3.5.2 Antiparallel SNARE complex formation……..…...…….....92
3.5.3 Meaning of SN25CC(G43D) construct eliminating high smFRET…….....93
3.5.4 Diffusion of mobile SNAP-25 molecules ……..…...……..97
3.5.5 Timing of SNARE binding and release……..….....…..98

Chapter 4. Summary……...103
4.1 Conclusions of in vivo smFRET method……103
4.2 Biological conclusions found using method……..…...……104
4.3 Future work ……..…...……..105
4.3.1 Improving live cell smFRET system ……..…...……105
4.3.2 Future studies of SNAREs with smFRET *in vivo*……..107

References……...110

LIST OF TABLES

Table 2.1 Summary of dye-labeled protein constructs and labeling information…...…27

Table 3.1 Data table of % highFRET for various constructs……...75

LIST OF FIGURES

Figure 1.1 FRET efficiency versus distance of dye molecules…….....8

Figure 1.2 Schematic of SNARE complex formation on a membrane……..…15

Figure 2.1 Schematic of SNAP-25 construct label site locations when in and out of SNARE complex……...21

Figure 2.2 Location of SNAP-25 label sites on crystal structure of SNARE complex….22

Figure 2.3 *In vitro* characterization of SN29NN construct…….23

Figure 2.4 Layout of custom built TIRFM setup……35

Figure 2.5 Diagram of near-TIRFM illumination……40

Figure 2.6 Schematic of basic live cell smFRET experimental setup…….41

Figure 2.7 Images of autofluorescent background from cells and coverslips……...46

Figure 2.8 Example image of smFRET signal from SN25CC injected into a BS-C-1 cell……...49

Figure 2.9 Example image of smFRET signal from SN29NN injected into a PC-12 cell……....…….50

Figure 2.10 Effect of various additives to photobleaching time *in vivo*……57

Figure 3.1 Intensity traces of two smFRET events…….66

Figure 3.2 Screen shots over time of smFRET event from Figure 3.1……67

Figure 3.3 Additional intensity traces of smFRET events…….69

Figure 3.4 Histogram of FRET values for injection of SN25CC into BS-C-1 cell…….70

Figure 3.5 Histograms of %highFRET for protein constructs injected into BS-C-1 cells…….....76

Figure 3.6 Histograms of %highFRET for protein constructs injected into PC-12 cells……...77

Figure 3.7 Histograms of %highFRET for control protein constructs injected into BS-C-1 cells……..78

Figure 3.8 Example image of smFRET signal from SN25CC(G43D) injected into a BS-C-1 cell…….……79

Figure 3.9 Measurement of %highFRET from multiple injections into same cell……....81

Figure 3.10 Scatterplot overlay of high FRET events over time for SN25CC injected into a BS-C-1 cell……...……95

Figure 3.11 Tracking of individual high FRET SN25CC molecule over time in a BS-C-1 cell……....…96

Figure 3.12 Residence times of high FRET SN25CC molecules in BS-C-1 cell…….…...…99

LIST OF ABBREVIATIONS

smFRET (single molecule fluorescence resonance energy transfer)

TIRFM (total internal reflection microscopy)

NA (numerical aperture)

SNARE (soluble N-ethylmaleimide sensitive fusion protein attachment protein receptor)

SN1 (N-terminal SNARE binding domain in SNAP family protein)

SN2 (C-terminal SNARE binding domain in SNAP family protein)

SN25 (SNAP-25)

Sb (synaptobrevin-2, residues 1-96)

Syx (syntaxin-1)

DIC (differential interference contrast)

Chapter 1. Introduction to Method and Biological System of Study

The focus of this research was to develop a system capable of measuring the folded state of an individual protein by using fluorescence resonance energy transfer (FRET) in a live cell. Achieving high enough signal to image and track a single fluorescently-labeled protein inside the optically noisy environment of a living cell required overcoming a number of obstacles. I begin by describing the methods employed to image and track proteins within live cells as well as the strategies used to overcome the myriad obstacles associated with *in vivo* single molecule imaging. I also describe why these methods are essential to this process and how they combine into a novel technique capable of something unavailable through other means: measurement of the dynamic conformational state of a single protein in real-time in a live cell. After I will discuss the biological system used to prove the utility of this method and provide evidence of its capabilities with novel findings in this system.

1.1 Overview: Methods

The implementation of single molecule FRET to determine the conformation of a protein in a live cell requires the use of multiple techniques. First, I describe the value of single molecule methods. Then I explain FRET and how it is implemented in a single molecule system followed by a discussion of total internal reflection fluorescence microscopy (TIRFM). Following this I give a summary of the issues with implementing these methods in the environment of a living cell. I conclude by explaining how the combination of these methods within a live cell is an important step in determining biological information of proteins at the nanoscale that is unavailable through any other means.

1.1.1 Single Molecule Measurements

Single molecule methods have become a prevalent tool in biology as they allow the study of individual dynamics that can often be lost when studying populations of molecules (Xie 1996; Weiss 2000). In particular, localizing specific molecules, their interactions with specific partners as well as the kinetics of these reactions often cannot be done in bulk samples.

Proteins are particularly well-suited for single molecule studies as an individual protein's function is often dependent on interactions with numerous small molecules (e.g. calcium, ATP) (Yildiz, Forkey et al. 2003), other proteins (Weninger, Bowen et al. 2008), DNA (Sass, Lanyi et al. 2010) and their randomly fluctuating folded state (Weninger, Bowen et al. 2003). However, the majority of these studies require purified samples studied *in vitro*, with these various interactive factors added in buffer conditions to simulate real conditions. This prompts the goal of utilizing single molecule techniques in a live cell, as individual species localize in a dynamic manner dependent on the myriad interactions and local heterogeneities within the complex environment of the cellular milieu (Sako and Yanagida 2003). Studying the time trajectory of a single molecule allows the measurement of multiple reaction pathways and transient intermediate states that are hidden in bulk solutions. In fact, exact distributions of molecular properties can be accumulated without having to synchronize the cascades of reactions typical in cells.

Tracking of single molecules in cells has been utilized for more than a decade. Initial studies successfully implemented single molecule fluorescence spectroscopy by imaging small molecules at the plasma membrane to track diffusion (Schmidt, Schutz et al.

1996; Saxton and Jacobson 1997) and to measure their intracellular enzymatic turnover (Lu, Xun et al. 1998). More recent studies have successfully imaged and tracked single proteins (Lippincott-Schwartz, Snapp et al. 2001) and viruses (Seisenberger, Ried et al. 2001) in an *in vivo* setting. The majority of live cell protein studies rely on fluorescent moieties being expressed by the cell (An and Almers 2004), which make concentration levels (and therefore isolation of single molecules to image) very difficult to control. As a result, I expressed and fluorescently labeled proteins of interest externally and microinjected them into cultured cells at levels sufficient for single molecule detection (see section **2.1** for biological constructs). Another host of challenges comes from acquiring sufficient signal:noise to image single molecule FRET signal within the optically noisy environment of a live cell (Blow 2008; George 2008). I describe these difficulties in detail in section **1.2.4** and how I managed to overcome them throughout Chapter **2**.

1.1.2 Fluorescence Resonance Energy Transfer (FRET)

The primary technique I used to study the conformation of proteins in this work is fluorescence (or Förster) resonance energy transfer (FRET). FRET is a non-radiative dipole-dipole interaction between two fluorophores in which the emission spectrum of a donor overlaps with the excitation spectrum of an acceptor. It is a quantum mechanical process likened to resonant oscillator coupling by Theodor Förster who first proposed and developed FRET theory (Forster 1946). This landmark work established the equations to measure FRET quantitatively from empirical measurements of the spectra and excitation lifetimes of the fluorophores (Forster 1948). Derivation of the FRET equations is out of the scope of this work, but is detailed elsewhere (Clegg 1996).

The rate of energy transfer from the donor to the acceptor fluorophore depends on a number of factors. Most simply, measuring the intensities (I) of the donor and acceptor dyes experimentally allows the calculation of FRET efficiency from the equation:

$$E = \left(\frac{I_{Acceptor}}{I_{Acceptor} + I_{Donor}} \right) \quad \textbf{Equation 1.1}$$

where E is the efficiency of energy transfer (range 0-1). FRET efficiency can be more directly defined with the equivalent equation derived from the specific properties and locations of the dyes:

$$E = \left(1 + \left(\frac{R}{R_0} \right)^6 \right)^{-1} \quad \textbf{Equation 1.2}$$

where R is the separation of the donor and acceptor dyes and R_0 is the characteristic distance of the two dyes at which half the energy is transferred. R_0 is defined as:

$$R_0 = 2.11(\kappa^2 n^{-4} Q_D J(\lambda))^{1/6} [in\ nm] \quad \textbf{Equation 1.3}$$

where n is the index of refraction of the medium between the dyes, Q_D is the quantum efficiency of the donor in the absence of the acceptor and J(?å is the overlap integral between the donor emission and acceptor excitation. ?7epresents the orientation of the transition dipoles of the resonating dyes and is defined as:

$$\kappa = \cos(\theta_T) - 3\cos(\theta_D)\cos(\theta_A) \quad \textbf{Equation 1.4}$$

where ?|T is the angle between the transition dipole of the donor and acceptor while ?|D and ?|A are the angles between the dipoles and a vector linking them. ? is averaged over the range of orientations of donor and acceptor dipoles occurring during the measurement interval.

The R_0 values for both dye pairs used in my experiments (Cy3 and Cy5 as well as Alexa 647 and Alexa 555) are about 5 nm (Weninger, Bowen et al. 2003) assuming orientational freedom of the dyes attached to the proteins (Dale and Eisinger 1974). This orientational freedom has been shown for these protein constructs in previous work and was confirmed with control experiments discussed in section **3.3.1**. Figure 1.1 shows the graph of the FRET equation using an R_0 value of 5 nm. As can be seen, the efficiency E can be effectively measured if R is in the range of 2-8 nm. The sensitivity of FRET on this scale makes it an ideal tool for studying proteins, as folding and binding interactions largely happen on the nanometer scale. Measuring FRET requires the fluorescence signal to be split into the emission wavelength ranges of both dyes (shown as green for Cy3/Alexa 555 and red for Alexa 647/Cy5 throughout this paper). This is achieved through a dichroic mirror and selective filters for each individual color.

For simplicity, FRET signal is often referred to as high, mid or low. High FRET refers to the case where $R<R_{0,}$ when the dyes are close enough for the donor to transfer sufficient energy such that the acceptor releases the majority of the photonic emission . Low FRET refers to $R>R_0$, when the dyes are separated enough such that the donor photonically emits the majority of the photonic energy. Mid FRET is when $R\sim R_0$. These terms are illustrated schematically in the right of Figure 1.1. The constructs I used were strategically designed to exist in either a high or a low FRET state depending on protein conformation as is described in section **2.1**.

1.1.3 Single Molecule Fluorescence Microscopy and FRET

Fluorescence imaging of single molecules has only been possible since the early 1990s. With the laser power density required for sufficient photonic emission from a single fluorophore (~50W cm^{-2} laser power density was used for all FRET experiments), stable fluorescent dyes are a necessity along with cameras or photodiodes capable of detecting photons in the tens. As a result, single molecule FRET (smFRET), which requires sufficient signal:noise to measure two fluorescent dyes simultaneously, was not achieved until 1996 (Ha, Enderle et al. 1996). Since then, only two reports of smFRET being employed to study interactions in live cells exist.

One group (Sako, Minoghchi et al. 2000) was able to use single molecule methods to count the population of the small protein Epidermal Growth Factor (EGF) binding to the surface of a living cell. A mixture of EGF bound to Cy3 and Cy5 dyes was added outside a cell and individual dimers of Cy3-EGF and Cy-5 EGF could be detected by FRET signal while simultaneously tracking the mobility of the protein in a dimerized state.

A second group (Murakoshi, Iino et al. 2004) succeeded in using smFRET between the small molecule GTP and the small G-protein Ras to prove the sequence of events in a cell after addition of EGF. Cells were transfected with a yellow fluorescent protein-Ras construct and microinjected with Bodipy-GTP. After external exposure to EGF, smFRET was observed between the GTP and Ras, proving the sequential binding interaction. Further, the single molecule technique allowed Ras to be simultaneously tracked while measuring FRET and showed a slowing of diffusion in the membrane upon activation.

While these studies used smFRET in a live cell context, both were only able to show ligand-protein interactions while neither application was able to address protein

conformational changes related to function. As will be detailed in section 1.2.3, I have been able to measure the conformational state of a single protein in a live cell using smFRET with the ability to simultaneously track its movement over time. This is a novel use of FRET that provides information unavailable through any other means.

1.1.4 Total Internal Reflection Fluorescence Microscopy

One technique that is helpful to lower the optical noise associated with imaging in a life cell is total internal reflection fluorescence microscopy (TIRFM) (Roy, Hohng et al. 2008; Simon 2009). This method uses epifluorescent microscopy as the laser input comes through the objective lens to illuminate the sample after it is focused on the back focal plane of the lens. However, with the use of a high numerical aperture (NA) objective lens (NA=1.4 is required to image in a live cell with a typical index of refraction of 1.38 (George 2008)), and when the laser is aligned sufficiently toward the outer edge of the back focal plane to achieve a critical angle of 61.5 º for the glass-cell interface, the excitation output will be totally internally reflected due to the difference in indices of refraction. The result is an evanescent wave, an electric field that decays exponentially into the cell capable of exciting fluorophores. The depth of this field, d, can be calculated using:

$$d = \frac{\lambda}{4\pi}\left(n_1^2 \sin^2\theta - n_2^2\right)^{-\frac{1}{2}} \quad \textbf{Equation 1.3}$$

where ?×s the wavelength, n_1 and n_2 are the indices of refraction for the glass coverslip and cell, respectively, and ?{s the incident angle of the laser (Axelrod 2003). This depth, which is essentially the 1/e intensity value, penetrates 60-190 nm into the cell depending on how steep the angle is set at in my system. However, it is important to note that much of my data

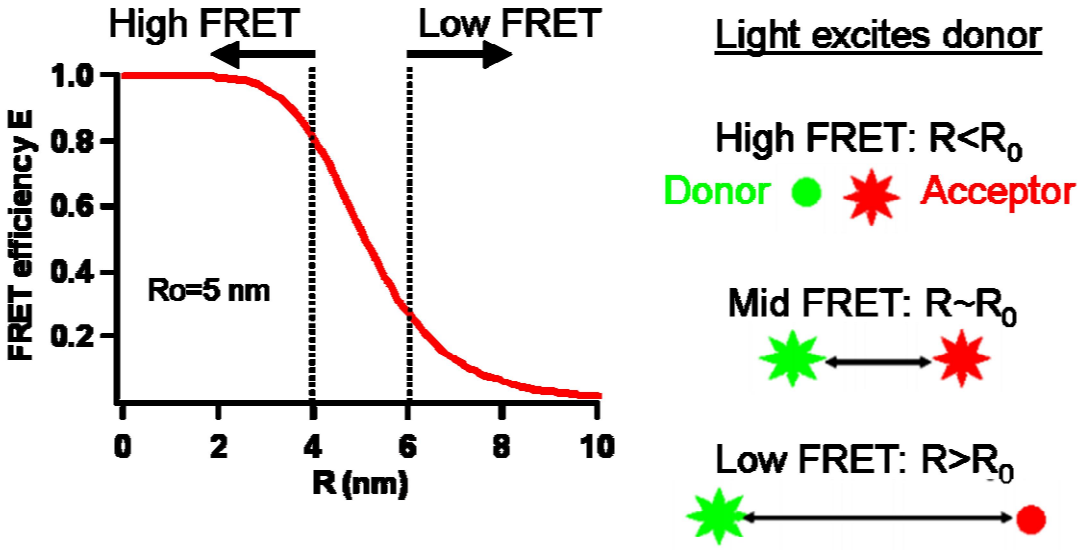

Figure 1.1

***Left*: FRET efficiency graphed for donor and acceptor dyes with an R_0 of 5 nm. *Right*: Schematics of FRET between single dye pairs. High FRET refers to the case where the dyes are close and the majority of the donor energy is transferred to the acceptor. Low FRET is when the dye separation is far enough such that the donor emits most of its energy photonically.**

was taken in “near” TIRFM mode as described below and would excite molecules much deeper into the cell. This was important for minimizing the background fluorescence typical of the live cell itself as well as from fluorescent samples in the bulk of the cell as only a small portion of it is excited (Axelrod 2003). TIRFM is also useful for selectively studying molecules near the cellular membrane attached to the coverslip due to the short path of the evanescent wave.

Another important aspect of the custom-built TIRF system is the ability to alter the laser alignment into the objective lens such that it enters at slightly less than the critical angle. This achieves “near” TIRFM, in which the laser is not totally internally reflected and exits the objective lens at an oblique angle. This method is described in more detail in section **2.2.2**. I used both full TIRFM and near-TIRFM to acquire data.

1.2 Overview: Significance of Technique

Single molecule FRET has been used extensively in an *in vitro* context. Its dynamic, nanoscale resolution provides an ideal tool for measuring the dramatic movements in proteins as they move from an unfolded to a folded state. As the majority of proteins become functional in the folded state, the ability to track proteins over time as they fold becomes especially important. Therefore, applying this method in a live cell context provides an unprecedented measure of nanoscale dynamics in an *in vivo* environment, the complexities of which can not be simulated in solution.

1.2.1 Protein folding

A foremost goal in molecular biology is determining how structure influences function. Protein folding, the process by which the amino acid chain transforms into a three-dimensional structure from a random coil, is a particularly prominent vein of this research, as many proteins have shown the necessity of proper folding into a final structural form to become functional. SNARE proteins, used exclusively in this study, particularly fit this paradigm as they are intrinsically disordered in solution and fold into their functional state upon binding to their cognate partners. However, the dynamic manner in which an intrinsically disordered polypeptide turns into a fully functional structure is largely unknown for many proteins.

The primary force that guides a protein into its folded state is the sequence of the amino acid chain itself. Localized energy fluctuations dependent on solvent, surrounding ions and temperature then provide microenvironments sufficient for folding of the polypeptide chain. The properties of the amino acids within the sequence itself largely guides how these factors influence folding (Anfinsen 1973). For one, hydrophobic amino acid residues within the chain naturally group together to form waterless pockets within proteins while hydrophilic amino acids remain on the outside portions. Hydrogen bonding also has a major affect (Pace, Shirley et al. 1996). Meanwhile, positively and negatively charged amino acids as well as bulky side chains can influence binding interactions. Some of these interactions are with other proteins, particularly a subset of proteins known as chaperones, which influence how the polypeptide folds into a final protein with higher order structure. SNARE proteins, in particular, only find the necessary energy to fold into a higher order structure known as an aøhelix when they find their cognate partners (Sutton, Fasshauer

et al. 1998; Scales, Chen et al. 2000). This is driven by charged interactions within the amino acid sequence and a lack of bulky side chains within the structure. Meanwhile, a host of accessory proteins also seem to influence how these intrinsically disordered SNARE proteins find and interact with each other (Ungar and Hughson 2003). How these dynamics interactions happen within an organism and influence protein folding is a major open question in many biological systems. This is particularly true due to disease states often associated with misfolded proteins (Selkoe 2003). The open questions on how SNAREs fold into functional complexes are discussed in section **1.3.3**.

FRET is an ideal tool to study protein folding as it is sensitive at the nanoscale, where many of these dramatic folding events take place. Further, strategic use of smFRET allows the dynamic tracking of these proteins with knowledge of their folding state, which in a live cell context provides unprecedented resolution of single proteins folding. This strength is explained in more detail in section **1.2.3**.

1.2.2 Importance of live cell work

Studies of proteins and how they interact *in vitro* have unveiled the function of a number of life's devices. However, the complex environment within a cell often makes the study of biological phenomena difficult to interpret outside of a live cell context. To truly understand the biologically relevant behavior of molecules it is essential to observe them as they function within the complex networks of regulatory and signaling cascades of living cells (Kitano 2002). Biological functions emerge from the interplay of numerous interacting components within these networks (Bork, Jensen et al. 2004). Techniques done in a test tube in buffer solution cannot come close to simulating such interactions.

The challenges in unraveling detailed molecular function within cells arise from this high degree of intracellular complexity (Csete and Doyle 2002). Biomolecules often take part in multiple pathways in intermediate and transient states as they move throughout the cell. They are also influenced by molecular crowding effects (van den Berg, Wain et al. 2000). Therefore, it can be important to resolve each individual molecule as it functions in a cellular environment. This is the impetus for developing smFRET in live cells, as this technique has proven capable of measuring the distribution of such intermediate and transient protein folding events *in vitro*. Pioneering the use of smFRET *in vivo* is an essential step in determining protein function in their complex, native environment.

1.2.3 What smFRET can achieve in a live cell

As detailed in section **1.1.1** and **1.1.3**, single molecule studies have provided a number of interesting results only available through the study of the isolated molecule. Meanwhile, *in vivo* bulk FRET studies have shown a number of interesting results, including detection of ensembles of molecules favoring particular conformations (An and Almers 2004) and the large-scale interplay of binding reactions (Itaka, Harada et al. 2004). However, the bulk nature of these studies does not allow conformational measurement of individual molecules—including infrequent or transient states—or stoichiometric determination of binding events. Further, the location and timeframe of such conformational changes or binding events is difficult to achieve when imaging a large number of molecules throughout a cell.

Therefore, there is large demand for being able to use smFRET within a live cell context. I worked toward this goal by creating protein constructs capable of folding into a

different conformation only when they attach to their endogenous binding partners within a cell. This way, I was able to prove the possibility of measuring single molecule conformational changes of an individual protein and monitor single binding events. Further, I succeeded in measuring the location where these events took place and monitor their timecourse. I detail the strategic design of the biological constructs I used to successfully implement *in vivo* smFRET in section **2.1** and the biological system of study I was able to learn more about using this technique in section **1.3**.

1.2.4 Difficulties of smFRET *in vivo*

Implementing smFRET detection in a live cell required overcoming a number of obstacles. As detailed above, the biggest obstacle is detecting the signal—typically on the order of 10 photons per time bin for a single fluorophore (Ram, Ward et al. 2006)—above the optically noisy autofluorescent background of a live cell. Using TIRFM on specific types of cultured cells, selected for their flat shape and kept in particular conditions that I found to lower autofluorescence helped me achieve smFRET. These strategies are detailed in sections **2.3-2.4**. Another problem is the autofluorescence of the glass coverslips at the laser powers required for single molecule imaging. The ~50W cm^{-2} green laser line creates background fluorescent signal from the impurities within the glass, requiring efforts to find pure samples as explained in section **2.3.2**. An additional difficulty of live cell imaging is the short time until photobleaching of fluorescent dye molecules in the cytoplasm. Photobleaching of dyes, caused by the high powered laser in concert with the available oxygen throughout the cellular milieu structurally altering the fluorescent molecules, often inhibits sufficient imaging times to measure kinetics. Strategies to extend this time until photobleach are detailed in section

2.4.3. Finally, ensemble FRET studies commonly use transfected protein chimeras with expressed fluorescent proteins as a donor-acceptor pair. Variable expression levels make single molecule application of this approach difficult. Therefore, I expressed, purified and labeled recombinant proteins with small, organic fluorophores and microinjected them into cells as explained in section **2.3.3**.

1.3 Overview: Biological System of Study

Membrane fusion is an essential process within eukaryotic cells as materials are transported between cellular compartments. Biological membranes resist spontaneous fusion and as a result highly conserved protein machinery has evolved to mediate membrane fusion reactions (Bock, Matern et al. 2001). The SNARE (soluble N-ethylmaleimide sensitive fusion protein attachment protein receptor) family of proteins is implicated in catalyzing membrane fusion in addition to lending targeting and specificity to vesicle tracking (Brunger 2001; Tamm, Crane et al. 2003; Jahn 2004). While the best-studied SNARE complex involves calcium-dependent neurotransmitter release in neuronal synapses (Brunger, Weninger et al. 2009), SNAREs are involved in fusion pathways throughout all higher organisms (Rossi, Salminen et al. 1997) and show surprising redundancy despite the myriad systems involved with membrane fusion (Antonin, Fasshauer et al. 2002). My lab has experience with a particular neuronal complex found in synapses that forms between SNAP-25, syntaxin and synaptobrevin (Oyler, Higgins et al. 1989; Weninger, Bowen et al. 2003).

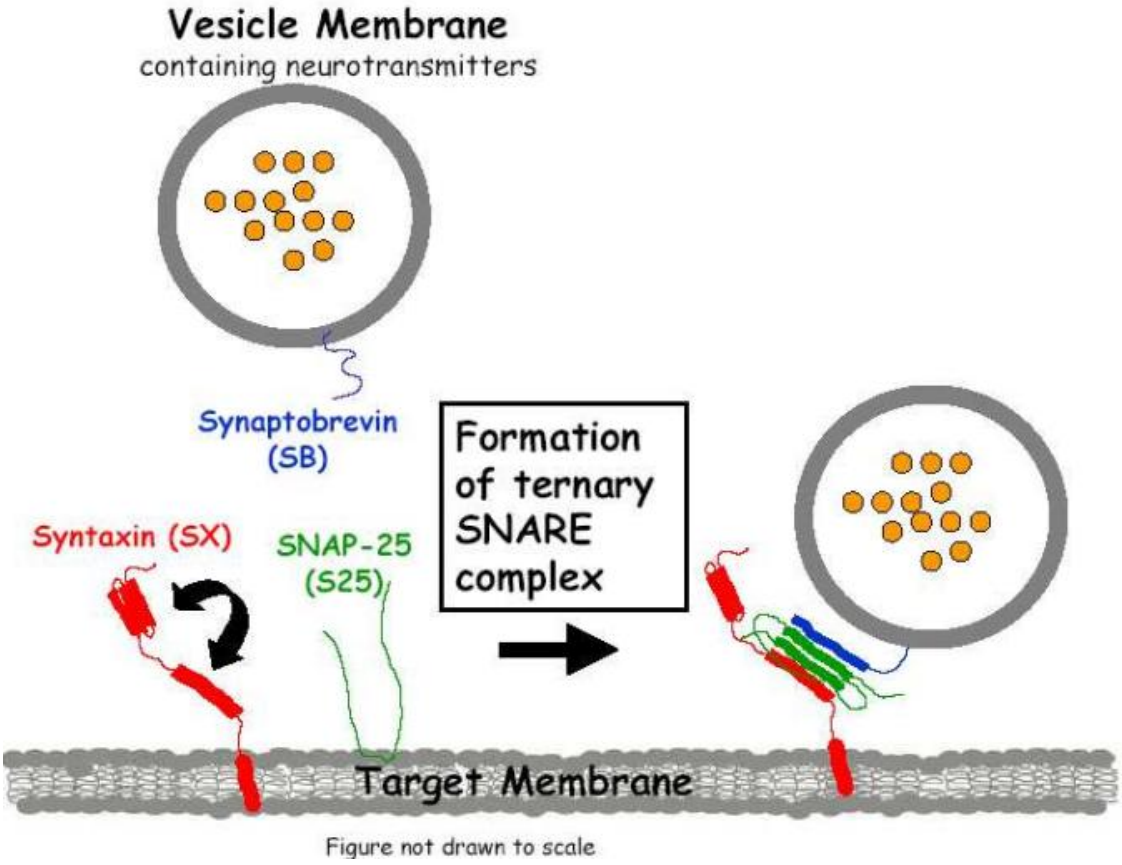

Figure 1.2

Schematic of SNARE complex formation. The membrane-localized proteins SNAP-25 and syntaxin come into contact with vesicular-localized synaptobrevin to form ternary SNARE complex that theoretically pulls the apposing membranes together and drives membrane fusion.

1.3.1 SNARE proteins

During trafficking of vesicles SNAREs on the target cellular membrane bind with SNAREs on the vesicle to form a complex of 4 parallel alpha helices. This is shown schematically in Figure 1.2. The particular complex shown here is a combination of the vesicular protein synaptobrevin with the membrane proteins SNAP-25 and syntaxin and is referred to as ternary complex. Synaptobrevin and syntaxin each have 1 SNARE binding domain while SNAP-25 contributes 2 SNARE binding domains. Only 3 other SNARE proteins also possess 2 domains: SNAP-23 (Ravichandran, Chawla et al. 1996), SNAP-29 (Steegmaier, Yang et al. 1998) and SNAP-47 (Holt, Varoqueaux et al. 2006), each of which is named for its respective molecular weight. This family of SNAP proteins are structurally similar to SNAP-25, can also bind with various isoforms of syntaxin and synaptobrevin and have shown the ability to substitute for SNAP-25 in some SNARE complex formations (Ravichandran, Chawla et al. 1996; Steegmaier, Yang et al. 1998; Holt, Varoqueaux et al. 2006).

I decided to study SNAP-29 in addition to SNAP-25, a protein my lab is familiar with, to learn how these proteins might differentially act *in vivo*. SNAP-29 is distinct from SNAP-25 in a number of ways. First, it is not localized predominantly in the brain like SNAP-25 but has more ubiquitous expression in all tissues tested within the human body (Steegmaier, Yang et al. 1998) and binds to the plasma membrane and intracellular vesicles equally well (Hohenstein and Roche 2001). SNAP-29 also lacks palmitoylation sites, membrane-localizing cysteines found in SNAP-25, making it more likely to be found in the cytoplasm and forcing its membrane targeting to be dependent on interactions with syntaxin (Steegmaier, Yang et al. 1998). SNAP-29 is thought to inhibit SNARE complex disassembly

but in a noncompetitive manner from SNAP-25, which implies that its function is involved with modulation of the recycling of the component members of SNARE complex (Su, Mochida et al. 2001; Wang and Tang 2006). Other work has shown that this inhibitory effect of SNAP-29 on SNARE complex disassembly does not coincide with an influx of calcium, but instead is active at a particular frequency of synaptic activity (Pan, Cai et al. 2005). Such studies are beginning to determine how SNAP-29 differentially acts in synapses from other SNAP proteins in an effort to answer a general question in SNARE biology: how do the multitude of SNAREs with such structural similarities—there are 35 distinct SNAREs in humans—orchestrate the multitude of separable membrane fusion events in cells (such open questions are addressed more extensively in section **1.3.3**)? And more universally: how is this related to human health?

A number of studies have begun to address this question for SNAP-29 and how disorders arise from abnormal regulation of vesicular fusion (Wonodi, Hong et al. 2005). One study found a mutation in the gene that promotes the expression of SNAP-29 is associated with chromosome 22-linked schizophrenia (Saito, Guan et al. 2001). A deletion in the SNAP-29 gene has also been linked to 70% of cases of a disorder called velocardio-facial syndrome, which is also associated with increased prevalence of psychiatric disease including schizophrenia and bipolar disorder (Carlson, Sirotkin et al. 1997). Finally, the importance of SNARE machinery during brain development is highlighted by a point deletion in a gene expressing SNAP-29 that was found to cause an extremely debilitating syndrome termed CEDNIK (Sprecher, Ishida-Yamamoto et al. 2005). Symptoms of this disease include poor vision, severe neuropathy and abnormal skin barrier formation, which allude to the importance of SNAP-29 in development. In addition, vesicles found in the skin

and fibroblasts were abnormal with a generalized defect in vesicle fusion and trafficking. All of these studies underscore the importance of SNAREs in the organization of membrane fusion and why techniques like smFRET—capable of contributing to the knowledge of SNARE function as well as many proteins throughout the body—are necessary for the advancement of human medicine and related technology.

1.3.2 SNARE folding

The SNARE proteins SNAP-25 and SNAP-29 are ideal candidates for study with smFRET as they undergo a large conformational change when entering SNARE complex. These proteins are intrinsically unstructured until they come into contact with their SNARE binding partners and subsequently fold into parallel alpha-helices (Bock, Matern et al. 2001). Using the known crystal structure of SNAP-25 (Sutton, Fasshauer et al. 1998) in complex allowed me to strategically design mutation sites for dye-labeling that can report entry into SNARE complex with changes in FRET emission (Weninger, Bowen et al. 2003). I similarly designed the mutations of SNAP-29 as I did for SNAP-25 as there is evidence supporting the claim that the structures formed for different members of the family are remarkably similar (Scales, Chen et al. 2000; Antonin, Fasshauer et al. 2002). The strategic design for the 3 major constructs used in my research and a description of the fluorescence dye labeling approaches are located in sections **2.1** and diagrammed in Figure 2.1.

1.3.3 Open questions concerning SNAREs

While SNARE proteins have been intensely studied there are a number of unanswered questions concerning how their structure leads to function. In particular:

- How do various members of the SNARE family, many of which share remarkably similar sequences and binding domains, selectively coordinate the distinct membrane fusion events throughout an organism (Ungar and Hughson 2003)? For example, there are over 50 different neurotransmitters that must be selectively released by vesicular fusion within the brain.
- What are the molecular mechanisms that mediate the folding of SNAREs into a complex? Are interactions largely stochastic, targeted by localized expression, or mediated by binding interactions with lipid domains, tethering factors, or other accessory proteins (Ungar and Hughson 2003; Brunger, Weninger et al. 2009)?
- Do associations found *in vitro*, such as binary complex (Weninger, Bowen et al. 2008) or anti-parallel SNARE complex (Weninger, Bowen et al. 2003), exist in a physiological context?

My results from studying SNAP-25 and SNAP-29 using smFRET in a physiological context suggest answers for many of these questions. Specifically, I was able to show SNARE complex formation of SNAP-25 injected into a cell that does not express the protein natively, hinting at the universal nature of SNARE binding interactions. Additional results indicate the formation of anti-parallel SNARE complex and temporally differentiable bound states from SNAP-25 *in vivo*. These results, and how they address many of the open questions above, are discussed in detail in section **3.5**.

Chapter 2. Strategies for implementing smFRET *in vivo*

The use of smFRET *in vivo* to determine individual protein conformation has not been achieved because of the inherent difficulty of measuring two-color signal from single molecules in the optically noisy environment of a cell. I used a number of strategies to overcome these obstacles. First, I strategically designed dual-labeled SNAP-25 and SNAP-29 constructs such that they emitted low FRET when not in complex but could yield either low or high FRET depending on dye location when folded into SNARE complex. Second, I employed TIRFM as well as near-TIRFM imaging techniques to selectively excite only small slices of the cell while still being able to view multiple fluorescent molecules at once. Third, I experimented with multiple types of glass and cleaning methods to eliminate as much background noise as possible from autofluorescence of coverslips. Fourth, I experimented with multiple types of cultured cells and growth media to eliminate unwanted background. Maintaining healthy cells and selecting for cells with low autofluorescence also proved essential to achieving smFRET. Finally, incubating cells with additives to the growth media allowed me to extend the duration of dye fluorescence before photobleach.

2.1. Overview: Design of biological constructs

The use of site-directed mutagenesis allows precise labeling of proteins with robust, small-molecule dyes. I used the known crystal structure of SNAP-25 SNARE complex (shown in Figure 2.2) to find strategic locations for dye labeling. Mutating cysteine into these specific sites, a typically uncommon amino acid with a thiol residue, allowed fluorescent labeling of maleimide-terminated thiol-reactive dyes.

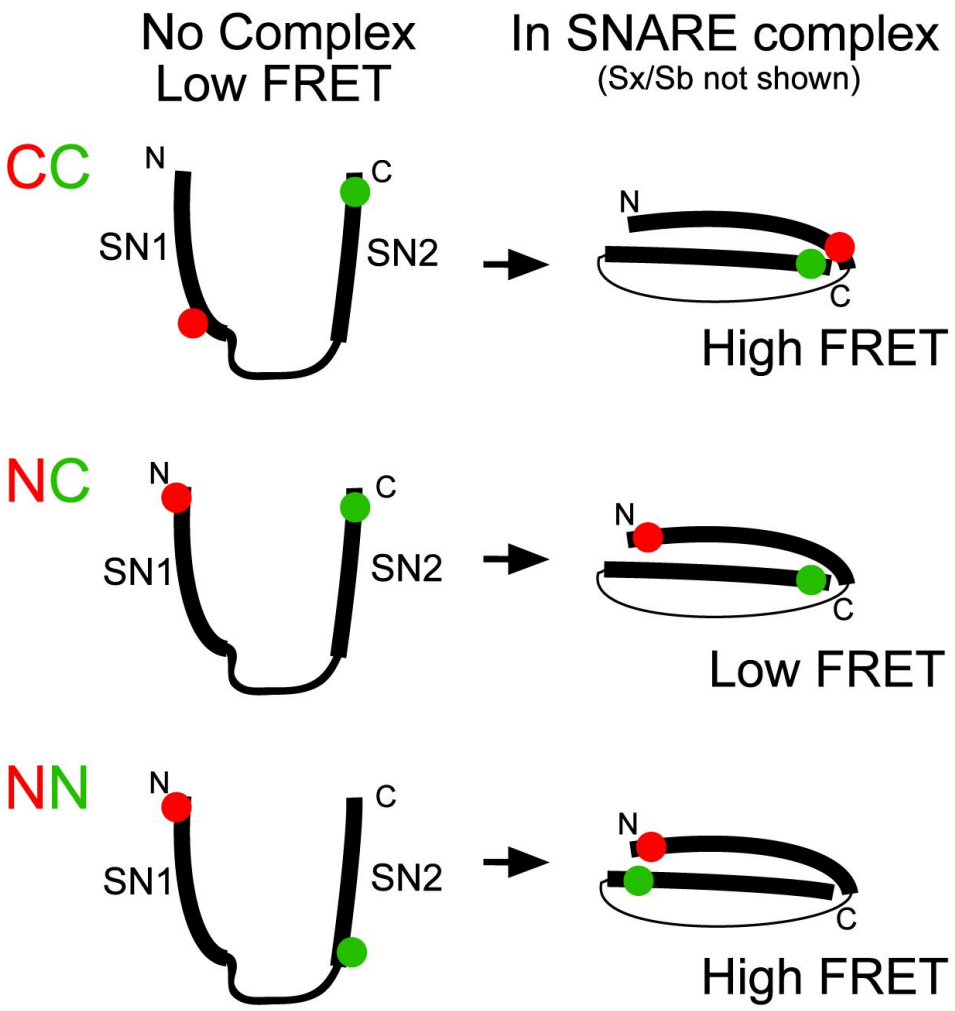

Figure 2.1

Schematic of SN25CC, SN25NC and SN29NN label site locations. Isolated SNAP-25 and SNAP-29 (no complex, left) are unstructured, resulting in low FRET because of the large separation of the label attachment sites. When they enter SNARE complex (right; synaptobrevin and syntaxin are not shown) the SN25CC and SN25NC constructs yield high and low FRET states, respectively, while SN29NN yields high FRET. Red and green circles represent the approximate label sites, each of which has a 50% chance of being Cy3 (or Alexa 555) or Cy5 (or Alexa 647) in a construct with 100% labeling efficiency.

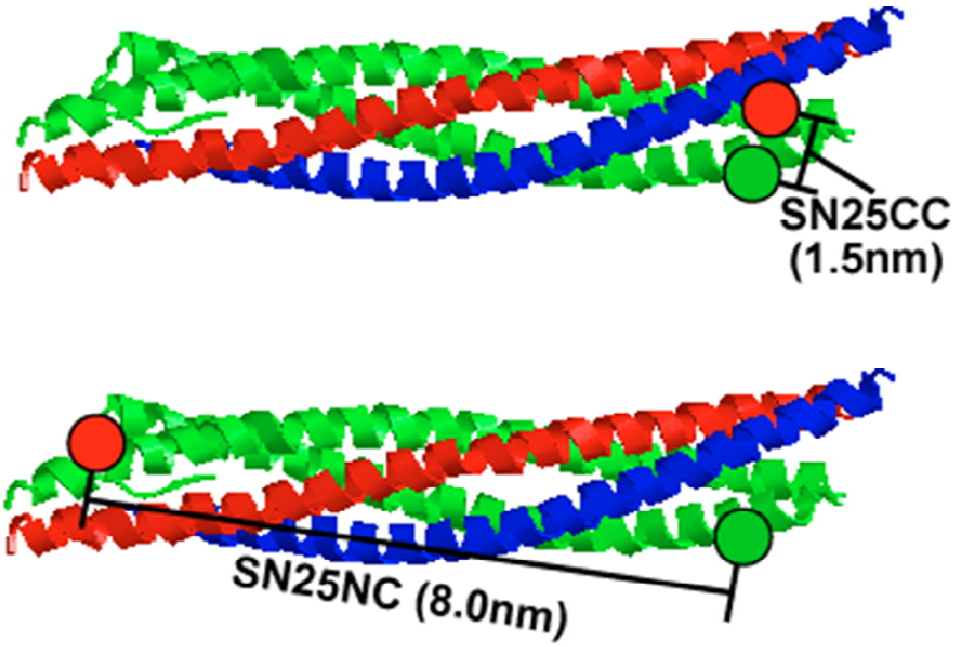

Figure 2.2

Location of label sites in assembled SNARE complex (Protein Data Bank identifier : 1sfc; syntaxin, red; synaptobrevin, blue; SNAP-25, green; (Sutton, Fasshauer et al. 1998)). The SN25CC was designed such that dye distances are less than 2 nm apart in the final SNARE complex and give high FRET. SN25NC was designed so dyes are 8 nm apart in parallel complex and give low FRET. While there is no solved crystal structure for SNAP-29, studies indicate that it forms SNARE complex in a very similar manner to SNAP-25. As a result, SN29NN is expected to look like the above structures with both dye-label sites on the N-terminal sides of the SN1 and SN2 domains (schematically, the left side of both green alpha helices shown above, as shown in Figure 2.1).

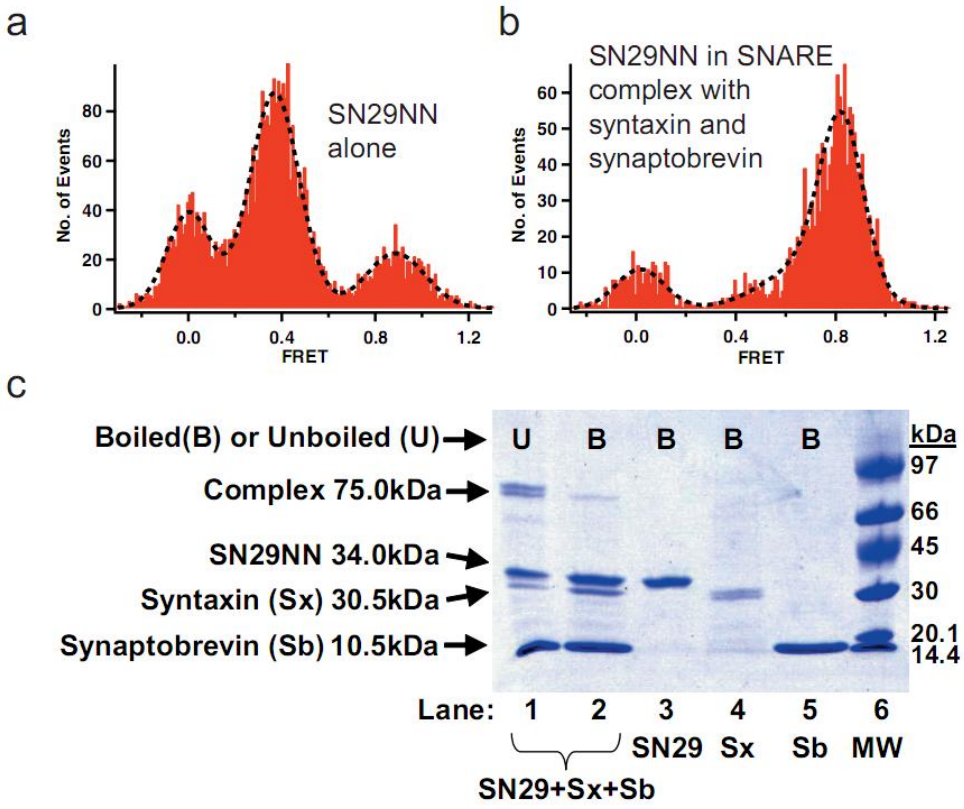

Figure 2.3

(a) SN29NN labeled with Alexa 555 and Alexa 647 was encapsulated inside liposomes tethered to a quartz surface and analyzed for single molecule FRET. The FRET distribution is dominated by a low FRET peak (0.37). A smaller FRET peak at 0.9 is likely due to protein aggregation. The FRET=0 peak is due to acceptor blinking and bleaching. (b) SN29NN labeled with Alexa 555 and Alexa 647 was assembled into SNARE complex with syntaxin (Sx) and synaptobrevin (Sb) and measured for smFRET as in a. The FRET peak revealed emission around 0.82, reporting entry into SNARE complex by a change from low FRET to high FRET. (c) SDS-PAGE (10-15% gradient phast gel with Coomassie staining) analysis reveals SNAP-29 forms an SDS resistant complex with syntaxin and synaptobrevin. Molecular weight markers are in lane 6. Lanes 1 and 2 contain a mixture of SN29NN (unlabeled), syntaxin and synaptobrevin without boiling (lane 1) or with 5 minute boiling in SDS loading buffer (lane 2). Lanes 3-5 contain the individual protein samples (at the same final concentrations used in lanes 1 and 2) as indicated. An SDS-resistant complex with molecular weight between 66 and 97 kDa is visible in lane 1 that disappears upon boiling in lane 2.

This external labeling of proteins and subsequent microinjection into the cell avoids the complications of expressing transfected fluorescent proteins *in vivo* (Giepmans, Adams et al. 2006). These moieties suffer from being prohibitively large (typically 20x the molecular weight of the Cy or Alexa dyes used in my experiments), possess weak quantum yields and typically must be attached to the end of the polypeptide chain to avoid disturbing the functionality of the protein of interest. Further, transfected fluorescent proteins are hard to localize within the cell and can be difficult to express at single molecule concentrations (Giepmans, Adams et al. 2006). Using the microinjector I have much greater control of the location and concentration of fluorescent protein within the cell.

I designed dynamic SNAP-25 and SNAP-29 constructs capable of changing in FRET value depending on their conformation *in vivo*. In order to prove that I could use FRET to monitor single protein conformation I needed to do a number of controls to account for possible false positive signals. A simple control was injecting only buffer into a cell to show that the acceptor channel does not show false FRET events. A second control involved injecting an equimolar mixture of SNAP-25 singly-labeled with either Alexa 555 or Alexa 647, termed SN25C as only a single cysteine substitution was made at the K76 site (the first C in Figure 2.1, top), to prove that SNAP-25 does not randomly aggregate to give smFRET signal. Another key control used the SN25CC construct with the mutation G43D, an amino acid substitution that prevents SNARE complex formation due to the insertion of a larger, charged aspartic acid side chain (Loranger and Linder 2002). Final controls involved injecting double-labeled synaptobrevin, a SNARE protein with one SNARE binding domain that does not dramatically fold like SNAP-25 or SNAP-29, to ensure SNAREs do not non-specifically bind after injection in live cells and give false FRET signal. Two synaptobrevin

constructs were used, termed Sb-NC_5_72 and Sb-NC_28_72 for the amino acid locations of their dye labels.

2.1.1 Strategic mutations and dye-labeling

SNAP-29 has no native cysteine residues, while SNAP-25 has 4 on palmitoylation sites that tether the protein to membranes. These 4 cysteines were removed in all proteins used in this study without loss of complex-forming function (Weninger, Bowen et al. 2003). Therefore, by mutating the codons in the plasmid DNA that expresses my protein, 2 amino acids can be changed to cysteine to create specific dye-labeling locations that covalently link to maleimide dyes. In this manner, I was able to make proteins capable of single molecule FRET dependent on the distance between the label locations. Once this new protein is created, the final dye-labeled construct must be tested to ensure there is no loss of function. In particular for SNAP-25 and SNAP-29, they must be able to form SNARE complex when incubated with their binding partners syntaxin and synaptobrevin. Therefore, mutations were made in regions at the ends of the SNARE binding domains of SNAP-25 and SNAP-29, termed SN1 and SN2 as shown in Figure 2.1, to avoid inhibiting SNARE complex forming ability of these proteins.

The SN25CC and SN25NC constructs, each of which is labeled with Cy3 and Cy5 as described below, have full functionality as shown in previous work (Weninger, Bowen et al. 2003). For SN29NN, I had to create SNARE complex and use *in vitro* FRET experiments to prove the proper activity of the labeled protein and to ensure my FRET construct design came out as planned. This is detailed in section **2.1.3**.

I created dye-labeling locations on the outside of SNAP-25 and SNAP-29 according to the known crystal structure to avoid internal-facing residues or potential sites of steric repulsion capable of inhibiting covalent modification. Proteins were incubated with a tenfold molar excess of maleimide dyes at pH 7.4 for 4 h, followed by PD10 gel filtration and extensive dialysis to remove unbound dye. Experiments with double-labeled protein used equimolar mixtures of donor and acceptor dye. The two cysteines were not selective for specific dyes, so 50% of double-labeled molecules had one donor and one acceptor, and the other double-labeled molecules had either two donors or two acceptors. Since I am able to image molecules one at a time, I have the ability to select for only those with one donor and one acceptor by keeping traces in which the acceptor and donor photobleach in single steps. Intensity trace analysis is discussed extensively in section **3.1.1**. Dye-labeling efficiencies of double-labeled proteins and probe types for each are summarized in Table 2.1. I used the donor-acceptor pairs Alexa 555/Alexa 647 and Cy3/Cy5 as they both have similar spectra with an R_0 close to 5nm (Weninger, Bowen et al. 2003), giving them ideal sensitivity in the range of my SNARE construct designs.

2.1.2 SN25CC and SN25NC

SNAP-25 with Cy3 and Cy5 dyes covalently attached to cysteine substitutions at K76C and Q197C is termed SN25CC as both dye label locations are C-terminal to the 2 SNARE binding domains as shown in Figure 2.1, top. SN25NC keeps the Q197C label site and uses a second site N-terminal of the SN1 domain, Q20C, such that the distance between the αcarbons of these two mutations is 8 nm, as opposed to 1.5 nm for the SN25CC label sites (Figure 2.2). While these distances give an idea of expected dye separation, carbon

Table 2.1

Summary of protein constructs used in this study with dye labeling information. SN25 stands for SNAP-25 while Sb stands for synaptobrevin-2 (residues 1-96).

Protein Construct	Fluorescent Dye (including pairs)	Mutation sites for dye labels	Labeling efficiency (donor)	Labeling efficiency (acceptor)
SN25CC	Cy3 and Cy5	K76C and Q197C	53%	43%
SN29NN	Alexa 555 and Alexa 647	R51C and Y198C	50%	46%
SN25NC	Alexa 555 and Alexa 647	Q20C and Q197C	48%	56%
SN25C (donor)	Alexa 555	K76C	46%	-
SN25C (acceptor)	Alexa 647	K76C	-	92%
SN25CC (G43D)	Alexa 555 and Alexa 647	K76C and Q197C	112%	42%
Sb_NC_5_72	Alexa 555 and Alexa 647	A5C and A72C	28%	26%
Sb_NC_28_72	Alexa 555 and Alexa 647	S28C and A72C	45%	40%

linker regions of the dyes will extend this distance and lower FRET. Another protein-dependent event potentially affecting FRET values is the worm-like chain properties of intrinsically disordered proteins like SNAP-25. While SNAP-25 becomes ordered when it folds into an α-helical chain in SNARE complex, random chain dynamics can make label locations separated by many amino acids stay closer together than the extended polypeptide length when the protein is free in solution (Ohashi, Galiacy et al. 2007). This is explained below in consideration of the FRET values found for *in vitro* FRET experiments of isolated SN25CC and SN25NC. It should also be pointed out that these results are for proteins in buffer solution. Isolated protein might act differently in a live cell context with such phenomena as molecular crowding potentially having an effect (Chebotareva, Kurganov et al. 2004).

Human SNAP-25 plasmid DNA encoded into the pet28c vector was kindly given by the A.T. Brunger Lab at Stanford University. Purification and FRET characterization of these constructs are extensively described by previous work (Weninger, Bowen et al. 2003) and the various techniques used are elaborated on in section **2.1.3**. Briefly, proteins were expressed in E. coli BL21(DE3) cells with thrombin-cleavable, 6-His tags and purified under native conditions using combinations of Ni^{2+}-NTA, ion exchange and gel filtration chromatographies. The 6-His tag was removed using thrombin.

When SN25CC is alone in solution it yields FRET=.27 (U.B. Choi and K.R.Weninger; unpublished data) but when in complex with syntaxin and synaptobrevin gives a FRET value of .9 (Weninger, Bowen et al. 2003). The same works have shown that SN25NC gives .3 FRET both in and out of SNARE complex formation. However, occasionally SN25NC will yield high FRET signal, indicative of the SNARE domains

binding in a backwards or “anti-parallel” formation (Weninger, Bowen et al. 2003). I explain evidence for such anti-parallel SN25NC formations *in vivo* from my smFRET data in section **3.5.2**. The FRET values of .27 for these two SNAP-25 constructs moving freely in solution (but encapsulated within a tethered liposome for imaging purposes) is higher than anticipated based solely on amino acid separation, indicating compaction as expected from random coil effects (U.B. Choi and K.R.Weninger; unpublished data). For my smFRET data *in vivo,* however, I would not expect to find such FRET values as cytoplasmically injected proteins diffuse in an isotropic solution. The events I am able to image only occur on the timescale of the 100ms frame length I image for (see section **2.3.1** for detailed microscope parameters) and are therefore restricted to when the protein binds in place. If SNAP-25 does bind in place before folding into SNARE complex, it is expected to lose the intrinsically disordered properties it has in solution. This would separate the dye label sites closer to what is expected from the actual polypeptide length. Therefore, low to mid FRET values like the .3 reported for SN25CC and SN25NC encapsulated in tethered liposomes *in vitro* are not expected for smFRET data within the cell. Instead, the large distance between the label sites (121 amino acids for SN25CC and 177 amino acids for SN25NC) should yield FRET zero, as is shown in FRET histograms for my *in vivo* data (section **3.2.3**).

2.1.3 SN29NN

Similar to SN25CC, the SN29NN construct was designed to yield high FRET signal when folded into SNARE complex and low FRET signal when isolated. This was based on alignment of SNAP-29 with the known crystal structure of SNAP-25, as the two proteins show similar properties in previous assays (Steegmaier, Yang et al. 1998; Scales, Chen et al.

2000). Unlike SN25CC, SN29NN used two mutation sites on the two N-termini of the SNARE binding domains (Figure 2.1, bottom) as these proved not to alter function. The mutations created in SNAP-29 to make SN29NN were R51C and Y198C, which align well to previous label sites used to create a high FRET construct with apposing N-terminal label sites in SNAP-25 (Weninger, Bowen et al. 2003). Since SN29NN was created uniquely for this project it required a great deal of work to purify this relatively unstable protein and prove the efficacy of the SN29NN construct. This included working out a denaturing purification protocol, the conditions necessary to for SN29NN to form SNARE complex *in vitro* and testing this SNARE complex on the microscope using smFRET to prove the label sites do indeed create a protein capable of high and low FRET signal as predicted by structural similarity to SNAP-25.

Human SNAP-29 in a pet28c vector was kindly given by the Z.-H. Sheng at NIH in Bethesda, MD. The pet28c vector provides kanamycin resistance and attaches a 6-histidine tag at the N-terminal end of my protein to allow purification with Ni^{2+}-NTA chromatography (Schmitt, Hess et al. 1993). The SNAP-29 plasmid was expressed in E. coli BL21(DE3), a cell line with an inducible lac operon that provides an induction trigger for protein expression upon addition of the non-metabolized lactose analog IPTG. Cultures were grown in terrific broth (Sambrook, Fritsch et al. 1989) with 50 µg ml^{-1} kanamycin sulfate to an optical density at 600 nm of 1.0 at 37 °C while shaking. The temperature was decreased to 24°C, 0.5 mM IPTG was added and cells were collected after 8–10 h. Lowering the temperature for expression of the protein inhibits the formation of inclusion bodies within the bacteria, which are difficult to break up in purification and cause the desired protein to be insoluble (Baneyx 1999).

Initial attempts at purifying SNAP-29 under native conditions resulted in the vast majority of my protein becoming insoluble and lost in the pellet during ultracentrifugation. As a result, I used a denaturing purification protocol for SNAP-29 (Schmitt, Hess et al. 1993). Cells were resuspended at 0.2 g ml^{-1} in lysis buffer (10 mM Tris, 100 mM NaH2PO4 and 5 M urea (pH 8.0)), disrupted by sonication and centrifuged at 10,000g for 30 min at 4°C. Supernatant was bound to Ni^{2+}-NTA beads for 1 h rotating at 4 °C. Beads were washed with lysis buffer at pH 8.0, lysis buffer at pH 6.8 and then eluted in pH 5.9 lysis buffer. SNAP-29 at 50–100 µM aggregated unless urea was present above 2 M. SNAP-29 was dialyzed into buffer A (20 mM Tris and 2.5 M urea (pH 7.3)) and then purified on a MonoQ column on a linear gradient in buffer A from 0 to 1 M NaCl (peak elution, ~225 mM NaCl). Molecular weight and purity were verified by SDS-PAGE electrophoresis. The 6-His tag was not removed from SN29NN as usual thrombin cleavage techniques do not work properly in denaturing conditions (high urea). I did not find any evidence the 6-His tag inhibited function in any way.

I verified that the SN29NN construct formed SDS-resistant SNARE complex *in vitro* with separately purified syntaxin and synaptobrevin. SN29NN, syntaxin and synaptobrevin were mixed in that order at 1:2:5 (molar ratio) with urea always present at 2.5 M. The mixture (<0.1 ml) was dialyzed against 1 liter of buffer (20 mM Tris and 300 mM NaCl (pH 8.0), 2 mM ßémercaptoethanol, 5% (vol/vol) glycerol) with a Slide-A-Lyzer MINI Dialysis Unit. The dialysis buffer was preheated to 37°C before the sample was added. After the protein mixture in the dialysis unit had been in 37°C buffer for 10 min, the dialysis flask was placed at 4°C for 12 h while stirring. SDS-PAGE of the resulting complex (Figure 2.3) showed the SN29NN-containing SNARE complex was SDS-stable without boiling and

dissociated upon boiling in SDS buffer. This is typical for SNARE complex formation, as boiling is required to break up the tight associations formed by SDS-resistant SNARE complex.

In order to prove that SN29NN gave FRET signal as expected, I encapsulated single molecules of the protein (in and out of complex) inside 100 nm diameter, biotinylated liposomes (Boukobza, Sonnenfeld et al. 2001), which were immobilized on a biotinylated-BSA and streptavidin-coated surface in a chamber between a quartz microscope slide and a glass coverslip. I measured smFRET from the immobilized proteins using prism-type TIRFM, with the same filters and detection used for *in vivo* work (section **2.3.1**). SN29NN was diluted in urea-free buffer so that final urea was <7 mM before liposome encapsulation. I found FRET from isolated SN29NN to be 0.37 (Figure 2.3.a), which is similar to results for similar isolated SN25CC as described above. Meanwhile, FRET from SN29NN SNARE complex was measured by the liposome encapsulation method as 0.82 (Figure 2.3.b). These results align with the results described above, which show FRET from SN25NC and SN25CC in parallel, SNARE complex with syntaxin and synaptobrevin to be 0.3 and 0.9, respectively. Therefore, SN29NN is a viable construct capable of reporting high and low FRET when in and out of SNARE complex.

2.1.4 SNAP-25 control constructs

A number of control constructs were created from SNAP-25 to prove that high FRET signal in cells is a result of SNARE complex formation. The first involved purifying SNAP-25 with only the K76C mutation, termed SN25C as it is C-terminal to the SN1 domain, and labeling this cysteine with either Alexa 555 or 647. I mixed equimolar amounts of SN25C

singly labeled with each kind of dye and microinjected them into cells at the same concentration as other SNAP-25 constructs. This was done to ensure that smFRET signal I saw from SN25CC and SN25NC is not a result of these proteins self-aggregating or forming unexpected dimers that could potentially give false FRET signal.

Another important control was an adaptation of the SN25CC construct with the point mutation G43D. This mutant protein shows normal kinetics and membrane localization within cells despite its inability to interact with syntaxin (Loranger and Linder 2002). Therefore, I created this mutation in SN25CC as SNARE complex assembly should not be possible without the ability of this protein to interact with syntaxin. Indeed, I found that the single point mutation at G43D eliminated high smFRET signal from the SN25CC, giving strong evidence that such high FRET is an indicator of SNARE complex formation. This is further discussed in section **3.3.2** while biological implications are detailed in section **3.5.3**.

2.1.5 Synaptobrevin control constructs

Dye-labeled synaptobrevin constructs were also used as controls to prove SNARE proteins do not non-specifically bind and give false high FRET signal. Synaptobrevin is a binding partner of SNAP-25 that only has one SNARE domain. It would be expected that if synaptobrevin non-specifically bound to other labeled synaptobrevins or aggregated in some way with endogenous SNARE proteins that high FRET signal could occur from the jumble of proteins. The soluble fragment (residues 1-96) of rat synaptobrevin-2 was expressed and purified as previously described (Bowen, Weninger et al. 2004). Two synaptobrevin constructs were used, one with label sites at S28C and A72C termed Sb-NC_28_72 and a second with closer label sites at A5C and A72C termed Sb-NC_5_72. Both were double-

labeled with Alexa 555 and Alexa 647 and microinjected into live cells. High FRET was absent for all injections with these constructs as shown in section **3.2.3**.

2.2. Overview: TIRFM alignment

Total internal reflection fluorescence microscopy was essential to overcoming the background fluorescence of cells caused by laser excitation. I manually set up a custom-built TIRFM system as this allowed me to adjust the optical path for different objective lenses and TIRFM modes. A commercially available TIRFM system from Olympus did not have such flexibility. In particular, the ability to enter near TIRFM mode was essential for making smFRET imaging work in cells.

2.2.1 Custom built alignment of TIRFM

The schematics of the system are detailed in Figure 2.4. A Gaussian profile beam is initially expanded and then collimated to create a wide, uniform beam behind the microscope (expanded beam schematically represented by the area between the dotted lines). The expanded beam is reflected by a mirror through a final lens with a focal length equal to the distance from it to the back focal plane of the objective lens. The vertical micrometer adjustment allows movement of this last lens independent of the mirror. This provides a way to align the focus of the laser onto the focal plane of different objective lenses. The horizontal micrometer adjustment is able to move the final lens and the mirror in unison, allowing displacement of the entire beam to the outer edge of the objective lens but still in

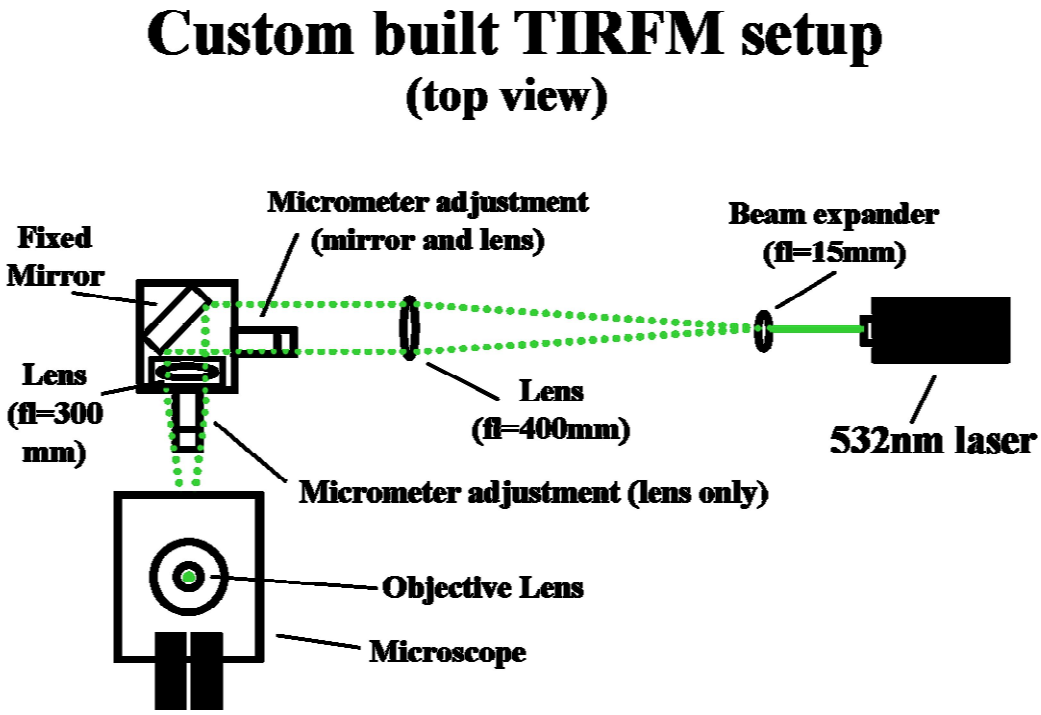

Figure 2.4

Layout of custom built TIRFM setup.

the focal plane in order to enter TIRFM mode. Adjusting the laser horizontally in this way allows manual adjustment from full to near TIRFM.

Two different oil-immersion objective lenses were used: a 60x with NA=1.45 and a 100x with NA=1.4. The necessity of high numerical aperture oil immersion lenses is detailed in section **1.1.4**. Both lenses were used for data acquisition with the 100x used more often for smaller cells.

2.2.2 Imaging with near TIRFM

Near TIRFM occurs when the laser enters the objective lens on the outside edge of the back focal plane slightly lower than the critical angle of 61 º required for total internal reflection of the beam. As a result, the laser does exit the objective lens, but at a very steep angle such that it only excites a slice of the cell above the focus of the lens before exiting the cell as shown in Figure 2.5. This allows illumination of molecules at a higher distance from the coverslip into the cell than full TIRFM, in which the evanescent wave only travels 100-200 nm above the coverslip. Near TIRFM can prove important depending on the location of the microinjected molecules and the depth of z-direction illumination desired. The direct excitation from the laser in near TIRFM can selectively excite the fluorophores as well without creating too much autofluorescence due to the oblique exit angle of the beam. This can often lead to higher signal:noise than full TIRFM (Tokunaga, Imamoto et al. 2008).

2.3. Overview: Imaging and microinjection

In addition to the TIRFM setup, there are a number of important components of the microscope that are essential to achieving smFRET detection *in vivo*. These include a an

objective lens made of low autofluoresce materials with high numerical aperture, dualview splitter capable of dividing the fluorescence signal output from the objective into two spectrally resolved bands and an ultra-cooled emCCD camera capable of detecting single photons at a time. Another important part of imaging was maintaining clean solutions as typical room debris can be highly fluorescent under green laser illumination. Solutions of proteins were filtered, coverslips were cleaned extensively and a number of coverslips were tested in order to find the brand with the purest glass. The last essential component of the smFRET setup is the microinjector, which allows precision delivery of dilute amounts of protein while minimally disturbing cells.

2.3.1 Experimental setup

Imaging was performed on a custom built setup centered on an Olympus IX-71 microscope as diagrammed in Figure 2.5. Dye-labeled molecules are excited by a 7 mW, 532 nm laser line within the cell in epifluorescent mode and the signal passes back through the objective onto a Photometrics Dualview. The Dualview splits the fluorescence into donor and acceptor spectral ranges using a Chroma 645dcxr beamsplitter and filters the individual channels using an HQ585/70m for the donor and HQ700/75m for the acceptor. This spectral filtering is ideal for the emission spectra of Alexa 555 and 647 or Cy3 and Cy5. Signal was then passed onto a Roper Scientific Cascade 512:B electron-multiplying charge-coupled device (emCCD) camera capable of detecting the sparse fluorescence signal from single molecules. The result is a split of the same image in two different spectral bands on a computer screen. I also used a differential interference contrast (DIC) device mounted above the sample to locate cells and take brightfield images before fluorescence analysis.

As typical photon collection rates by high numerical aperture microscope objectives from single molecules are limited (Ram, Ward et al. 2006), an emCCD camera was used to overcome the many sources of noise. These include the read noise, dark current and the photon shot noise inherent to light detection. Read noise, which derives from the analog to digital signal conversion, is negligible at millisecond exposures when on-chip gain is used in these cameras (O'Grady 2006). This comes at the cost of an amplification noise factor inherent to emCCDs, which increases the inherent shot noise by a factor of 1.4 (Andor-plc 2010). The cooling in the camera reduces the dark noise—derived from heat energy in the silicon lattice that makes up the CCD (Andor-plc 2010)—to 1 electron per pixel per s (Cascade 512:B manual), which is negligible. Therefore, camera-derived noise in the signal I measure from the tens of detected photons from each single molecule is almost wholly due to shot noise, which comes out to the square root of the number of photons times the amplification noise factor.

Cultured cells were grown on round glass coverslips. These were placed in a Bioscience Tools heated imaging chamber. This consists of a circular metal tray that holds the coverslip around the edge, an O-ring about the same perimeter as the coverslip and a metal clasp that puts enough force on the O-ring to create a seal in order to hold media during imaging. Cells were heated from an electric power supply with a metal ring that fits around the cover slip tray. I found cells kept in media close to 37 ºC had lower autofluorescence (Figure 2.7) and maintained a healthy phenotype on the microscope for much longer. Unhealthy cells likely autofluoresce due to increased production of endogenously fluorescent molecules (Zipfel, Williams et al. 2003).

An Eppendorf Femtojet microinjector was used to inject sample into cells. The microinjector arm is mounted on the microscope stage at an angle high enough to enter the culture dish unimpeded. Details on microinjection strategies and parameters are in section **2.3.3**.

Low autofluorescence oil from Olympus (IMMOIL-F30CC) was another important component of the setup. Using oil with an index of refraction close to glass is important to avoid aberrations in imaging as the oil bridges the gap between the objective lens and the coverslip. I found this oil to have notably less autofluorescence under green laser illumination than other brands in comparison tests.

Sequences of images were taken every 100ms using custom acquisition software programmed in C. Only molecules localizing in place could be imaged at this resolution, as diffusing soluble molecules appear blurred at these exposures (although stopped motion imaging can be used to image such molecules (Xie, Yu et al. 2006)). smFRET could be imaged within cells for tens of seconds after injection despite constant illumination as fluorescent protein would often come in focus from the bulk of the unilluminated cell. Those fluorescent molecules constantly excited by the laser could last on the order of many seconds, as shown by the sample traces in Figures 3.1-3.3. However, many proteins would bind and unbind, yielding only brief FRET signal.

2.3.2 Backgrounds of glass coverslips

The autofluorescence of glass by the green laser illumination is a major impediment to epifluorescence imaging as the excitation and fluorescence emission must cross through the coverslip. Impurities within the glass seem to be the major source of this

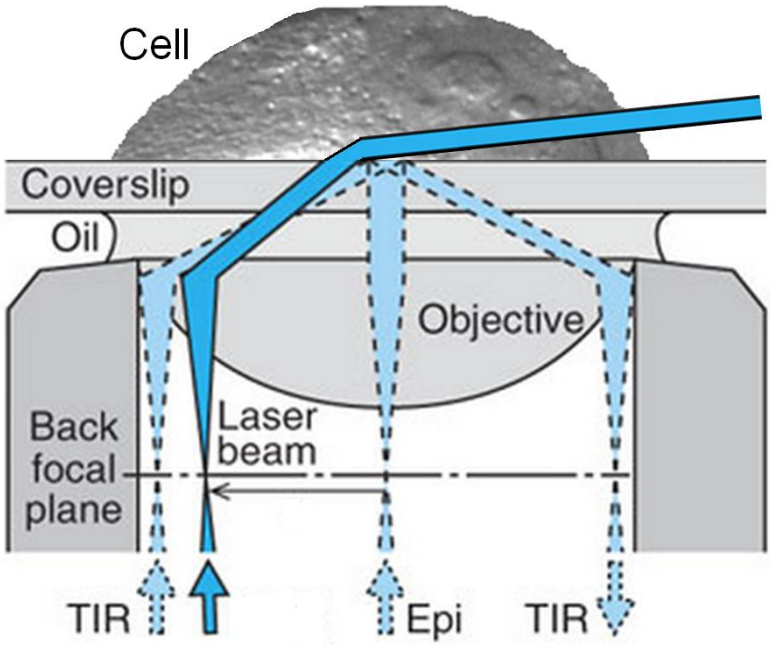

Figure 2.5

Diagram of illumination in near-TIRFM mode. Offset of the illumination beam through the objective slightly away from TIRFM allows the beam to cross through the cell and only illuminate a thin slice. Image modified from (Tokunaga, Imamoto et al. 2008).

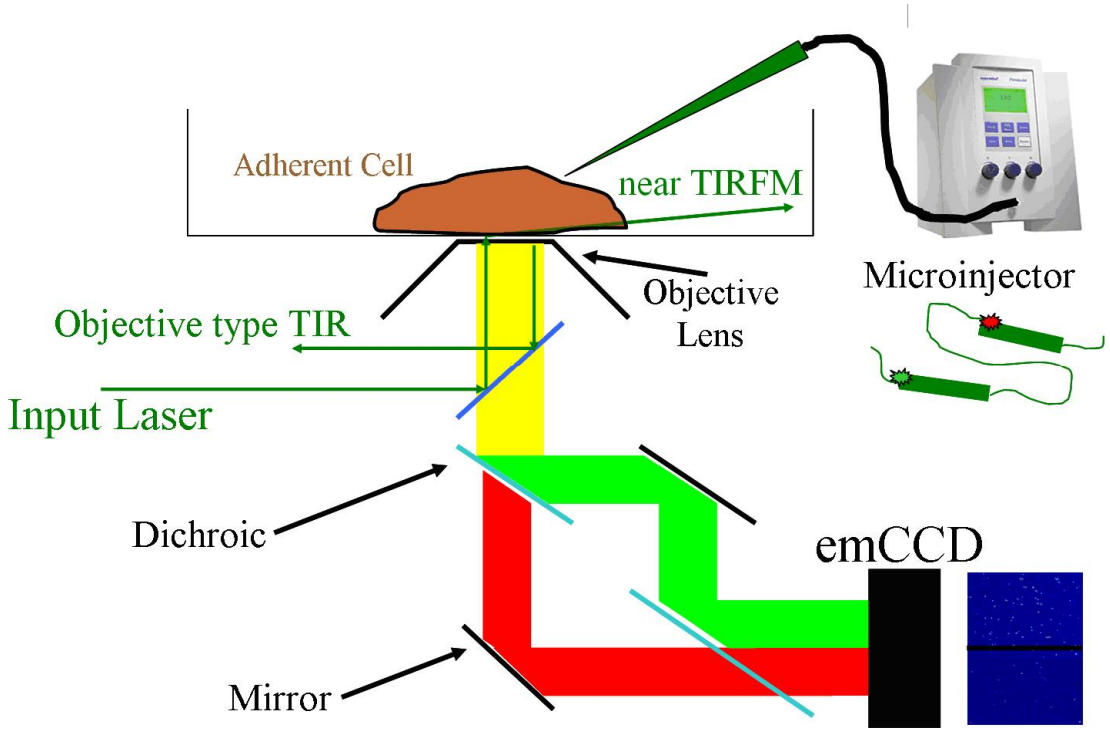

Figure 2.6

Schematic of basic live cell smFRET experimental setup.

autofluorescence, as different types of glass (german glass, soda lime, etc.) did not seem to give more or less background. I tried imaging with VWR, Bellco, Electron Microscopy Sciences and Fisherbrand #1.5 glass coverslips. Of these, Fisherbrand, which is made by Erie Scientific (25CIRCLE#1.5D), had the lowest fluorescence background.

Extensive cleaning of coverslips was also essential to eliminating background. Coverslips were briefly exposed to a propane torch flame to remove oil and then sonicated for 15 minutes each in a sequence of acetone, ethanol, potassium hydroxide and deionized water. After many rinses in deionized water, coverslips were autoclaved for use with cell culture. The PC-12 cultured cell line required poly-L-lysine (PLL, Sigma P1274) for growth on glass, which was added to the coverslips at .1 mg mL^{-1} for >1 hour and then rinsed off >5x with de-ionized water to remove excess. PLL did not alter the background fluorescence of the glass. I also attempted to use fused quartz (pure silica) coverslips due to their relatively low autofluorescence under green laser illumination. The relative background intensity difference between glass and quartz coverslips was notable as shown in Figure 2.7. Unfortunately, silica has a lower index of refraction than glass that causes spherical aberrations in the image (Friedman, Chung et al. 2006). This increases the point spread function of the single molecule, thereby increasing the amount of accumulated noise over the greater area measured. While the position of the optics can be altered to accommodate for the different index of refraction for quartz versus glass (Friedman, Chung et al. 2006), the objectives are designed for use with glass coverslips, making epifluorescence imaging through quartz problematic (Private communication, Nick George, Olympus, Pennsylvania). As a result, while I was able to see smFRET signal on quartz coverslips, I found higher signal: noise with glass coverslips.

2.3.3 Microinjection

I used an Eppendorf Femtojet microinjector to insert dye-labeled recombinant protein into cells. The microinjector uses detachable glass capillaries with .5 µm inner diameter tips capable of gently piercing the cell membrane and delivering contents via slight back pressure without harming the cell. I pipetted the various proteins into the back end of the capillary for each separate experiment at concentrations ranging from 10-100 nM in 50 mM Tris, 150 mM NaCl (ph 7.4), 1 mM DTT except for SNAP-29, which was injected in this buffer including 50-75 mM urea remaining after dilution from stock containing high amounts to maintain protein stability. Proteins were generally pure and devoid of aggregates after purification preparations. However, unfrozen or particularly concentrated protein was sometimes filtered through a .2 µm microcentrifuge filter membrane to ensure it did not clog the microinjector tip. Upon injection protein rapidly diffused outward from the tip insertion point as can be seen in videos online (http://www.nature.com/nmeth/journal/v7/n3/suppinfo/nmeth.1421_S1.html).

The amount of protein injected is not precisely known; however, I calculated the injection volume to be close to 10% of the cell volume by comparing the total fluorescence intensity of cells injected with ~125 nM of SN25CC in epifluorescent imaging mode with single molecules from the same injection in TIRFM mode. However, I expect this to be an overestimate based on my calculations below.

The background-subtracted intensity (using the average intensities of the cell under laser illumination before injection) for each pixel in the center of a cell injected with 125 nM SN25CC in epifluorescent imaging mode was 3660. As the area of the cell is about (50x50)

μm^2 and the area of each pixel is (.27x.27) μm^2, a cell covers 185x185=34,000 pixels. The background-subtracted intensity for a single molecule was about 500 in each pixel on an area dominated by 4 pixels. The integrated signal from a single molecule is thus 2000. Therefore, I estimate I injected (34,000*3660)/2000 molecules per cell, which is 63,000 SN25CC proteins. Since I injected with 250 nM of labeled protein, I can use the number of molecules to estimate the volume of the protein solution injected to be 4.2E-13 L. As the cell is expected to be 5 µm in height (Sato, Nagayama et al. 2000), the volume of the cell is estimated at 1.3E-11 L, making the injection volume 3% of the total cell volume.

I expect this might be an upper limit on the injection volume as I only measured in areas with uniform fluorescence while in epifluorescent mode. Areas such as the nucleus (where I have observed protein will not enter unless directly microinjected inside) did not have such uniform fluorescence, meaning the assumption that the whole area of the cell had an intensity near 3660 is an overestimate. Previous works have cited similar equipment injecting in the range of tens to hundreds of femtoliters (Capecchi 1980; Seeley, Keith et al. 1983) while my injection estimate is about 400 femtoliters. Therefore, I expect injection volume of BS-C-1 cells was likely somewhere between to 1-5% of the cell, with the test data given above closer to the 10% range as a particularly well-injected cell was used to measure this data.

PC-12 cells were injected in a similar manner but with lower protein concentration and less backpressure in order to inject less liquid into these smaller volume cells. Previous work has found viability of PC-12 cells to be around 80% with an injection volume 30% of the cell volume (Seeley, Keith et al. 1983). I expect an injection volume well less than this

value as I found injections of PC-12 required sufficiently low concentrations to image single proteins.

I do not anticipate the amount of protein I added altering the biological relevance of my results. My method required sufficiently low concentrations to image individual proteins. In comparison, bulk studies that required concentrations high enough to measure SNARE complex formation using fluorescence signal throughout the cell still found relevant biological data (An and Almers 2004). While this bulk work was able to find a ceiling at which additional expressed protein no longer had an effect on the cell, our single molecule observations were done with less injected protein than their lowest concentration measurements. Therefore, it is unlikely that exogenously added protein at the levels we used was anywhere near a biologically effective ceiling. Further, injections of SN25CC mixed with either 100x molar synaptobrevin, 50x molar SNAP-25 wild type or 200x molar SNAP-25 all displayed complex formation despite the abundance of competing protein. The similarity of the results in these injections is discussed further in section 3.4.3.
Clogging of the microinjector tip was common, likely a result of protein from within the imaging media or the tip aggregating or drying. In order to avoid the latter, when the microinjector tip was not in use it was kept at a height well out of range of the laser to avoid photobleaching the sample but still within the media. In addition, a very slight back pressure was maintained on the tip at all times as flow was necessary to avoid clogging and keeping imaging media from entering the tip. The small amount of fluorescent protein leaking into solution was largely irrelevant for data acquisition as protein can not penetrate the cell membrane on its own and imaging was done deep within the cell.

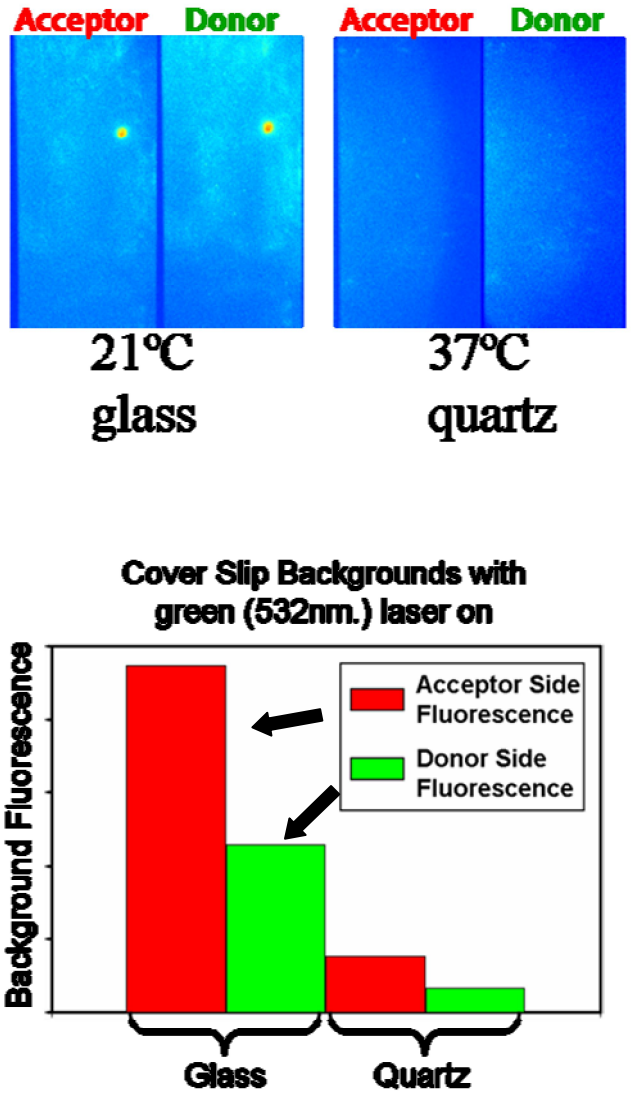

Figure 2.7

Images of autofluorescent background from cells and coverslips. (Top) Dualview fluorescent images of cells under green illumination. Background fluorescence is notably lower for cells grown on quartz coverslips and maintained at 37 °C on the microscope. (Bottom) Background fluorescence of bare coverslips under green laser illumination. Autofluorescence is notably lower for quartz coverslips, particularly in the acceptor channel (Friedman, Chung et al. 2006).

I selected cells to microinject based upon their flat, isolated appearance in the brightfield DIC image along with relatively low autofluorescence under green laser illumination in comparison to other cells. I would often inject cells while under DIC illumination to ensure proper filling and then would turn the lamp off and turn the green laser on 2-5 seconds after injection. However, once I became experienced with the microinjector, successful, non-invasive filling of the cell became highly probable and I was able to do this while under only green laser illumination (Figure 2.8, top). This allowed me to avoid the 2-5 second delay before imaging and instantly view the fluorescent proteins upon injection.

Direct viewing during injection became important as protein injected into a specific area remains at a localized high concentration for only a short time and I found binding times for proteins to be on the scale of hundreds of milliseconds (see section **3.4.3** for binding time data and section **3.5.5** for biological implications). After all microinjections and subsequent imaging was complete, I took DIC images of the cells to verify cell morphology—a good determinant of cell health—was not affected by the microinjector or laser illumination (Figure 2.8, bottom). I was also able to show these potentially harmful phenomena did not measurably impact the biological significance of the study by measuring *in vivo* smFRET data before and after continuous laser illumination and multiple microinjections as described in section **3.3.5**.

In full TIRFM mode the microinjector tip is invisible as the evanescent wave travels at most 200 nm above the coverslip and microinjection is designed to take place on top of the cells, which are about 5000 nm in height (Sato, Nagayama et al. 2000). The microinjector tip was largely invisible in near TIRFM mode as well so long as the laser coming out of the cell

was angled in the opposite direction as the microinjector tip (in the case of Figure 2.6, the laser would exit to the left).

2.4. Overview: Cell culture and media additives

Two different cultured cell types were used in my experiments. BS-C-1 cells, derived from monkey kidneys, and PC-12 cells, derived from rat brains, were used due to the differential protein expression expected from their respective tissue type. Imaging within cultured cells was tricky due to autofluorescence, making cell culture techniques and health of the cells on the microscope important for success. I also was able to extend the life of dyes, which photobleach quickly under powerful laser illumination within high-oxygen environments like cells, by using a combination of antioxidants and triplet state quenchers. I proved the utility of these additives by injecting polystyrene beads labeled with many Alexa 647 dyes (the acceptor fluorophore used in all experiments) into cells and measuring photobleaching rates.

2.4.1 Cell types and culture

The primary cell type used in experiments for *in vivo* smFRET imaging was BS-C-1, a line that originates from African green monkey kidney epithelium (Hopps, Tjio et al. 1963). These cells are large, grow quickly to confluence and maintain a flat morphology, making them ideal for easy microinjection and TIRFM imaging (Figure 2.8, top).

A second cell type used in experiments were PC-12 cells, a line derived from a rat adrenal pheochromocytoma (Greene and Tischler 1976). These cells have a more ball-like

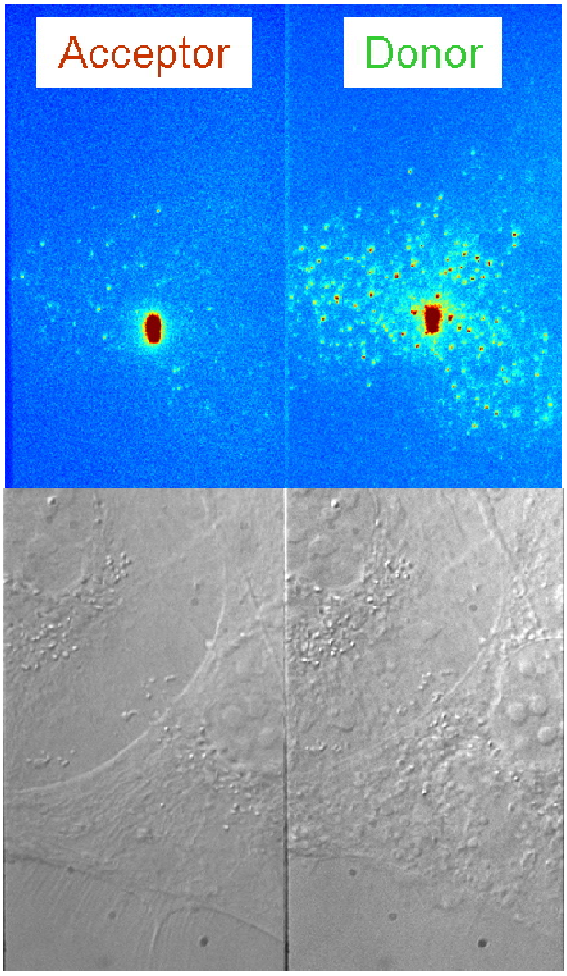

Figure 2.8

Example of smFRET imaging after injection of SN25CC into a BS-C-1 cell during green laser illumination. The left shows the acceptor channel (selected for Alexa 647 emission) and the right shows the donor channel (selected for Alexa 555 emission). Points of light on the top left represent single molecule FRET while points of light on the right are directly excited donors. The bottom left image is the DIC image taken before microinjection while the bottom right image was taken post-injection to show the lack of perturbation from microinjection and illumination of the cell. The bright spot in the center of the fluorescence image is the microinjector tip, which is viewable in near-TIRFM mode. The fluorescence image was taken from 500-600ms after the beginning of the injection. Each of the four channels is 68 µm wide and 107 µm tall.

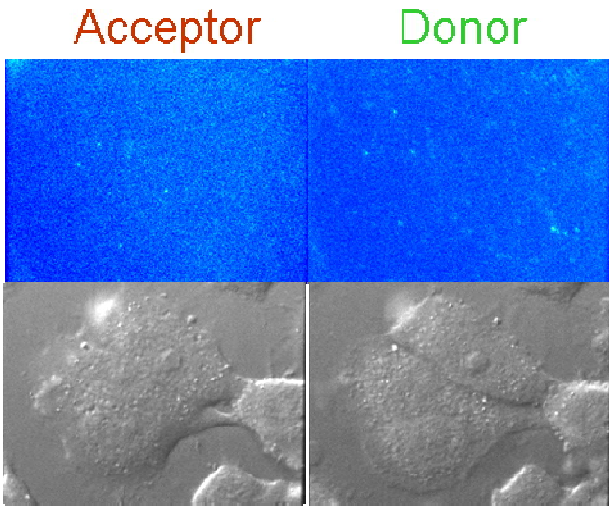

Figure 2.9

Example of smFRET imaging after injection of SN29NN into a PC-12 cell during green laser illumination using the same emission channels as in Figure 2.8. However, this image is from an injection in full TIRFM mode as opposed to the near-TIRFM imaging used during that injection. Four clear, bright smFRET events can be seen in the acceptor channel. The bottom left and bottom right DIC images are the same areas in the fluorescence image taken before and after the data acquisition. These brightfield images show minimal perturbation of the cell. Each of the four channels is 68 µm wide and 36 µm tall.

appearance than BS-C-1 with a smaller area and greater growth in the z-direction. The smaller size makes finding an ideal flat area for imaging difficult to find. PC-12 cells are largely used for their ability to differentiate and form neurites after addition of nerve growth factor. As I did not find an appreciable difference in the binding and conformation of my proteins using smFRET analysis within PC-12 and differentiated PC-12 cells, I only performed thorough data analysis on smFRET in undifferentiated PC-12 cells. However, attention to SNARE protein conformational state in the neuronal projections of differentiated PC-12 cells versus the cell body was out of the spectrum of this work, and could provide interesting results concerning localized SNARE protein expression and activity as these proteins are expected to be more active at sites of membrane fusion such as the presynaptic ends of neurons. As it is, I found similar results in PC-12 and BS-C-1 cells, indicative of the promiscuity of SNAREs between different tissue types. Evidence for this and the implications for SNARE biology are presented in chapter **3**.

Both cell types were grown using standard cell culture methods (Hopps, Tjio et al. 1963; Greene and Tischler 1976). Briefly, BS-C-1 cells were grown to ~80% confluency on coverslips in modified Eagle medium (DMEM) with 10% heat-inactivated fetal bovine serum (FBS) and 1% gentomycin. PC-12 cells were grown to ~50% confluency on coverslips coated with poly-L-lysine in DMEM with 10% horse serum, 5% FBS and 1% pen-strep. Coverslips were cleaned and sterilized as described above and stored in sterilized water. Seed passages were grown on ThermoFisher Nunclon plastic dishes and split every 7-10 days with 75% of the media changed every 2-3 days. All cell culture was done under sterile conditions in a flow-hood and reagents were purchased from HyClone.

To reduce background fluorescence while imaging, at least 2 hours beforehand I changed the cell culture media to 37 ºC fluorescence-free MEM from Gibco with 20mM HEPES and 1% gentomycin. Phenol red, used as a visual pH indicator, is particularly autofluorescent and needs to be removed from the media around the cells. Media was changed a second time directly before imaging to remove any residual phenol red. All imaging media also had Trolox from Sigma and cyclooctatetraene (COT) from Alfa Aesar added to the imaging media at least 12 hours before incubation with cells. These were added to extend the time until photobleach of dyes, as explained in section **2.4.3**.

2.4.2 Imaging in cultured cells

Imaging single fluorophores *in vivo* requires overcoming a great deal of cellular autofluorescence from such molecules as flavins and flavoproteins between 400-600 nm (Aubin 1979; Benson, Meyer et al. 1979). This background signal is dependent on cell health, cell type and growth conditions. I found BS-C-1 cells grown in DMEM and switched to fluorescence-free DMEM (without phenol red) from Gibco at least an hour before imaging had particularly low autofluorescent signal. These cells maintained low autofluorescence for many minutes on the microscope when kept at 37 ºC while imaging. Imaging for greater than 30 minutes was not typically done as evaporation of media would begin to compromise cell health as indicated by cells changing in morphology and detaching from the coverslip.

PC-12 cells were notably harder to image within, largely because of their greater thickness in the z-direction, which creates more volume for endogenous autofluorescent intracellular molecules to interact with the laser. This was not a problem in full TIRFM mode, but as explained above, near-TIRFM was often preferred for locating and exciting

single molecules desired for imaging. As a result, injected protein in BS-C-1 cells was typically imaged in near-TIRFM mode while in PC-12 cells full TIRFM was more likely. This is evident when comparing Figure 2.8 and 2.9, as the former shows an injection in near-TIRFM mode—evidenced by the laser interacting with the microinjector tip—while the latter shows an injection in full TIRFM where less of the cellular background is visible but only a few molecules are viewable within the thin excitation layer of the evanescent wave. Videos of these injections can be seen online at: http://www.nature.com/nmeth/journal/v7/n3/suppinfo/nmeth.1421_S1.html.

An important strategy for employing smFRET *in vivo* was selecting for cells of ideal morphology with low autofluorescence. For example, in the DIC images of Figure 2.9, the PC-12 cells in the center of the image are particularly flat and show low autofluorescence in the acceptor and donor channels as seen by the fluorescent image at the top. However, the cells at the bottom right of the DIC image—that were not injected—show a more rounded morphology with less apparent flat areas. These cells would be notably more difficult to microinject and would be more likely to show autofluorescent signal based on their greater height. As cells can show a surprisingly stochastic level of protein expression (Cai, Friedman et al. 2006), the simple process of sorting through multiple cells for those with potentially lower amounts of the autofluorescent proteins listed above is an important part of achieving smFRET imaging. I estimate of the total BS-C-1 cells visually inspected in a healthy batch, I would find about 10% that I deemed relatively flat with low autofluorescent signal and no encroaching neighbors limiting microinjection. This number was closer to 5% for PC-12 cells. Of the cells in which I attempted microinjection as an experienced user with the microscopy setup properly aligned, I estimate I was able to successfully inject and

measure smFRET in about 25% of them. This number fluctuated largely based on cell type (PC-12 are more difficult to microinject due to their small size), cell health, structural soundness of the microinjector tip and slight microscopic adjustments.

Another potential method of lowering autofluorescence within a cell is photobleaching, in which the laser lowers the background signal after extended illumination. I attempted to avoid photobleaching due to phototoxicity concerns and could often avoid it by coupling the techniques above in a healthy cell. However, cells were often photobleached for 10-60 seconds and some illumination was unavoidable in order to find cells with lower background. In order to test the impact such illumination had on the biology of my system, I microinjected protein into cells and took data before and after 2 minutes of laser illumination (the most that would ever be used) to determine if it changed the smFRET measurements for my proteins. As shown in section **3.3.5**, laser illumination did not seem to alter the biological findings in my system.

2.4.3 Improving dye properties with media additives

One of the biggest obstacles of smFRET *in vivo* is the compromised time until photobleach of dyes (Blow 2008). In particular for my system, Alexa 647 often only fluoresces a few seconds before photobleaching, although Alexa 555 lasts appreciably longer (notice the abundance of donor-Alexa 555 molecules in the right of Figure 2.8 compared to the few acceptor-Alexa 647 molecules on the left). Various media additives were used as a means extending dye life and avoiding unwanted dye states. These additives are used to remove oxygen from the system, which can cause physical breakdown of fluorophores, and avoid transfer of dyes to a triplet state.

The antioxidants Trolox and cyclooctatetraene (COT) were mixed into imaging media at least 12 hours before being added to cells. This time was necessary for Trolox to solubilize within the media while accumulated light was essential for the chemical to reach its active state (Cordes, Vogelsang et al. 2009). While the reduction of oxygen by these 2 antioxidants could have an effect on lengthening time until dye photobleach, they are mostly used as triplet state quenchers (Rasnik, McKinney et al. 2006). A triplet state is a potential relaxation state for an excited electron within a fluorophore that competes with fluorescence emission and traps the dye in a dark state. Avoiding this so-called blinking into and out of dark states enhances quantum efficiency of the dyes and maintains uniform FRET traces (Rasnik, McKinney et al. 2006). A trace with blinking would oscillate between high and low FRET signal and would limit data acquisition. However, I did not see such dark states, which are easily recognizable due to their fast on/off oscillations, in my *in vivo* smFRET traces.

I also tried adding a combination of the chemicals glucose oxidase and catalase to the imaging media to see how it affected dye bleaching within the cell. These enzymes are commonly used *in vitro* to extend dye life by removing oxygen from solution, which in concert with laser excitation effectively destabilizes fluorescent dyes and causes photobleaching (Rasnik, McKinney et al. 2006; Roy, Hohng et al. 2008). They accomplish this by turning glucose and O_2 into gluconic acid and water, which results in a net loss of O_2 in solution. While this system works when the enzymes are in direct contact with the solution, it was not known if less oxygen in the media would have a similar effect within the cell.

To quantify the effect of these chemicals in cells I used fluorescently labeled polystyrene beads. Amino-polystyrene microspheres (0.1 µm; Polysciences) were labeled with NHS-Alexa Fluor 647 per manufacturer's instructions at densities of near 50 dyes per bead. Labeled microspheres were diluted in buffer (50 mM phosphate and 150 mM NaCl (pH 7.4)), placed in a bath sonicator for 15 minutes to avoid aggregation and microinjected into BS-C-1 cells. The beads were brighter than
single dyes and diffused more slowly, which simplified tracking and analysis of photobleaching rates. I measured photobleaching of the microsphere-attached Alexa Fluor 647 inside cells after 4 hour incubation in fluorescence-free medium with a mixture of 2 mM Trolox and .2 mM Cot. For experiments with oxygen scavengers, just before imaging, 240 µg ml-d1 glucose oxidase, 50 µg ml-d1 catalase (both from Sigma) and 2% glucose were added to the medium. Fluorescence of Alexa Fluor 647 was directly excited using objective-type near-TIR with 1.5 mW of 635 nm laser light, observed through a 650 nm long-pass filter and recorded with an emCCD. The beads were tracked in the 10 Hz movies by custom Matlab software, background subtracted intensity timecourses were extracted and the decay of the fluorescence intensity was fit to single exponentials as shown in the inset of Figure 2.10. The average of the time constants for multiple tracked beads in several cells with various combinations of additives is plotted in Figure 2.10.
The antioxidants Trolox and Cot negligibly extended dye lifetimes on their own, while the oxygen scavenging system of glucose oxidase and catalase showed a strong improvement. The combination of these additives (right) had the longest time constant of all—improving the dye lifetime by a factor of four. Background-corrected intensity time courses were fit to an exponential decay function ($e^{-t/tJ}$; inset) and resulting time constants (t$\emptyset$) were averaged over

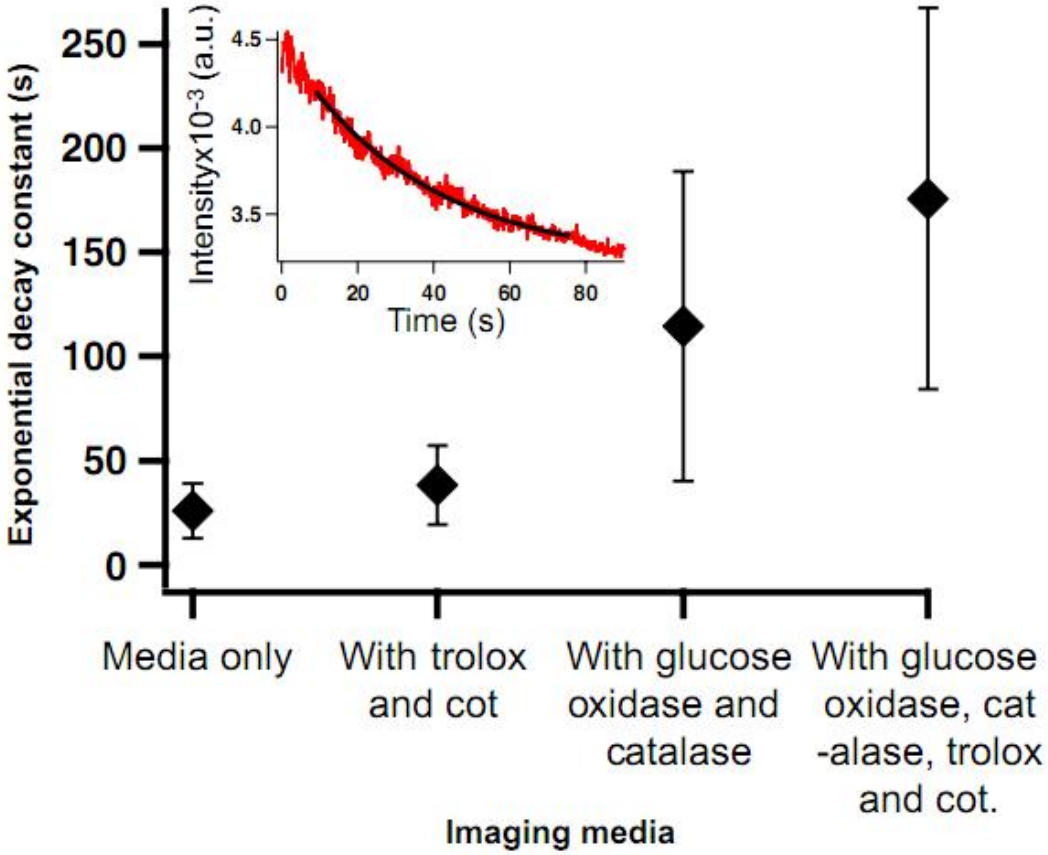

Figure 2.10

Effect of various additives to photobleaching time *in vivo*. Inset: example of single, tracked bead as the dye molecules photobleach over time. The graph is fit with a single exponential.

multiple tracked beads (N=47, 80, 19 and 27 left to right on graph). Error bars show one standard deviation of the average. The inset of Figure 2.10 is an example of a raw (not background subtracted) intensity time course for a tracked bead as it diffused in a cell. Success of bead injection was shown by slow diffusion of the bead within the cell, as beads outside the cell diffuse at an appreciably faster rate.

2.5. Step by step process of data acquisition

Here I summarize the typical sequence of steps necessary for smFRET data acquisition. I assume that dye-labeled protein is already prepared, the TIRFM system is properly aligned and cultured cells are at proper confluence on coverslips as described above.

- **Change the growth media of the cells to imaging media with Trolox and Cot at least one hour (but preferably 4-12 hours) before experiments.** Cells should be washed to ensure all growth media is removed by gently adding warmed imaging media (or ringer buffer) before final imaging media as even small amounts of phenol red will cause noticeable cellular autofluorescence. Imaging media should be made the night before for proper solubilization of Trolox and left under lights for Trolox to fully reach antioxidant potential. It is also possible to solubilize Trolox by shaking in heated media under more intense light (see (Cordes, Vogelsang et al. 2009) for more information) for about an hour.
- **Turn the emCCD and laser on at least 15 minutes before data acquisition.** The emCCD camera is ultra-cooled and needs time to cool down so signal is stable. Some lasers require time to reach stable power levels.

• **Pipette dilute protein into microinjector tip.** It is important not to do this too long before having the cells on the microscope, as the tip will often dry out and clog if not kept in solution. As described below, once the imaging chamber was on the microscope I would keep the tip in the media off to the side at all times to maintain flow conditions. I prefer setting up the microinjector before placing the cells on the microscope as there is a limited time window for healthy cells as described in the next step.

• **Place coverslip with cells in imaging chamber and add at least 2mL prewarmed media before placing on heated microscope stage.** As the imaging chamber is kept at 37 ºC on the microscope and open to air for microinjection evaporation becomes an issue. I occasionally changed the imaging media while the chamber was on the microscope, but this is difficult to do without disturbing cells. More frequently I would have multiple coverslips of cells ready and use each for a maximum of 30 minutes. Changes in pH from a lack of CO_2 (cultured cells in this study were grown in typical 5% CO_2), localized temperature fluctuations and evaporating water all likely contribute to this limit.

• **Align the microinjector tip such that it stays tens of micrometers above the cell top.** While microinjection can be system-dependent, I found keeping multiple set points with the Femtojet to be important. In this way, the tip could be moved to a set location in solution but out of the way of stray laser illumination when searching for cells. A second set point was kept tens of micrometers above the cell for active microinjection. I generally selected the final microinjection height by placing the tip next to a cell and gently moving the tip in the x-y plane to touch the side of the cell at the highest point in which it was still possible to touch the cell. Injecting into the top of the cell is essential

for minimal perturbation, as the tip can physically alter the shape of the cell or even pull it off the plate if it travels too far inside.

• **Inspect cells in brightfield DIC mode to find ideal areas for microinjection.** Flatter areas are easier to microinject and tend to have more uniform background autofluorescence.

• **Turn brightfield off and laser on to briefly inspect background of cell.** There was a high variability in autofluorescence backgrounds for both cells types used and selecting the right cell was important. If cellular background is prohibitively large, this autofluorescence can be bleached by laser illumination. As there are potential concerns with phototoxicity this was not the ideal method of data acquisition and could often be avoided with healthy cells in proper media. However, cells were often photobleached for 10-60 seconds and some illumination was unavoidable in order to find cells with lower background. I show in section **3.3.5** how laser illumination did not alter the biological findings in my system. Testing how phototoxicity alters the biological system of study in such a way is an important control for any live cell study.

• **Turn laser off and brightfield on to center cell for microinjection and take DIC image.** Knowing the location of injection can be important for a number of biological reasons. This last DIC view also allows centering of the microinjector tip on a flat area within the cell.

• **Inject cell**. This was done in one of two ways. In the beginning I injected cells with the DIC imaging on to ensure successful injection. This can be evidenced by piercing of the membrane and often a temporary bulge within the cell. As I became more experienced, I was able to microinject without the aid of brightfield imaging. In this case,

I would start recording data, open the laser shutter and then microinject all in less than a second. Successful injection is evident from the pulse of fluorescence staying within the outline of the cell body. This is particularly evident on the donor side as Alexa 555 lasts longer than Alexa 647 in my experiments, as seen in the top right of Figure 2.8. This proved important, as the most protein binding is seen when protein is still localized around the injection point before it diffuses into the bulk of the cell. Before injecting in this manner, I would usually take a quick couple second movie of the cell under only green laser illumination to record the cellular background before injection.

- **Inject cell again if desired.** If good signal was measured after a successful injection, I often found injecting a second time tens of seconds later would be equally successful. This method of double injection was also useful in a number of tests, such as the results shown in **3.3.5**.
- **Turn laser off and take a second DIC image of the cell post-microinjection.** Visual inspection is important for showing the cell was unaffected by injection as shown in the before and after DIC image of Figure 2.8. Data was not used if cells looked largely different in the before and after pictures as this is an indication of a compromised cell. Frequently the microinjector tip would disturb the cell enough to move it completely away from the injection site, obscuring data and often injecting protein onto bare glass. Such nonspecific binding could cause the protein to take any shape and even create false smFRET signal if the dyes happen to be close enough together, proving the importance of controlling microinjection.
- **Find a new cell out of the illumination range of the previous one.** As neighbors of the previous cell are likely to have received many seconds of laser illumination it is

necessary to move at least far enough away from the effective beam area of the previous attempt (~200 µm).

- **Stop taking data when cells begin to ball up and lift off coverslip.** As described above, this happened in my system after about 30 minutes, although sometimes cells could stay healthy for up to an hour. Unhealthy cells are harder to microinject, tend to have higher autofluorescence and provide a less biologically applicable environment.

Chapter 3. Results and Discussion

3.1 Overview: Data Analysis

I wrote custom software written in Matlab to analyze movies of data. I measured smFRET signal of many molecules by automating the process of locating particles that met a certain intensity threshold in the acceptor or donor channels and extracting traces of data over time. I confirmed such traces were of single molecules by measuring single drops and rises in intensity to and from background levels. Accumulating the data from these traces allowed me to quantify the FRET signal for different proteins microinjected into different cell types *in vivo*.

3.1.1 Data extraction

Points of light were localized in either the donor or acceptor channels of the movies by requiring the mean intensity of 9 pixel areas to be 3–8 times above the standard deviation of the background. The threshold was adjusted on a cell-by-cell basis for reliable identification and verified by eye. The identified spots were mapped to the complementary donor or acceptor channel, background was subtracted (calculated pixel by pixel using the mean value of the 16 pixels surrounding a 3x3 pixel region of interest) and intensity timecourses were extracted.

Single molecules were confirmed by the emission levels as well as single-step transitions at the beginning and end of events as shown for the two intensity traces in Figure 3.1. The presence of anticorrelated intensity jumps of the donor and acceptor intensities, where the acceptor dye emission vanishes owing to bleaching and the donor dye emission

rises simultaneously, confirmed smFRET interactions. An example of anticorrelation is shown in the top of Figure 3.1, with sequences of images used for this trace shown in Figure 3.2. Different kinds of smFRET traces are described in detail below in section **3.2** while many more examples are shown in Figure 3.3.

3.1.2 %highFRET

To compare the efficiency of generating high smFRET events across different proteins and different injections of multiple cells, I measured the percentage of high FRET events (%highFRET). This was done to normalize high acceptor emission events to the total single molecules imaged per cell as precise injection efficiencies—and therefore intracellular concentrations of proteins—varied. %highFRET is defined as the number of high FRET events (#highFRET, FRET > 0.7) divided by the sum of #highFRET and low FRET (#donorOnly, FRET < 0.7) events (%highFRET = 100 × #highFRET / (#highFRET + #donorOnly)) for each of the first ten frames after an injection during a 10 Hz movie. Those ten values of %highFRET accumulated for
around ten cells were assembled into histograms for the different combinations of proteins and cells used (Figure 3.5-3.7). The averages of these datasets are compared in
Table 3.1. This quantity represents the amount of high FRET resulting from SNARE complex formation relative to the total amount of protein injected. Details of more advanced analysis on single-particle tracking and residence time analyses are explained in section **3.4**.

3.2 Overview: Proof of method and data accumulation

As measuring the conformation of a single protein using smFRET has not previously been achieved within a cell it was important to prove the efficacy of this method. To do this, I had to achieve signal: noise high enough to image an acceptor and a donor dye above the noisy background of a cell. Therefore, initially proving the method required me to measure the background-subtracted intensities of single spots in both spectral channels and find signal characteristic of FRET within the traces. After initially achieving this step, I began to accumulate the smFRET values into FRET histograms to determine if the value *in vivo* is close to that expected for my protein constructs. Upon proving a consistent high FRET as expected for my constructs, I then started measuring the percentage of located molecules that gave high FRET signal (%highFRET) to get an idea of how the different proteins acted within the two cell types studied. The accumulation of this data began to tell me interesting things about the conformational biology of SNAREs.

3.2.1 Examples of data traces

Two examples of traces taken from single dual-labeled proteins injected into a cell and imaged in the acceptor and donor channels are shown in Figure 3.1. Both of these are SN25CC (see Figure 2.1 for a reminder of the protein constructs) injected into BS-C-1 cells, as shown in Figure 2.8.

The top trace is referred to as an anticorrelated FRET trace, and is an indication of FRET signal from a single donor and single acceptor pair. In this trace, in which there is only green laser illumination that can only excite the donor molecule, the initial signal comes from the acceptor, indicating FRET from an excited donor to the acceptor. Using Equation

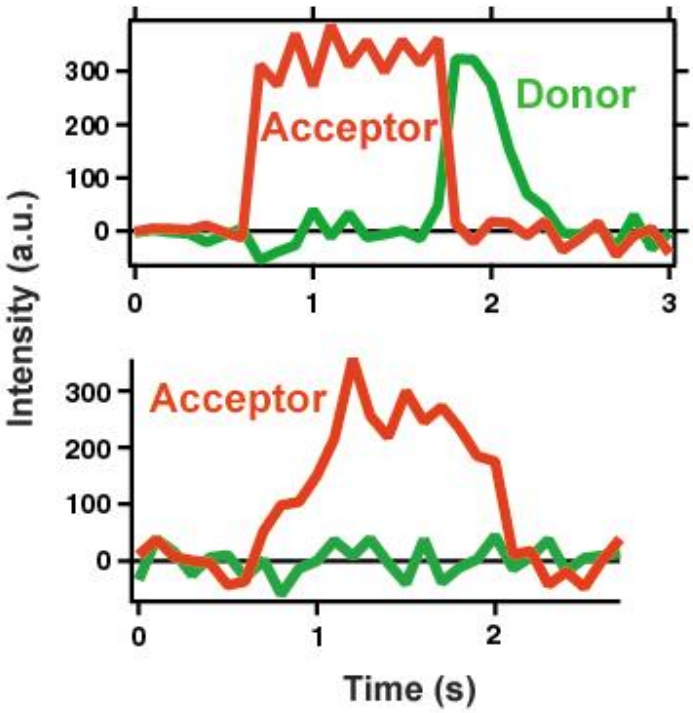

Figure 3.1

Example traces of two different kinds of smFRET events, an anticorrelated trace (top) and a transient binding trace (bottom). Both are from SN25CC injected in BS-C-1 cells with green laser illumination.

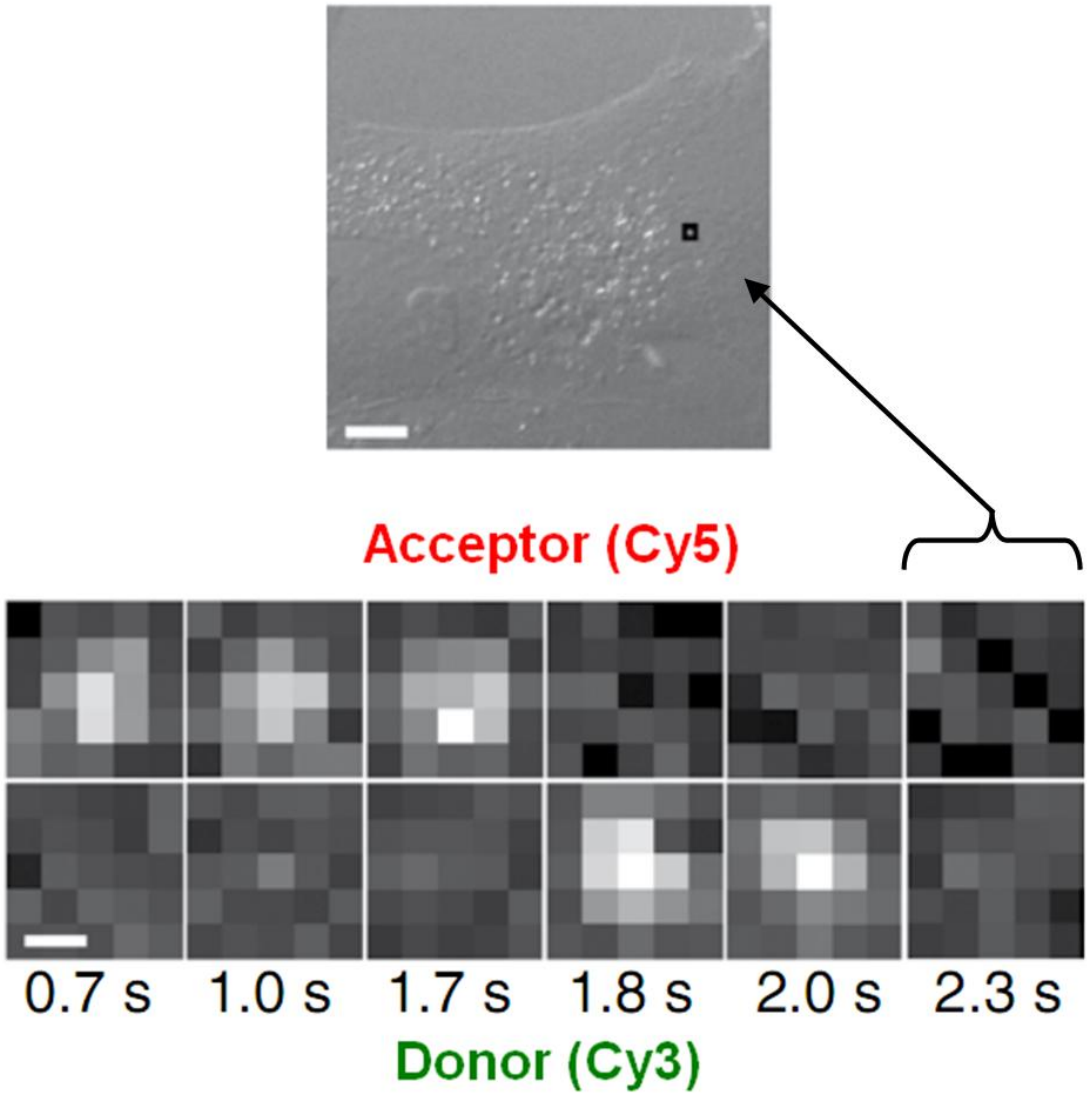

Figure 3.2

Screen shots of the same anticorrelated smFRET event shown in the top of Figure 3.1. The square on the DIC image of the cell above indicates the location shown in the boxes below. Each of the adjoining top and bottom squares is the same region imaged within different spectral bands for the two dyes. The scale bar in the DIC image is 10 µm, the scale bar in the fluorescence image represents .5 µm.

1.1, it is clear that the FRET that is seen from .7 to 1.8 seconds is close to 1, making it high FRET. This is an indication that the SN25CC protein has found its binding partners and folded into SNARE complex, therefore bringing the 2 dyes into close apposition such that they give off this high FRET signal. At about 1.8 seconds, the acceptor signal goes to background in one 100 ms frame, which is referred to as a single step photobleach. This is indicative of there only being a single acceptor molecule. As the acceptor photobleaches, the donor molecule can no longer releases its energy through transfer to the acceptor and begins to radiate fluorescence as a regular dipole in space. Then, at a little after 2 seconds, the donor molecule intensity drops to zero

However, many high smFRET events did not show this anticorrelation. Commonly, high acceptor emission would commence and end abruptly without donor emission, as shown in the bottoms of Figure 3.1 and Figure 3.3. Because the acceptor bleached faster than the donor in my system, this observation suggests fast SNAP-25 and SNAP-29 binding and unbinding. Characterization of binding times is described in section **3.4.3**. Molecules with low FRET emission, where only the donor molecule shows a single step rise in intensity, are indicative of membrane localization without SNARE complex formation. Such localized proteins did not typically show such transient binding as seen for smFRET events.

3.2.2 Histogram of FRET values

A FRET histogram (Figure 3.4) for single-molecule events occurring in the injection shown in Figure 2.8 of SN25CC in BS-C-1 cells was assembled by accumulating the average FRET emission level for each molecule detected within 0.2 s (FRET < 0.5) and 1.0 s (FRET

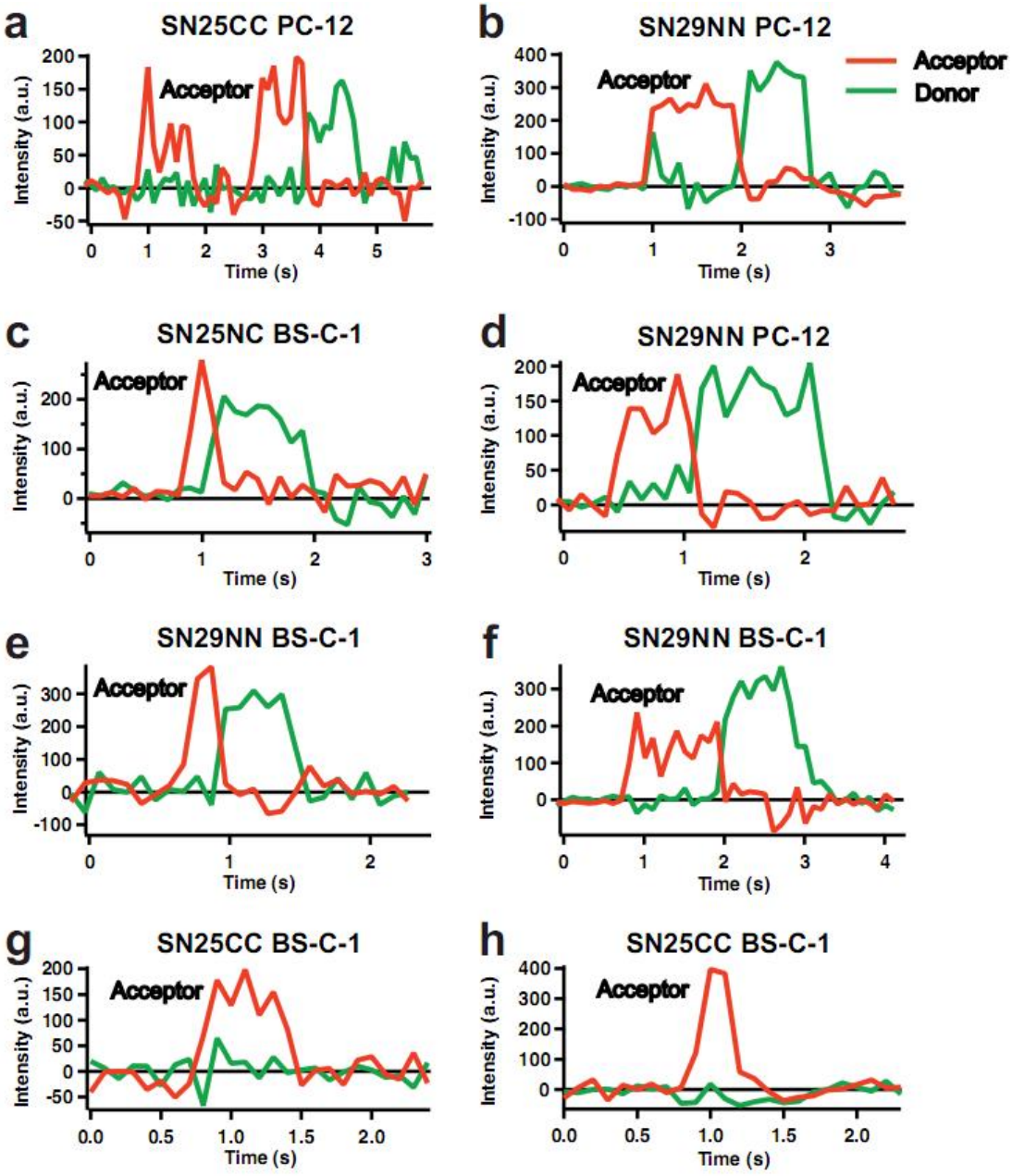

Figure 3.3

Additional examples of smFRET intensity traces.

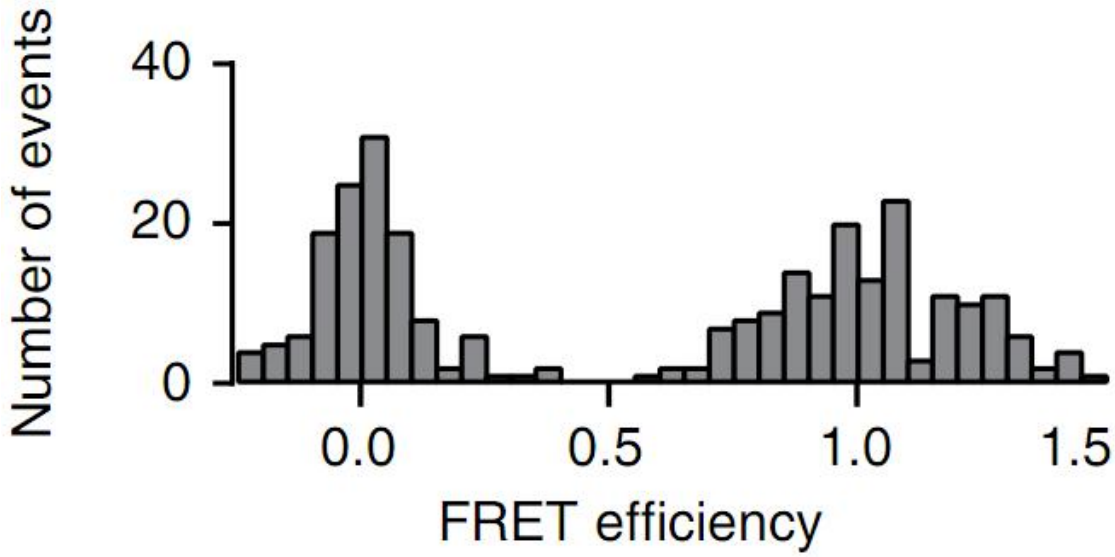

Figure 3.4

FRET histogram for the same SN25CC injection in a BS-C-1 cell shown in Figure 2.8. FRET signal measured for each individual molecule imaged over the course of the movie was averaged and accumulated into a histogram. High FRET events (FRET>.5) were accumulated for .2 seconds and low FRET events (FRET<.5) were accumulated for 1 second to sufficiently populate both peaks. The low FRET peak is narrower due to the higher signal: noise of the donor molecule.

> 0.5) after injection. The different duty cycles yielded sufficient populations in both peaks. This FRET efficiency histogram was consistent with expectations from the structure of the SNARE complex as described in section **2.1** and shown in Figures 2.1-2.2. Correcting the areas under the two Gaussian-shaped peaks near FRET efficiencies of 0 and 1 by the duty cycle of detection yielded %highFRET for this cell to be 22%, consistent with the value reported in Table 3.1 for many more cells.

3.2.3 Histograms of %highFRET

%highFRET, which details how many of the single proteins imaged is in a high FRET state and therefore forming SNARE complex, was accumulated as a means of measuring protein conformational differences in different cells. The dual-labeled proteins SN25CC, SN29NN and SN25NC were microinjected into both BS-C-1 and PC-12 cells and histograms of the number of high FRET events imaged over multiple cells were created. Figure 3.5 shows the results for the three protein constructs in BS-C-1 cells. While SN25CC and SN29NN are expected to yield high FRET signal, it was unknown whether SN25NC could yield high FRET signal *in vivo* as this would require anti-parallel SNARE complex formation (see section **3.5.2** for details). As shown, all 3 labeled constructs were able to form SNARE complex with endogenous BS-C-1 proteins. However, SN25CC most efficiently formed complex, over twice as much as SN29NN and SN25NC (see Table 3.1 for average %highFRET values and number of cells averaged over).

The %highFRET results for the 3 proteins in PC-12 cells are shown in Figure 3.6. As in BS-C-1 cells, all the proteins display high FRET events when microinjected into the cell, indicating the formation of SNARE complex with endogenous binding partners within PC-12

cells. In this case, individual SN29NN molecules are the most likely to form complex, while each of the SNAP-25 constructs have remarkable similar histograms of %highFRET values at an average of about half that of SN29NN.

3.3. Overview: Controls

A number of controls were important for proving the efficacy of smFRET within a live cell. First, all protein constructs had to be tested *in vitro* to ensure they could form SNARE complex with the addition of dye labels and give the signal expected from the dye label locations in the crystal structure. Once I felt confident in my protein constructs, I had to prove the signal I saw in the acceptor channel was not somehow a false positive FRET event. I used a number of methods to prove that the smFRET signal was indeed indicative of SNARE complex formation. A very important control was mutating a single amino acid in the SN25CC construct expected to prevent complex formation and finding that it no longer displayed smFRET signal. I also injected single-labeled SNAP-25 to determine if false FRET signal might derive from dimers or aggregates of the proteins. In addition, other labeled SNARE proteins that are not expected to give smFRET signal were injected to ensure they did not somehow fold or aggregate to give false signal. Finally, smFRET events were monitored before and after microinjection and extensive laser illumination to prove that these essential components of the live cell smFRET technique did not somehow affect the biological signal being measured.

3.3.1 *In vitro* work on FRET constructs

The protein constructs used in this study were designed largely by studying the crystal structure of the SNAP-25 SNARE complex (Sutton, Fasshauer et al. 1998). Dye-label locations were strategically made such that clear high and low FRET signal could be seen when SNAP-25 is in and out of complex as detailed in section **2.1**. While FRET results for SN25CC and SN25NC have previously shown that these constructs gave low and high signal as expected (Weninger, Bowen et al. 2003), SNAP-29 has never been used in a smFRET study. Further, even though SNAP-29 has remarkable sequence similarity to SNAP-25 (Steegmaier, Yang et al. 1998), there is no crystal structure of SNAP-29 SNARE complex, and also no proof that dye-labeled SNAP-29 can form SNARE complex. As a result, I used the crystal structure of SNAP-25 SNARE complex to design the SN29NN construct with the intent of it showing high FRET in complex and low FRET out of complex. As detailed in section **2.1.3**, I used *in vitro* experiments to prove that SN29NN gave this desired FRET signal and was able to form complex when mixed with its binding partners syntaxin and synaptobrevin. This *in vitro* work was essential before using SN29NN *in vivo*, as I can now interpret *in vivo* smFRET results with the knowledge of its expected signal and functionality.

3.3.2 Mutated construct eliminates high FRET signal

One concern with smFRET data *in vivo* is the possibility of the high smFRET signal expected from the protein constructs when they enter SNARE complex somehow being a false positive. In order to help disprove this possibility, I mutated, expressed and purified recombinant SN25CC protein with the point mutation G43D, as published work has shown this prevents SNAP-25 from binding with syntaxin (Loranger and Linder 2002). This should

inhibit SNAP-25 SNARE complex formation and possibly prevent SN25CC, which has had the 4 membrane-tethering palmitoylation sites removed, from localizing to membranes *in vivo*.

As expected for the SN25CC(G43D) construct, no high smFRET signal was visible upon injection into BS-C-1 cells (Figure 3.7 and Table 3.1). An example of this lack of high FRET upon injection of the G43D mutant into a BS-C-1 cell is shown in Figure 3.8. Injection of SN25CC (without the mutation) into these same cells instantly yielded high smFRET as usual. Surprisingly, SN25CC(G43D) was still able to localize to the membrane within the cell as evidenced by signal in the donor-only channel (Figure 3.8). If such protein was not bound in place imaging of these single molecules would be impossible due to blurring in the 100 ms resolution used in all experiments. Implications for SNAP-25 and SNARE proteins in general from this *in vivo* SN25CC(G43D) data are discussed in section **3.5.3**.

3.3.3 Imaging singly-labeled SNAP-25

Another potential source of false positive smFRET signal would be the dimerization or aggregation of SNAP-25. If such self-binding happened with SN25CC, for example, the dye pairs could potentially be any number of distances apart and give high FRET signal that would not be indicative of SNARE complex formation. In order to test for this possibility, I created a SNAP-25 construct with only one dye label site, termed SN25C, and created a mixture of this protein bound to Alexa 555 and Alexa 647. In my system, SN25C labeled with Alexa 555 would be visible only in the donor channel as it localizes within cells,

Table 3.1

Data table of %highFRET for various constructs.

Protein	Cell Type	Mean %HighFRET	N (cells)
SN25CC	BS-C-1	15.7±6.2	10
SN29NN	BS-C-1	6.4±5.7	9
SN25NC	BS-C-1	6.8±3.1	11
SN25CC	PC-12	9.5±7.8	8
SN29NN	PC-12	19.2±6.8	7
SN25NC	PC-12	11.2±5.9	6
CONTROLS			
Sb-NC_28_72	BS-C-1	1.7±3.5	12
Sb-NC_5_72	BS-C-1	2.0±4.0	19
Mixture of SN25C-donor-only & SN25C-acceptor-only	BS-C-1	0.9±2.4	10
SN25CC G43D	BS-C-1	1.0±2.5	10

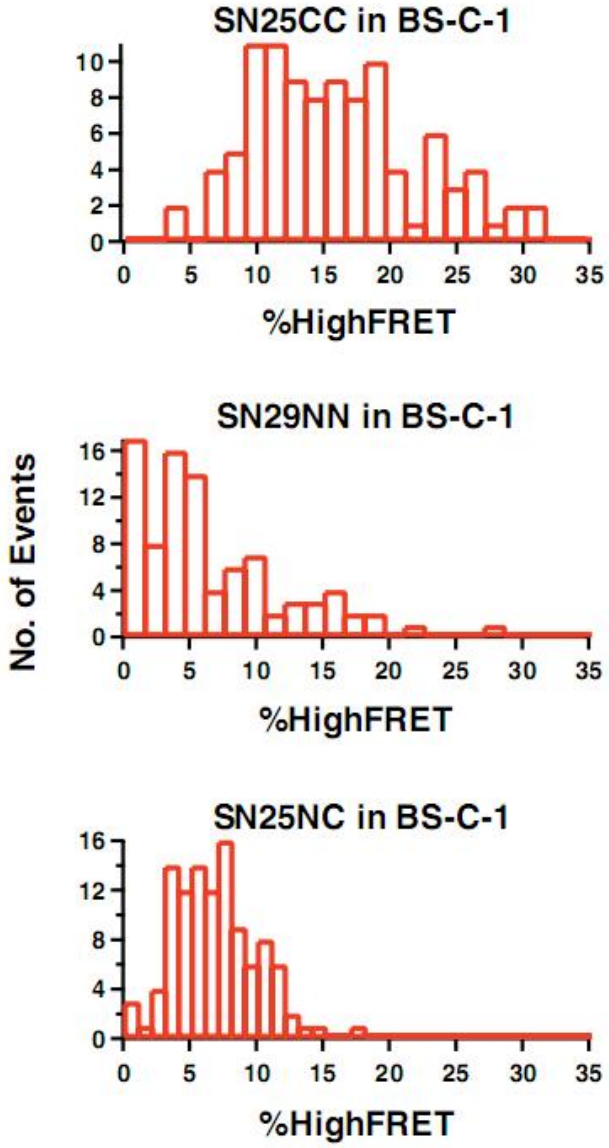

Figure 3.5

%highFRET measurements of primary protein constructs in BS-C-1 cells. Averages of these values are shown in Table 3.1.

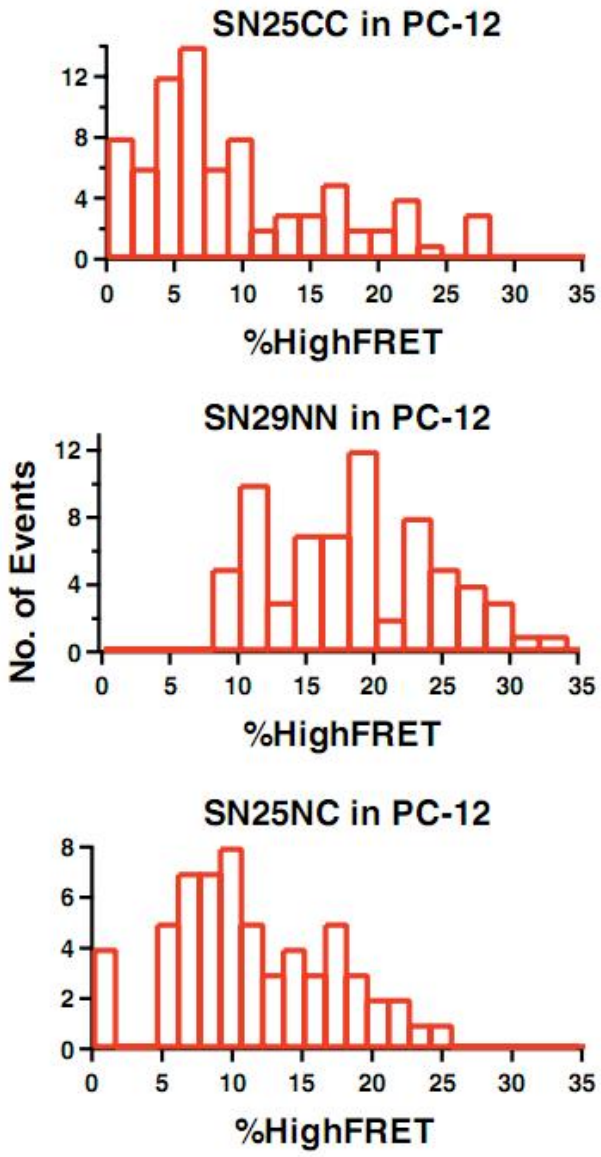

Figure 3.6

%highFRET measurements of primary protein constructs in PC-12 cells. Averages of these values are shown in Table 3.1.

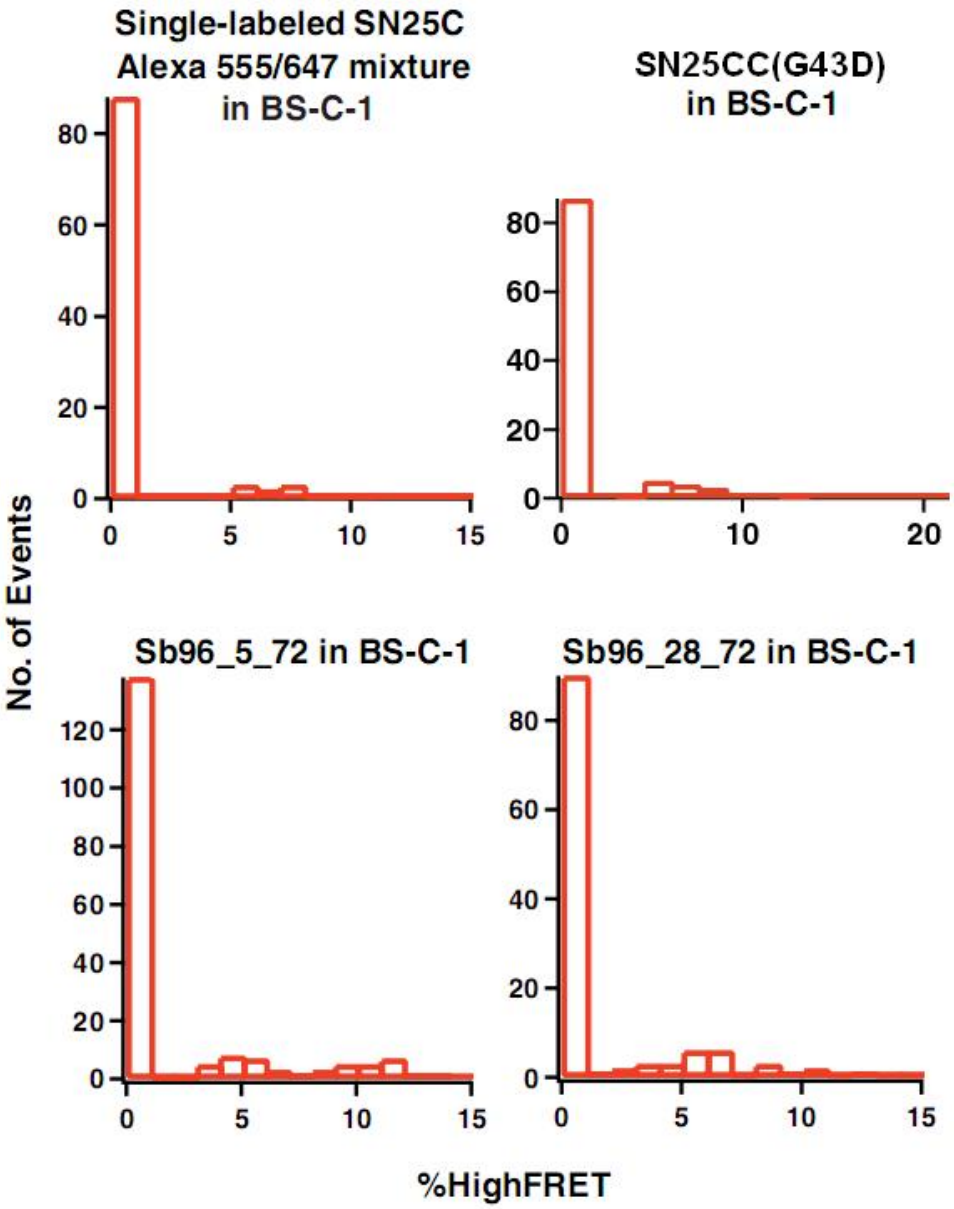

Figure 3.7

%highFRET for the control protein constructs injected into BS-C-1 cells. Averages of these values are shown in Table 3.1.

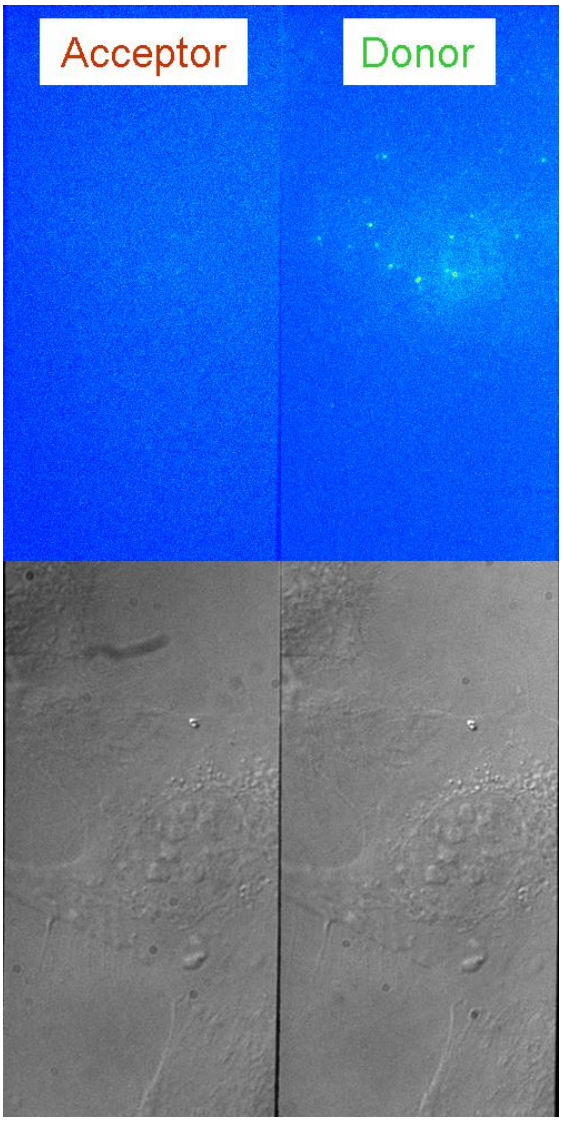

Figure 3.8

smFRET imaging of a BS-C-1 cell after injection of SN25CC(G43D). The lack of high FRET signal on the top left is indicative of the G43D mutation halting SNAP-25 complex formation. SN25CC(G43D) still binds within the cell, however, as donor molecules can be seen in the top right image. The bottom half is the DIC image through both channels. The fluorescence image is from 1.5-1.6 seconds after the beginning of the injection.

however, Alexa 647-bound SN25C would not be excited unless it is able to FRET with Alexa 555. This would only happen from non-specific dimerization or aggregation.

As shown in Figure 3.7 (and averaged in Table 3.1), no high FRET was visible when an equimolar mixture of SN25C labeled with each of these dyes was injected into BS-C-1 cells. This is expected as SNAP-25 is not known to dimerize or aggregate, but was an important control to ensure the recombinantly expressed protein constructs are functioning as expected when added to a live cell environment.

3.3.4 Imaging low FRET synaptobrevin construct

Two similar dual-labeled synaptobrevin constructs were also used as controls to further enhance the confidence that the smFRET signals resulted from SNARE complex formation. Synaptobrevin is a binding partner that along with SNAP-25 and syntaxin forms SNARE complex (Figure 2.2). Unlike SNAP-25, synaptobrevin only contributes one SNARE domain to the ternary complex. As a result, synaptobrevin should not have the dramatic folding that SNAP-25 does as it enters SNARE complex. With this expectation, I labeled synaptobrevin with a mixture of Alexa 555 and Alexa 647 at two sets of similar label sites such that they would give low or zero FRET in and out of complex: S28C and A72C, named Sb-NC_28_72 and label sites at A5C and A72C, termed Sb-NC_5_72. For these two constructs, the dyes are 44 and 67 amino acid away, respectively.

Somewhat counterintuitively, *in vitro* results have shown that synaptobrevin yields FRET signal close to .5 when confined within a tethered liposome (U.B. Choi and K.R.Weninger; unpublished data). This is due to the length of this flexible protein being much greater than the persistence length (Nelson 2004) (the persistence length is the length at

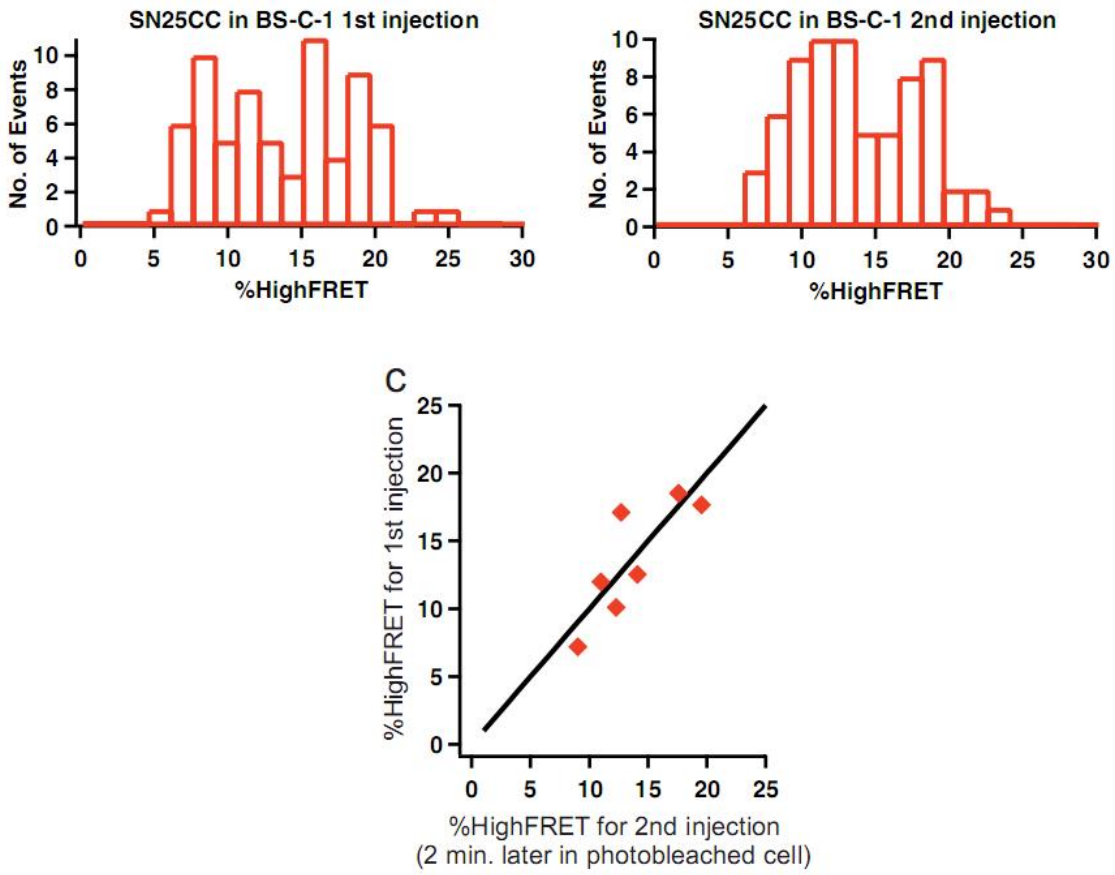

Figure 3.9

Measurements of %highFRET from 2 injections in the same cell separated by 2 minutes of laser illumination. The lack of difference between SNARE complex formation over the data acquisition regime is important for proving the smFRET technique does not negatively impact the biological message.

which a flexible chain maintains its stiffness; the persistence length of a metal chain would be the length of one link). As a result, with the protein able to move like a coiled piece of spaghetti in solution, the dye label separation averages out at distances much less than would be expected based on the length of the extended amino acid chain. Meanwhile, if one of these synaptobrevin constructs enters complex, it forms an alpha helix with a rigid chain length that measures .15 nm per amino acid (Nelson 2004). This keeps the dyes too far for high FRET in the synaptobrevin constructs, as the label sites would be 6.6 and 10.1 nm away for Sb-NC_28_72 and Sb-NC_5_72, respectively (note: the dyes are at the end of carbon linkers that also add 1-2 nm to the dye separation, contributing to the expectation of low FRET). And even if the labeled synaptobrevin constructs only localize to a membrane without entering SNARE complex, the restricted protein would not be expected to act like a random coil, in which the dyes would remain far apart based on the unfolded polypeptide length between them.

As expected, neither of the two synaptobrevin constructs yielded high FRET signal when injected into BS-C-1 cells as shown in Figure 3.7. This is an indication that no non-specific binding of the SNARE domains of the exogenously expressed proteins is occurring *in vivo*. Synaptobrevin did still localize to the membranes, however, as directly excited donor molecules could still be imaged at the 100 ms frame resolution. These events are indicated by the low FRET peak in the histograms of Figure 3.7, as donor-only signal with zero acceptor signal translates to zero FRET. The very low FRET in this case shows that once bound in place synaptobrevin does not move in a random coil manner and yield .3 FRET as shown in vesicle encapsulation experiments *in vitro*.

3.3.5 Ensuring microinjection and laser do not influence biological signal

A concern with the smFRET method in a live cell is how the stresses on the cell from the various techniques might negatively affect the cell and consequently the biology being studied. The biggest source of potential harm is phototoxicity (Grzelak, Rychlik et al. 2001; Potter and DeMarse 2001) from reactive species created by the strong laser illumination necessary for imaging single molecules. It is also possible that microinjection could negatively affect cells, although this technique has been used with great success in fluorescence studies and should be tolerated well if done properly.

To test for these effects, I injected SN25CC into the same BS-C-1 cells twice with 2 minutes of laser illumination in between. I then measured %highFRET from the first injection, allowed the proteins to diffuse and attached labels to photobleach, and then measured the %highFRET from a second injection. I injected protein of the same concentration and attempted to infuse the same amount with each injection to normalize the injection. I also visually inspected cells before and after this multiple injection regime to ensure there were no morphological changes in the cells.

Results for this multiple injection test are shown in Figure 3.9. The top left histogram shows the %highFRET values for the first 10 frames after injection for 10 different cells, which averaged out to 13.6 ± 4.8%. The top right histogram shows %highFRET for the first 10 frames after injection for the same 10 cells as in the top left, but after 2 minutes of 50W cm^{-2} green laser illumination, which came to an average of 13.7 ± 4.2%. The similar average values and the similar shape of the histograms is a strong indication that my experimental setup had little effect on the SNARE system used in this study. Further, I graphed the before and after %highFRET value for the average of the 10 values for each specific cell as shown

at the bottom of Figure 3.9. Each of the specific cells showed very similar before and after values, further supporting the above conclusion.

3.4. Overview: Advanced Single Molecule Data Analysis

While directly measuring the percentage of proteins showing high FRET signal in cells provided interesting results, these results did not fully take advantage of the individuation of signal from single molecules. Through further analysis, I was able to monitor the movement and binding time of each single protein within the cell while measuring smFRET signal. This allowed me to learn new information about the dynamics of SNARE complex formation that would be unavailable through any other means. Analyzing the numerous molecules within the cell required more intensive data analysis, however, requiring me to search through parameter space and measure the protein dynamics computationally with custom software. In this way I could automate the simultaneous tracking and thresholding of individual molecules over time.

3.4.1 Localizing smFRET events within cells

An advantage of single molecule experiments is localization of biological events to diffraction-limited fluorescence spots. For smFRET in particular, I was able to measure the conformational change of SNAP-25 as it folded into SNARE complex at specific locations within the cell over time. This is shown pictorially in Figure 3.10 for SN25CC injected into BS-C-1 cells. The start of each smFRET event is color-coded by time after injection and overlaid onto a DIC image of the cell. As can be seen, exogenous SNAP-25 diffuses through

the cell quickly and immediately forms SNARE complex with endogenous protein. The biological implications of this are discussed in section **3.5.1**.

To prove the resolution power of smFRET in cells, I recorded the squared distance of each event from the injection site (white circle) to measure the diffusion of the SNARE complex-forming protein in the cell over time. The results are diagrammed in the inset of Figure 3.10. As shown, sites of high FRET events traveled outward from the injection point quickly upon microinjection with the concentrated protein traveling outwards at 4 $\mu m^2 s^{-1}$ on average.

3.4.2 Tracking individual molecules

The ability to track individual molecules is an important aspect of single molecule experiments. I performed single particle tracking of high smFRET emitting proteins using standard methods (Saxton and Jacobson 1997) as shown in Figure 3.11. Individual molecules were first identified by requiring the mean background-subtracted intensity of 9 pixel areas to be 3–8 times above the standard deviation of the background, as described in section **3.1.1**. Then, a jump size was defined, which is the maximum distance a particle could travel and still be considered the same particle from frame to frame. The jump size was kept at .75 µm, as particles moving more than this over the 100 ms frame were likely not in the restrictive cellular milieu but outside the cell.

The coordinates of the center of the diffraction limited spot recorded for molecules with high smFRET were used to analyze mobility by finding ?â over each ?â, (100 ms frame rate) in order to solve for D:

$$D = \frac{(\Delta r)^2}{4\Delta t} \qquad \textbf{Equation 3.1}$$

The D value for each of the moving particles was then averaged. While the vast majority of high smFRET events (FRET >.7) from SNAP-25 did not move in the x-y plane, 3.5 ± 1.5% (N=10 cells) exhibited diffusive motion inside the cell greater than the noise detection limit while staying within the illumination height (typically many µm for near-TIRFM). For SN25CC in BS-C-1 cells the average D for 5 tracked, long-lasting mobile molecules was D = 0.27 ± 0.05 $\mu m^2 s^{-1}$. The average of 10 stationary particles yielded a noise limited resolving floor value of D = 0.045 ± 0.016 $\mu m^2 s^{-1}$. FRET efficiency histograms for tracked single molecules were similarly bimodal as in Figure 3.4 with peaks around 0 and 1. Successful microinjection was confirmed as protein molecules outside the cell diffused with D many orders of magnitude higher (the r in the equation below would be ~2 orders of magnitude smaller) and could not be reliably imaged with the frame rate used.

As SNAP-25 itself is expected to remain in place while forming SNARE complex, it is possible that it can give smFRET signal while bound to intracellular vesicles while they move through the cell. To estimate the believability of the above diffusion value for a vesicle, I assume vesicles to be at a fairly low concentration and generally spherical, in which case the Einstein relation (Nelson 2004) can be used:

$$D = \frac{kT}{6\pi\eta r} \qquad \textbf{Equation 3.2}$$

where k is the Boltzmann constant, T is temperature in Kelvin, ?-is the viscosity of the fluid and r is the radius of a vesicle. Assuming the cells are maintained at 37 ºC, the viscosity of the cell is 10-20x greater than that of water (.001 kg $m^{-1} s^{-1}$) (Luby-Phelps 2000), and the

diameter of a vesicle is 50 nm (Jahn and Sudhof 1994), D is expected to be .23-.45 $\mu m^2 s^{-1}$. This is very much in line with my result above. In addition, the diffusion of viral particles, which are of similar size to vesicles, has been measured in BS-C-1 cells to be .7 $\mu m^2 s^{-1}$ (Babcock, Chen et al. 2004), further proof of the mobile molecules I imaged being attached to vesicles. In comparison, I measured the leading edge of fluorescent protein immediately diffusing after microinjection at about 100 $\mu m^2 s^{-1}$, giving a clear indication that the single mobile proteins measured above are restricted by attachment to much larger particles.

In order to further probe how SNAREs bind and interact *in vivo*, I tried additional experiments using SN25CC microinjected along with large amounts (25 µM; 100-200x SN25CC molar concentration) of unlabeled soluble synaptobrevin (amino acids 1-96). Interestingly, injecting this excess SNARE protein increased the fraction of high FRET emitting SN25CC molecules that were mobile to 10.5 ± 3.4% (N=10 cells), 3x greater than SN25CC injected alone. This shows that increased synaptobrevin abundance alters the distribution of SNAP-25 acceptor sites within the cell's trafficking networks, as is further discussed in section **3.5.4**.

3.4.3 Differentiating biological events by binding times

Another important use of single molecule microscopy is the ability to measure timing of individual events and even measure rare or transient transitions. To prove this utility for smFRET *in vivo*, I tracked and measured residence times for all the particles over the course of each injection of SN25CC into BS-C-1 cells. The majority of high smFRET events seen in a cell were transient bindings, allowing the accumulation of a large amount of binding time data.

The residence time of a smFRET event is defined to be the number of consecutive frames in the same location that display donor and acceptor intensities characteristic of high FRET. This is shown graphically in the two traces Figure 3.3g and 3.3h, where the residence times are ~ 1 and 0.5 s, respectively. Anticorrelated events, such as those seen at the top of Figure 3.1 and Figure 3.3a through 3.3f, were not included in these measurements as they report time until acceptor photobleaching and not protein dwell time. High smFRET events of microinjected protein within the cell that terminate without anticorrelated donor recovery were indicative of protein binding in place, folding into a conformation capable of keeping the dyes in close apposition and unbinding. Only those smFRET events with characteristic intensities for single molecules were kept. Donor photobleaching could also account for such terminating high FRET traces, however, in my system acceptors typically bleach appreciably faster than donors.

Residence times of smFRET for injection of SN25CC into multiple BS-C-1 cells were extracted from movies using custom software and accumulated into histograms. The resulting histograms required double exponential functions for accurate fitting (excluding the first bin) as shown in Figure 3.12 and discussed further in section 3.5.5. I uncovered a fast binding state (0.05 s) less than the camera frame rate (100 ms) and a longer binding state (0.2 s) that occurred in ~10 % of events. Similar double exponentials were required for fitting of all residence time histograms with SN25CC in BS-C-1 cells (injections of SN25CC along with either 50x molar SNAP-25 wild type, 200x molar SNAP-25 wild type or 100x molar synaptobrevin gave similar dual-state residence times). The longer-lived state is likely limited by how long the dye lasts before photobleaching.

3.5. Overview: Implications for SNARE biology

While the primary purpose of my research was to prove the efficacy of using smFRET *in vivo* to measure dynamic protein conformation, I selected the SNARE system with the intent of learning more about many of the open questions in this field. My initial results, in which SNAP-25 and SNAP-29 both formed SNARE complex within both kinds of cells tested, speak to the ubiquity of SNARE proteins as well as their instant readiness for complex formation. I also proved that a result only seen *in vitro*, anti-parallel SNARE complex formation, also exists *in vivo*. The controls done with the SN25CC(G43D) mutant that did not form SNARE complex due to a single mutation in the SNARE domain of this protein also provide interesting results in comparison to past works, including a bulk FRET study using a similar construct to SN25CC. Finally, the smFRET technique allowed me to localize single proteins within a cell, track their diffusion within the cell while in SNARE complex and even measure differentiable binding states by monitoring this complex formation over time.

3.5.1 Instant SNAP-25 and SNAP-29 complex formation in multiple cell types displays the promiscuity of SNAREs

A major open question in SNARE biology is how these proteins are able to orchestrate the multifarious membrane binding events that occur intracellularly. It is becoming clear that accessory proteins that mediate SNARE complex formation are essential to membrane binding events (Weninger, Bowen et al. 2008), but these associative interactions do not appear to be enough to discriminate between very similar SNARE proteins of the same family (Scales, Chen et al. 2000). One hypothesis is that selective

binding of the various SNARE domains is driven by amino acid sequence specificity capable of correctly pairing off cognate proteins (Scales, Chen et al. 2000). A second theory is that different SNAREs are expressed locally in different tissues (Ungar and Hughson 2003). Another possibility is that accessory proteins regulate SNARE interactions.

My results strongly favor the idea that local SNARE expression is important to function *in vivo*. I showed both the SN25CC and SN29NN constructs could form SNARE complex in two vastly different cell types: kidney epithelial cells from monkeys and neuron-like adrenal cells from rats. The fact that SNAP-25, which is expressed almost exclusively in the brain and not in the kidney (Oyler, Higgins et al. 1989), can interact and even form complex with proteins expressed in kidney cells is a surprise. This is less impressive with SNAP-29, which is expressed in many tissue types including kidneys and the brain (Steegmaier, Yang et al. 1998). Further intriguing is the fact that both the SNAP-25 and SNAP-29 constructs were made from human protein, while the cell types used are derived from monkeys and rats. While the sequence similarity between these 2 proteins and their binding partners in monkeys and rats is very high (Advani, Bae et al. 1998), the ability of these proteins to function across species further enhances the idea that SNARE protein organization is not driven by sequence specificity.

The idea that SNARE proteins are not selective has been studied *in vitro* by purifying SNARE proteins and forming complex between various mixtures of cognate SNAREs (generally a combination of a syntaxin, synaptobrevin and SNAP protein) (Yang, Gonzalez et al. 1999). However, my work extends this to an *in vivo* context, where endogenously expressed accessory proteins are expected to affect such non-specific SNARE promiscuity. As my results show with SNAP-25 and SNAP-29 forming complex in 2 vastly different cell

types, SNAREs are able to remain promiscuous despite potential accessory protein interactions. These accessory proteins, such as synaptotagmin (Fernandez-Chacon, Konigstorfer et al. 2001), complexin (Li, Augustine et al. 2007; Maximov, Tang et al. 2009), munc (Deak, Xu et al. 2009), snapin (Ilardi, Mochida et al. 1999) and a‘-synuclein (Burre, Sharma et al. 2010), have all been shown to affect the capacity for and stability of complex formation and often subsequent membrane fusion. It is very possible such proteins influenced SNARE complex formation in my study, but clearly they did not prevent it.

Endogenous SNAREs were instantly ready to accept exogenously injected protein, with high FRET signal often occurring within a single 100 ms frame after microinjection. This is not completely surprising: immunoassay (Bajohrs, Darios et al. 2005) and binding studies in permeabilized cells (Lang, Margittai et al. 2002; Bar-On, Winter et al. 2008) indicate ~90% of the native syntaxin at the plasma membrane is available for forming SNARE complex, whereas exogenous SNAP-25 and synaptobrevin both rapidly assemble into SNARE complex on plasma membranes. My studies extend these conclusions to real-time analysis of fully intact, living cells. I was not able to exhaust SNARE complex formation by repeated injections of proteins, possibly indicating that turnover of these binding times are often transient and turnover of these proteins is high. This is expected in a system essential for the vesicular fusion that permits neuronal transmission on the millisecond timescale (Kuner, Li et al. 2008).

Another interesting finding came from injection of SN25CC with 100-200x molar excess of synaptobrevin (25 µM). I infrequently saw SN25CC protein give smFRET signal while moving within the cell: 3.5 ± 1.5% of molecules imaged within 10 injected cells exhibited diffusive motion with $D = 0.27 \pm 0.05\ \mu m^2\ s^{-1}$. As detailed above, this is possibly

due to binding of SNAP-25 on vesicles. However, upon injection of SN25CC with its cognate SNARE partner synaptobrevin, 10.5 ± 3.4% of SN25CC molecules studied within 10 cells yielded smFRET while moving with similar diffusive motion. This is an indication that the addition of synaptobrevin altered the distribution of SNAP-25 binding sites in the cell's trafficking networks. One hypothesis would be that the amount of endogenous synaptobrevin—a SNARE protein localized to vesicles—is a rate-limiting step in allowing SNAP-25 to bind, fold and form SNARE complex. Therefore, the overabundance I injected might have increased the interactions of SN25CC and vesicles such that complex formation was more likely on these diffusing organelles. The unique ability of smFRET to characterize the folding state of each individually imaged SNAP-25 as it moved throughout the cell allowed us to gain this information.

3.5.2 Antiparallel SNARE complex formation

Another interesting finding is the high FRET signal from the SN25NC construct. This construct is designed in such a way that in normal SNARE complex, in which the SN1 and SN2 domains of SNAP-25 bind with syntaxin and synaptobrevin in the same N to C direction, FRET signal should be low due to the dye separation (Figure 2.1, middle). A linker region in between the domains allows SN2 to start back at the N-terminal such that the 4 domains are in parallel (Figure 2.1, middle right). However, as has been shown *in vitro* (Weninger, Bowen et al. 2003), the SNARE domains are non-specific enough such that the SN2 domain of SNAP-25 can bind in the C to N direction in SNARE complex, thereby yielding high FRET signal in the SN25NC construct.

I was able to duplicate these results *in vivo* using smFRET. This is a bit surprising, as it is thought that accessory proteins might act as chaperones and prevent such less specific interactions from occurring. The SN25NC construct folded into complex and yielded high FRET signal in both BS-C-1 and PC-12 cells, albeit at rates slightly less than SN25CC and SN29NN (Table 3.1). This might imply a preference for the parallel four helix bundle as also shown *in vitro* (Weninger, Bowen et al. 2003).

This result points toward an additional regulating mechanism in the regulation of SNARE binding. It is possible that antiparallel complex formation alters the mechanistic force of the dramatic folding event thought to fuse membranes, or even alters the amount of complex formation happening at any one time as some ratio of bound cognate SNAREs are in a non-functioning conformation. Ideas for discriminating between these possibilities are discussed in section **4.3** on future work.

3.5.3 Meaning of SN25CC(G43D) construct eliminating high smFRET

I injected SN25CC with the mutation G43D in the SN1 domain of the protein into BS-C-1 cells to determine how it affected SNARE complex formation. I expected SN25CC to be unable to form complex based on previous works that have shown that this mutation eliminated interactions between syntaxin-1 and SNAP-25 *in vitro* and *in vivo* (Fasshauer, Bruns et al. 1997; Loranger and Linder 2002). I found that SN25CC(G43D) was unable to form SNARE complex as evidenced by the lack of smFRET signal, yet was still able to bind within the cell as shown by donor molecules staying in place for many seconds after protein injection (Figure 3.8).

The previous work on this SNAP-25 mutant has yielded mixed results. One work expressed a GFP-labeled SNAP-25 construct with the G43D mutation in cultured neuron-like cells and used immunoassays to prove it no longer bound to syntaxin (Loranger and Linder 2002). Interestingly, this construct was still able to localize to membranes *in vivo* via palmitoylation of the 4 cysteines in the linker region of SNAP-25 and also showed similar trafficking kinetics as the wild type protein in a neuronal cell line (membrane interactions were reduced in a non-neuronal cell line). All SNAP-25 proteins used in my studies had these 4 cysteines changed to serine for the purpose of strategic labeling of cysteines in other locations, thereby eliminating any such palmitoylation-dependent membrane tethering.

Another study using SNAP-25 constructs similar to ours but with large fluorescent protein moieties expressed within the cell on the N-termini of SN1 and SN2 (similar to Figure 2.1, bottom) used bulk FRET to determine SNAP-25-syntaxin interactions in PC-12 cells (An and Almers 2004). In one particular test, the authors used a construct with the SN2 domain removed but kept the SN1 chain and fluorescent probes intact along with the G43D mutation. Surprisingly, this G43D mutation did not eliminate interactions of the SN1 domain of SNAP-25 with syntaxin, but according to the authors appeared able to form some kind of binary complex.

These previous studies provide two different interpretations of how the G43D SNAP-25 mutant functions in cells. The first indicates this mutation eliminates interactions of SNAP-25 with syntaxin. The second claims the mutated SN1 domain of SNAP-25 can bind syntaxin without the SN2 domain present. While seemingly contradictory, it is possible that the SN2 domain can affect binding of syntaxin with SN1 even without complex formation. The binary complex of SNAP-25 and syntaxin has been shown elsewhere and is

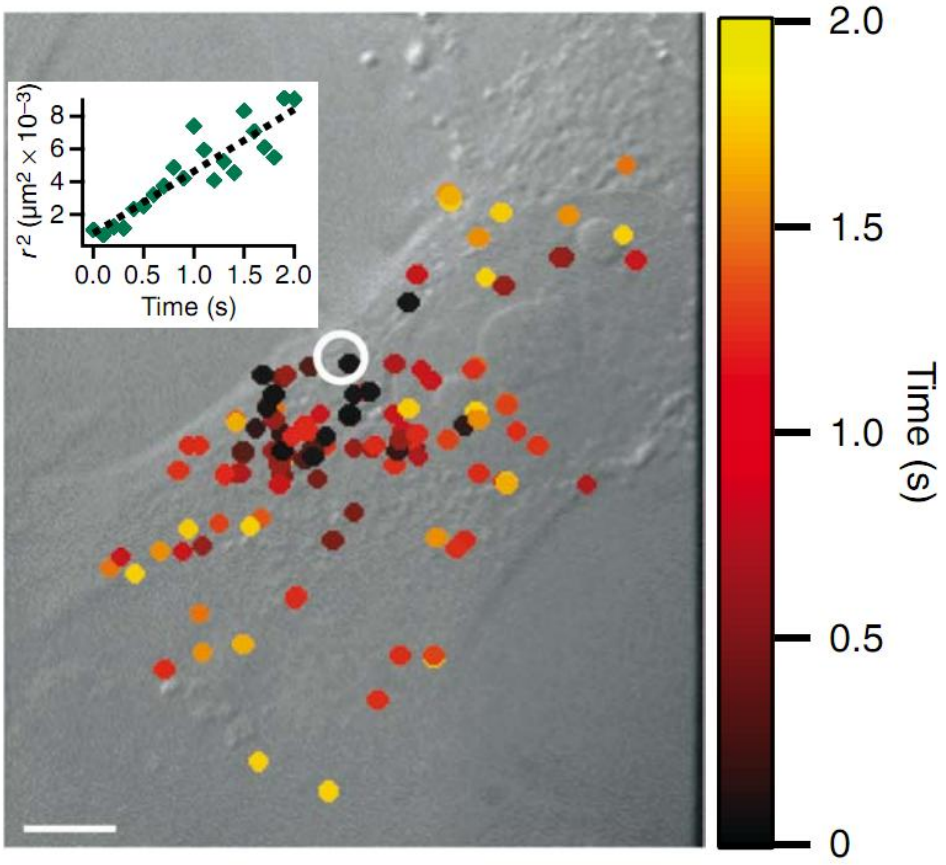

Figure 3.10

Scatterplot of high FRET events over time of SN25CC injected in a BS-C-1 cell. Inset is graph of average distance of high FRET events from injection site squared over time. Scale bar: 10 μm.

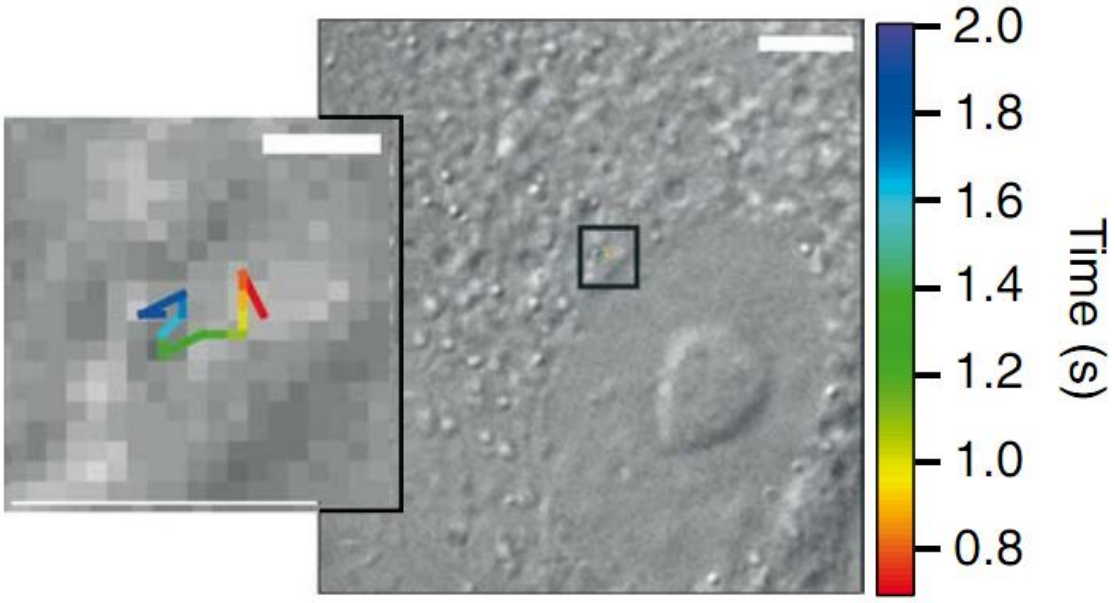

Figure 3.11

Tracking of individual high FRET, mobile SN25CC protein in BS-C-1 cell. Time after injection is color-coded. Inset is zoom of squared region. Scale bars: 5 µm, 1um (zoom).

theorized to promote the subsequent formation of ternary complex (Weninger, Bowen et al. 2008). Therefore, it is plausible that the G43D mutant, which is thought to prevent the tightly packed ternary complex (comprised of the 4 SNARE domains from syntaxin, synaptobrevin and SN1 and SN2 from SNAP-25) through steric and electrostatic forces of this charged amino acid (Fasshauer, Sutton et al. 1998), might not inhibit formation of a more loosely interacting binary complex.

The occurrence of this more loosely packed binary complex that would leave the SN1 or SN2 domain unfolded is a possible explanation for my G43D results. I have shown that this mutation eliminates high FRET signal and therefore complex formation, but still shows low FRET signal indicative of localized binding within the cell. The SNAP-25 might well be bound in place to a membrane-localized syntaxin that allows the stable donor fluorescence signal seen in Figure 3.8 without keeping the acceptor in close enough proximity for FRET. It is also possible that a stretch of basic amino acids in SNAP-25 permits membrane localization without the necessity of palmitoylation sites (An and Almers 2004). Such membrane binding would permit lateral diffusion within the membrane, which was visible in some but not the majority of molecules (see video of SN25CC(G43D) injection here: http://www.nature.com/nmeth/journal/v7/n3/extref/nmeth.1421-S4.mov). **3.5.4 Diffusion of mobile SNAP-25 molecules**

I found SN25CC diffusing within BS-C-1 cells at $D = 0.27 \pm 0.05\ \mu m^2\ s^{-1}$ while simultaneously yielding high FRET signal, indicative of complex formation. My calculations in section **3.4.2** explain the plausibility of these mobile SN25CC molecules being bound to vesicles based on this number. In addition, I found that simultaneous injection of 100x molar excess of synaptobrevin along with SN25CC made 3x as many

molecules display such mobility. This is an indication that the distribution of SNAP-25 acceptor sites within the cell's trafficking networks are altered by the overabundance of synaptobrevin. Synaptobrevin is the member of ternary SNARE complex that binds to vesicles and is thought to form complex with plasma membrane-localized syntaxin through intermediate SNAP-25 interactions that allow fusion of the two membranes (Duman and Forte 2003) or possibly pore formation (Dennison, Bowen et al. 2006). Therefore, it is not surprising that an abundance of synaptobrevin provides additional receptor sites for SNAP-25 binding to endogenous vesicles, which would cause this appreciable rise in SN25CC mobility. This is further evidence that those diffusing SNAP-25 molecules with high FRET signal are bound to vesicles.

3.5.5 Timing of SNARE binding and release

I found two differentiable SNARE complex dwell times from injection of SN25CC into BS-C-1. These were found by measuring high smFRET signal that disappeared without anticorrelation, which is indicative of binding and unbinding of SN25CC. The accumulation of these residence times for multiple injections of SN25CC in BS-C-1 cells (Figure 3.12) were best fit by a double exponential in all cases (including SN25CC injected with either 50x molar SNAP-25 wild type, 200x molar SNAP-25 wild type or 50x molar synaptobrevin in BS-C-1 cells), with the two states averaging out to around .05 and .2 seconds. 90% of these events were in the shorter state.

Fitting a single exponential on these accumulated dwell times yielded a χ^2 value of about 200 while segments of the plot did not stay within the 95% confidence interval. Fitting a double and triple exponential yielded a χ^2 of around 11 in both cases. However, the only

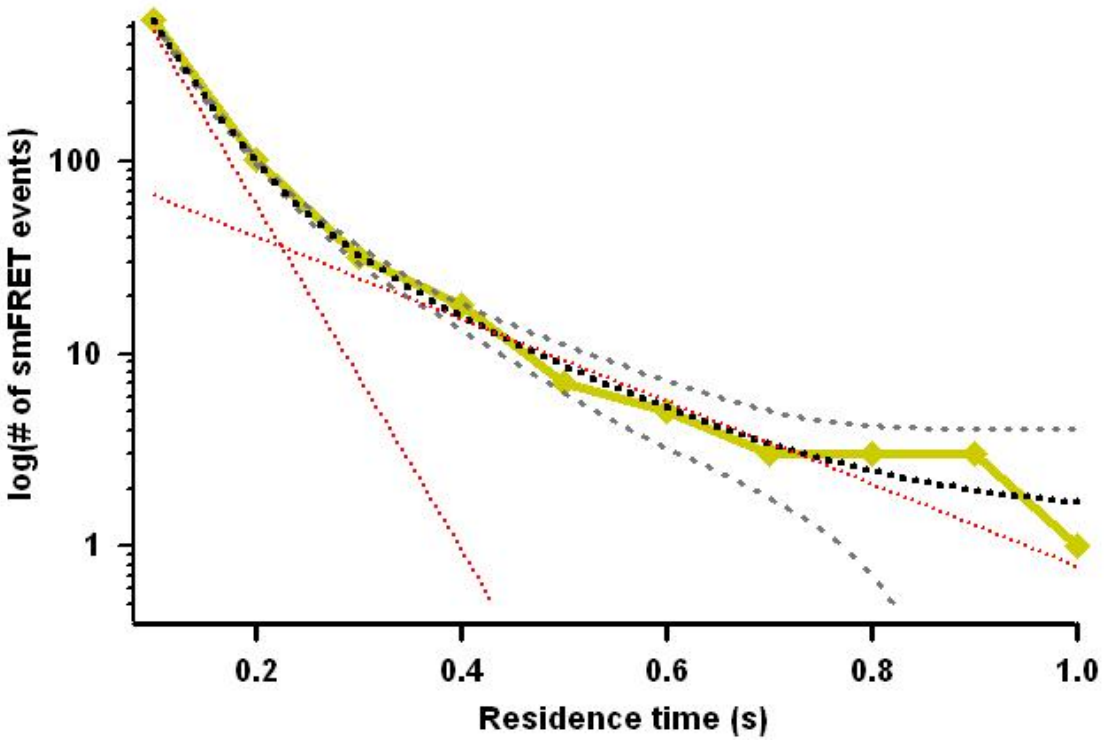

Figure 3.12

Residence times of tracked high FRET SN25CC events in BS-C-1 cell. A double exponential fit is shown with black dots, while the single exponential fits that comprise the double exponential fit are shown with red dots. 95% confidence intervals calculated by the Igor Pro fitting routine are shown in gray for the double exponential fit. Time constants for the two single exponential graphs are tO= .05 and 2 seconds.

solutions that fit a triple exponential state either required a negative coefficient or had lifetimes with a standard deviation (calculated in Igor Pro by assuming a normal distribution of uniform error around the fit parameters) many orders of magnitude larger than the predicted value. As shown in Figure 3.12, the data clearly falls within the 95% confidence interval of the double exponential fit. Further, I anticipate a two state process from results in SNARE biology as discussed below.

The ability to measure two states on the millisecond timescale is an intriguing result. There are 2 candidate mechanisms I would expect to take place on this timescale with 2 differentiable states capable of yielding high FRET signal. The first possibility is formation of two different SNARE complexes capable of folding SN25CC into a high FRET orientation. This could represent cis and trans SNARE complexes, which have previously been shown to adopt two-state kinetics (Bar-On, Winter et al. 2008). Cis-SNARE complex is when SNARE complex formation occurs on the plasma membrane without synaptobrevin being localized to a vesicle, while trans complex is the purported formation in which synaptobrevin is bound to a vesicle and complex formation pulls membranes together.

Another possible differentiable set of states is binary and ternary SNARE complex. It is theorized that SNAP-25 might initially fold when bound to syntaxin—possibly with the aid of accessory proteins like complexin, Munc13 and Munc18—which then allows subsequent binding of synaptobrevin to form ternary complex (Weninger, Bowen et al. 2008). These interactions would make sense with the timescales of my smFRET signal, as the initial interaction of SN25CC with syntaxin and accessory proteins would be a quick, potentially transient fold. Proteins are expected to function on such timescales (Henzler-Wildman, Lei et al. 2007). Then, if this complex found a synaptobrevin acceptor, SN25CC would continue

to give high FRET signal until disassembly of the complex. If not, the SN25CC molecule could just as likely unbind from the syntaxin depending on the local energy state and status of accessory protein binding. There is also evidence for membrane fusion, and therefore assembly and disassembly of SNARE complex formation, taking place on such hundred millisecond timescales (Kuner, Li et al. 2008).

It should be noted that these results were temporally limited: the 100 ms exposure time of each frame provides a lower limit while the photobleaching time of the acceptor (or donor, although the acceptor bleaches much faster in my system due to the greater photostability of the donor dyes) restricts measuring long-term smFRET signal. However, while acceptors dyes rarely lasted longer than 1 second for long-lived events (Figure 3.1 and 3.3 show many examples of anticorrelated smFRET lasting about this time), the vast majority of smFRET events were transient as indicated by the dwell times above (Figure 3.3g-h), an indication that the majority of high FRET traces are indicative of biological signal taking place within the temporal limits of my system. Unfortunately, any sort of long-term event that might take place over the course of many seconds would not be possible without extending the time the dyes last.

A final possibility for the dissociable smFRET times I measured is 2 different vesicle states, such as docking and fusion. A number of studies have shown that synaptic vesicles can undergo multiple binding and fusion states (Aravanis, Pyle et al. 2003; Gandhi and Stevens 2003). Each of these is expected to be modulated by SNARE protein interactions. Therefore, the 2 smFRET states I measure could well be the folding of SNAREs during vesicular binding and fusion. For example, one method of vesicular content release called kiss-and-run has been found to last 400-860 ms, similar to the timescales of one of my high

FRET binding states (Aravanis, Pyle et al. 2003; Gandhi and Stevens 2003). Therefore, it is possible I am measuring the transient folding of SNAREs as vesicles are brought close to membranes with the more prevalent shorter state and an actual vesicle content delivery event with the less common, longer one. Ideas for proving such SNARE-dependent vesicular release are detailed in section **4.3** on future work.

Chapter 4. Summary

I have shown the ability to use single molecule fluorescence resonance energy transfer within live cells to determine the conformation of an individual protein. This required the use of externally-labeled recombinant protein being microinjected into live cells and imaged under a specialized set of equipment ideal for low noise detection. This included a low autofluorescence, high numerical aperture objective lens, an ultra-cooled emCCD camera and low noise glass and oil. It also required maintenance of healthy cultured cells at physiological temperatures on the microscope in specialized media and a process of selecting ideal cells for microinjection and subsequent imaging. The combination of these methods allowed sufficient signal to simultaneously image acceptor and donor fluorescence molecules in two spectral bands necessary for smFRET. I proved the utility of this method by studying the large conformational change of single SNARE proteins as they entered into complex with endogenous protein *in vivo*. The ability to image such protein folding on the nanoscale and individuate the location and time of these transient events is a major advance in biomolecular research. I was able to prove this with multiple interesting findings of SNARE proteins using this novel method. I discuss future possibilities of smFRET in further elucidating the mechanisms of SNAREs in a live cell context.

4.1 Conclusions of in vivo smFRET method

Strategic design and labeling of protein constructs able to show significant conformational changes allowed me to overcome the many limitations of *in vivo* microscopy and determine dynamic information of individual proteins in a physiological environment.

While signal to noise as well as imaging time is limited through the use of organic fluorophores, I was able to individuate single SNARE proteins as they dynamically moved throughout a cell and folded in and out of SNARE complex. I proved the robustness of my constructs as indicators of the conformational state of proteins through numerous controls and have shown novel results using this system important to the understanding of SNARE biology.

This method is widely applicable to proteins in myriad systems due to its sensitivity on the nanoscale and utility in discriminating transient folding states of single molecules. Considering the exponential growth of single molecule methods in the literature—microscopy being one of the foremost components of this rise—utilization of this method first shown here should have a significant impact on elucidating the inner workings of the cell.

4.2 Biological conclusions found using smFRET

I proved the usefulness of smFRET by studying a number of different aspects of SNARE proteins. These exogenously grown proteins found their endogenous SNARE partners and folded instantaneously after injection, indicating that binding sites are immediately available for SNAREs during the normal resting state of cells. Another triumph was displaying the promiscuity of SNAREs *in vivo*. Both SNAP-25 and SNAP-29 were able to localize and form SNARE complex in 2 cell types derived from different tissues from different organisms. Further indicating this lack of specificity *in vivo*, I was able to show how SNARE proteins can form complex in an anti-parallel manner, in which the SNARE domains orient themselves in an opposite orientation to that expected from structure. This

had not been shown previously in a live cell context. I also proved the inability of SNAP-25 to bind syntaxin and form SNARE complex when the point mutation G43D is made in the SN1 domain, resolving a contradiction between two previous results. The ability to measure SNARE complex formation of each individual protein also allowed me to track and localize these events over time. I was able to track the diffusion of such SNAP-25 molecules while they formed complex and used this information to show the plausibility of such proteins being bound to intracellular vesicles. Finally, I was able to individuate the residence time of each SNAP-25 molecule that formed complex, resolving two distinct intracellular functions of this protein from their differing temporal signatures.

4.3 Future work

The successful implementation of smFRET *in vivo* provides an opportunity for studying nanoscale phenomena across the biological spectrum. While this initial method is currently limited by a number of factors technological improvements will make smFRET easier to implement in a live cell context. Further, the biological information gained from smFRET can be enhanced with the use of other exciting new methods. Even though this technique can be used universally for such protein folding events, I also discuss the opportunities to build off my success in the SNARE system and further resolve how these essential proteins orchestrate membrane fusion.

4.3.1 Improving live cell smFRET system

As single molecule methods continue to grow in popularity the market for improving fluorescence technologies continues to grow as well. As a result, it is expected that the

development of fluorescent probes that last longer before photobleach will continue. In particular, the use of quantum dots would provide a huge boost in monitoring nanoscale events with smFRET as they have vastly better quantum yield and time until photobleach compared to organic probes. Unfortunately, at this point commercially available quantum dots are tens of nanometers in diameter as they require significant coatings to make them functional for protein attachment, to keep them soluble and avoid toxicity to cells (Blow 2008). Such large probes are unmanageable when attached to proteins, particularly when using dye separations on the order of nanometers are required for FRET.

An enhancement to my method would be the use of a second laser color to further analyze single molecule dynamics. The use of two lasers, one each to directly excite both the acceptor and donor fluorophores, is typical in *in vitro* smFRET experiments. This requires alignment of both lasers in TIRFM mode and laser shutters to alternate between two color illumination. I used only green laser illumination to excite my donor dye for FRET and measured intensities characteristic of single fluorophores. However, directly exciting the acceptor molecule is a preferred way to prove only single dyes are present.

Another currently available improvement in the *in vivo* smFRET system would be the use of fluorophores with excitation further into the red and infrared part of the spectrum. It is well-known that cells autofluoresce less in this spectral range (Aubin 1979; Benson, Meyer et al. 1979), and nanometer resolution can still be achieved between such fluorophores as Alexa 647 and Alexa 750, which possess an R_o around 7 nm (equation 1.2).

A number of recent innovations in single molecule fluorescence microscopy also provide exciting ways to enhance data acquisition in cells while simultaneously measuring FRET. For example, nanometer localization of dyes using a technique like FIONA (Yildiz,

Forkey et al. 2003), PALM (Betzig, Patterson et al. 2006), or STORM (Rust, Bates et al. 2006) would allow improved tracking and give a better idea of the specific intracellular areas where smFRET events occur. The use of photoswitchable dyes, prevalent in these techniques, also affords opportunities to specifically excite groups of molecules, thereby adding temporal control to further enhance strategic imaging of specific molecules.

An additional technological advance that could aid in smFRET studies is the labeling of unnatural amino acids with fluorescent dyes. Recent work has shown the ability to site-specifically insert an unnatural amino acid into *E Coli* that can then be labeled with an azido fluorophore (Nguyen, Lusic et al. 2009). Using this method avoids having to use maleimide labeling chemistry to bind cysteines strategically mutated into proteins as done with my constructs. As a result, any native cysteines in a protein that are not desired for labeling do not have to be removed, as is currently done. This is important for maintaining the biological relevance of proteins with native cysteines, such as SNAP-25, as discussed below.

4.3.2 Future studies of SNAREs with smFRET *in vivo*

The great success displayed here studying SNARE proteins using smFRET in live cells can be extended in many directions. Using non-native amino acid labeling can permit smFRET studies of SNAP-25 with its native palmitoylation sites to determine how these alter complex dynamics *in vivo*. Injecting my SNAP-25 and SNAP-29 constructs into differentiated PC-12 cells and altering the Ca^{2+} and K^{+} concentration could also provide interesting physiological relevance of SNARE complex formation—particularly while monitoring release of neurotransmitter from these cells. Further, coinjection with botulism or

tetanus toxins could help to elucidate which SNARE proteins are participating in the complex formation shown with high FRET signal.

As just mentioned, strategic labeling of proteins with unnatural amino acids would also aid in future studies. Of particular relevance for my studies, the ability to strategically label SNAP-25 without having to remove the 4 cysteines that are palmitoylated *in vivo* would allow this protein to better localize to membranes and give a truer picture of its function. This method would also permit those amino acids change to cysteine for labeling in SN25CC, SN25NC and SN29NN to remain in their native state, an important goal in any study.

PC-12 cells have a unique ability to develop into neuron-like cells with neuronal projections—termed neuritis—when incubated with nerve growth factor. I successfully grew these differentiated cells on coverslips and was able to microinject them within the neurite regions. While I did not see any initial differences in SNARE complex formation in these differentiated cells, which are expected to have wholly different gene expression to go along with their morphological changes, they offer a whole new system ripe for future studies. One work in particular was able to show increased SNARE interactions in the neurites of these cells during exocytosis caused by incubations of Ca^{2+} and K^{+} (An and Almers 2004). My method would be able to localize single SNARE interactions within these neurons while monitoring the dynamic state of the protein. Further, neurotransmitters such as serotonin and insulin are released from differentiated PC-12 cells can be monitored during exocytosis (Zerby and Ewing 1996; Amatore, Arbault et al. 2008). This would provide a means of linking structural changes to function, as increased neurotransmitter release should accompany increased SNARE complex formation, which I can measure with the smFRET system. Such structure-functional studies could be carried out with many protein types to

detect multiple neurotransmitters and give unparalleled access to how SNAREs orchestrate vesicle exocytosis. For example, measuring neurotransmitter release of SN25CC versus SN25NC could determine how parallel and antiparallel SNARE complex formation affects function.

The use of specific proteases could also help strategically elucidate SNARE function in combination with smFRET. Oft-used toxins like botulism and tetanus, which specifically cleave syntaxin, synaptobrevin and SNAP-25 depending on the type, can be injected in concert with my constructs to determine how complex formation is affected by the loss of certain proteins. For example, monitoring smFRET signal of SN25CC coinjected with *Botulinus* neurotoxin C, which site-specifically cleaves syntaxin (Schiavo, Shone et al. 1995), could tease out the SNAP-25-syntaxin interactions responsible for high FRET signal seen *in vivo*. This method could help clear up many of the open questions in the literature about the wide variety of purported SNARE complexes seen both *in vitro* and *in vivo* (An and Almers 2004; Weninger, Bowen et al. 2008).

REFERENCES

Advani, R. J., H. R. Bae, et al. (1998). "Seven novel mammalian SNARE proteins localize to distinct membrane compartments." Journal of Biological Chemistry 273(17): 10317-10324.

Amatore, C., S. Arbault, et al. (2008). "Electrochemical monitoring of single cell secretion: Vesicular exocytosis and oxidative stress." Chemical Reviews 108(7): 2585-2621.

An, S. J. and W. Almers (2004). "Tracking SNARE complex formation in live endocrine cells." Science 306(5698): 1042-1046.

Andor-plc (2010). Unravelling Sensitivity, Signal to Noise and Dynamic Range – EMCCD vs CCD, Andor Technology plc.

Anfinsen, C. B. (1973). "Principles That Govern Folding of Protein Chains." Science 181(4096): 223-230.

Antonin, W., D. Fasshauer, et al. (2002). "Crystal structure of the endosomal SNARE complex reveals common structural principles of all SNAREs." Nature Structural Biology 9(2): 107-111.

Aravanis, A. M., J. L. Pyle, et al. (2003). "Single synaptic vesicles fusing transiently and successively without loss of identity." Nature 423(6940): 643-647.

Aubin, J. E. (1979). "Autofluorescence of Viable Cultured Mammalian-Cells." Journal of Histochemistry & Cytochemistry 27(1): 36-43.

Axelrod, D. (2003). "Total internal reflection fluorescence microscopy in cell biology." Biophotonics, Pt B 361: 1-33.

Babcock, H. P., C. Chen, et al. (2004). "Using single-particle tracking to study nuclear trafficking of viral genes." Biophysical Journal 87(4): 2749-2758.

Bajohrs, M., F. Darios, et al. (2005). "Promiscuous interaction of SNAP-25 with all plasma membrane syntaxins in a neuroendocrine cell." Biochemical Journal 392: 283-289.

Baneyx, F. (1999). "Recombinant protein expression in Escherichia coli." Current Opinion in Biotechnology 10(5): 411-421.

Bar-On, D., U. Winter, et al. (2008). "Imaging the assembly and disassembly kinetics of cis-SNARE complexes on native plasma membranes." Febs Letters 582(23-24): 3563-3568.

Benson, R. C., R. A. Meyer, et al. (1979). "Cellular Autofluorescence - Is It Due to Flavins." Journal of Histochemistry & Cytochemistry 27(1): 44-48.

Betzig, E., G. H. Patterson, et al. (2006). "Imaging intracellular fluorescent proteins at nanometer resolution." Science 313(5793): 1642-1645.

Blow, N. (2008). "Nanotechnology: Could it be a small world after all?" Nature 452(7189): 901-906.

Bock, J. B., H. T. Matern, et al. (2001). "A genomic perspective on membrane compartment organization." Nature 409(6822): 839-841.

Bork, P., L. J. Jensen, et al. (2004). "Protein interaction networks from yeast to human." Current Opinion in Structural Biology 14(3): 292-299.

Boukobza, E., A. Sonnenfeld, et al. (2001). "Immobilization in surface-tethered lipid vesicles as a new tool for single biomolecule spectroscopy." Journal of Physical Chemistry B 105(48): 12165-12170.

Bowen, M. E., K. Weninger, et al. (2004). "Single molecule observation of liposome-bilayer fusion thermally induced by soluble N-ethyl maleimide sensitive-factor attachment protein receptors (SNAREs)." Biophysical Journal 87(5): 3569-3584.

Brunger, A. T. (2001). "Structural insights into the molecular mechanism of calcium-dependent vesicle-membrane fusion." Current Opinion in Structural Biology 11(2): 163-173.

Brunger, A. T., K. Weninger, et al. (2009). "Single-Molecule Studies of the Neuronal SNARE Fusion Machinery." Annual Review of Biochemistry 78: 903-928.

Burre, J., M. Sharma, et al. (2010). "a‚Synuclein Promotes SNARE-Complex Assembly in Vivo and in Vitro." Science Published online.

Cai, L., N. Friedman, et al. (2006). "Stochastic protein expression in individual cells at the single molecule level." Nature 440(7082): 358-362.

Capecchi, M. R. (1980). "High-Efficiency Transformation by Direct Micro-Injection of DNA into Cultured Mammalian-Cells." Cell 22(2): 479-488.

Carlson, C., H. Sirotkin, et al. (1997). "Molecular definition of 22q11 deletions in 151 velo-cardio-facial syndrome patients." American Journal of Human Genetics 61(3): 620-629.

Chebotareva, N. A., B. I. Kurganov, et al. (2004). "Biochemical effects of molecular crowding." Biochemistry-Moscow 69(11): 1239-+.

Clegg, R. M. (1996). Fluorescence resonance energy transfer. Fluorescence imaging spectroscopy and microscopy. B. H. Ed XF Wang. New York, John Wiley & Sons: 179-252.

Cordes, T., J. Vogelsang, et al. (2009). "On the Mechanism of Trolox as Antiblinking and Antibleaching Reagent." Journal of the American Chemical Society 131(14): 5018-+.

Csete, M. E. and J. C. Doyle (2002). "Reverse engineering of biological complexity." Science 295(5560): 1664-1669.

Dale, R. E. and J. Eisinger (1974). "Intramolecular Distances Determined by Energy-Transfer - Dependence on Orientational Freedom of Donor and Acceptor." Biopolymers 13(8): 1573-1605.

Deak, F., Y. Xu, et al. (2009). "Munc18-1 binding to the neuronal SNARE complex controls synaptic vesicle priming." Journal of Cell Biology 184(5): 751-764.

Dennison, S. M., M. E. Bowen, et al. (2006). "Neuronal SNAREs do not trigger fusion between synthetic membranes but do promote PEG-mediated membrane fusion." Biophysical Journal 90(5): 1661-1675.

Duman, J. G. and J. G. Forte (2003). "What is the role of SNARE proteins in membrane fusion?" American Journal of Physiology-Cell Physiology 285(2): C237-C249.

Fasshauer, D., D. Bruns, et al. (1997). "A structural change occurs upon binding of syntaxin to SNAP-25." Journal of Biological Chemistry 272(7): 4582-4590.

Fasshauer, D., R. B. Sutton, et al. (1998). "Conserved structural features of the synaptic fusion complex: SNARE proteins reclassified as Q- and R-SNAREs." Proceedings of the National Academy of Sciences of the United States of America 95(26): 15781-15786.

Fernandez-Chacon, R., A. Konigstorfer, et al. (2001). "Synaptotagmin I functions as a calcium regulator of release probability." Nature 410(6824): 41-49.

Forster, T. (1946). "Energiewanderung Und Fluoreszenz." Naturwissenschaften 33(6): 166-175.

Forster, T. (1948). "Zwischenmolekulare Energiewanderung Und Fluoreszenz." Annalen Der Physik 2(1-2): 55-75.

Friedman, L. J., J. Chung, et al. (2006). "Viewing dynamic assembly of molecular complexes by multi-wavelength single-molecule fluorescence." Biophysical Journal 91(3): 1023-1031.

Gandhi, S. P. and C. F. Stevens (2003). "Three modes of synaptic vesicular recycling revealed by single-vesicle imaging." Nature 423(6940): 607-613.

George, N. B. (2008). Overcoming Optical Challenges to Live-Cell TIRF Microscopy. Biophotonics International: 30-33.

Giepmans, B. N. G., S. R. Adams, et al. (2006). "Review - The fluorescent toolbox for assessing protein location and function." Science 312(5771): 217-224.

Greene, L. A. and A. S. Tischler (1976). "Establishment of a Noradrenergic Clonal Line of Rat Adrenal Pheochromocytoma Cells Which Respond to Nerve Growth-Factor." Proceedings of the National Academy of Sciences of the United States of America 73(7): 2424-2428.

Grzelak, A., B. Rychlik, et al. (2001). "Light-dependent generation of reactive oxygen species in cell culture media." Free Radical Biology and Medicine 30(12): 1418-1425.

Ha, T., T. Enderle, et al. (1996). "Probing the interaction between two single molecules: Fluorescence resonance energy transfer between a single donor and a single acceptor." Proceedings of the National Academy of Sciences of the United States of America 93(13): 6264-6268.

Henzler-Wildman, K. A., M. Lei, et al. (2007). "A hierarchy of timescales in protein dynamics is linked to enzyme catalysis." Nature 450(7171): 913-U27.

Hohenstein, A. C. and P. A. Roche (2001). "SNAP-29 is a promiscuous syntaxin-binding SNARE." Biochemical and Biophysical Research Communications 285(2): 167-171.

Holt, M., F. Varoqueaux, et al. (2006). "Identification of SNAP-47, a novel Qbc-SNARE with ubiquitous expression." Journal of Biological Chemistry 281(25): 17076-17083.

Hopps, H. E., J. H. Tjio, et al. (1963). "Biologic Characteristics of a Continuous Kidney Cell Line Derived from African Green Monkey." Journal of Immunology 91(3): 416-&.

Ilardi, J. M., S. Mochida, et al. (1999). "Snapin: a SNARE-associated protein implicated in synaptic transmission." Nature Neuroscience 2(2): 119-124.

Itaka, K., A. Harada, et al. (2004). "In situ single cell observation by fluorescence resonance energy transfer reveals fast intra-cytoplasmic delivery and easy release of plasmid DNA complexed with linear polyethylenimine." Journal of Gene Medicine 6(1): 76-84.

Jahn, R. (2004). "Principles of exocytosis and membrane fusion." Gastroenteropancreatic Neuroendocrine Tumor Disease: Molecular and Cell Biological Aspects 1014: 170-178.

Jahn, R. and T. C. Sudhof (1994). "Synaptic Vesicles and Exocytosis." Annual Review of Neuroscience 17: 219-246.

Kitano, H. (2002). "Systems biology: A brief overview." Science 295(5560): 1662-1664.

Kuner, T., Y. Li, et al. (2008). "Photolysis of a caged peptide reveals rapid action of N-ethylmaleimide sensitive factor before neurotransmitter release." Proceedings of the National Academy of Sciences of the United States of America 105(1): 347-352.

Lang, T., M. Margittai, et al. (2002). "SNAREs in native plasma membranes are active and readily form core complexes with endogenous and exogenous SNAREs." Journal of Cell Biology 158(4): 751-760.

Li, Y. L., G. J. Augustine, et al. (2007). "Kinetics of complexin binding to the SNARE complex: Correcting single molecule FRET measurements for hidden events." Biophysical Journal 93(6): 2178-2187.

Lippincott-Schwartz, J., E. Snapp, et al. (2001). "Studying protein dynamics in living cells." Nature Reviews Molecular Cell Biology 2(6): 444-456.

Loranger, S. S. and M. E. Linder (2002). "SNAP-25 traffics to the plasma membrane by a syntaxin-independent mechanism." Journal of Biological Chemistry 277(37): 34303-34309.

Lu, H. P., L. Y. Xun, et al. (1998). "Single-molecule enzymatic dynamics." Science 282(5395): 1877-1882.

Luby-Phelps, K. (2000). "Cytoarchitecture and physical properties of cytoplasm: Volume, viscosity. diffusion, intracellular surface area." International Review of Cytology - a Survey of Cell Biology, Vol 192 192: 189-221.

Maximov, A., J. Tang, et al. (2009). "Complexin Controls the Force Transfer from SNARE Complexes to Membranes in Fusion." Science 323(5913): 516-521.

Murakoshi, H., R. Iino, et al. (2004). "Single-molecule imaging analysis of Ras activation in living cells." Proceedings of the National Academy of Sciences of the United States of America 101(19): 7317-7322.

Nelson, P. (2004). Biological Physics: Energy, Information, Life. New York, W.H. Freeman and Company.

Nguyen, D. P., H. Lusic, et al. (2009). "Genetic Encoding and Labeling of Aliphatic Azides and Alkynes in Recombinant Proteins via a Pyrrolysyl-tRNA Synthetase/tRNA(CUA) Pair and Click Chemistry." Journal of the American Chemical Society 131(25): 8720-+.

O'Grady, A. (2006). "A comparison of EMCCD, CCD and emerging technologies optimized for low light spectroscopy applications - art. no. 60930E." Biomedical Vibrational Spectroscopy III: Advances in Research and Industry 6093: E930-E930
278.

Ohashi, T., S. D. Galiacy, et al. (2007). "An experimental calibration of GFP-based FRET, with application to intrinsically unstructured proteins." Biophysical Journal: 369a-369a.

Oyler, G. A., G. A. Higgins, et al. (1989). "The Identification of a Novel Synaptosomal-Associated Protein, Snap-25, Differentially Expressed by Neuronal Subpopulations." Journal of Cell Biology 109(6): 3039-3052.

Pace, C. N., B. A. Shirley, et al. (1996). "Forces contributing to the conformational stability of proteins." Faseb Journal 10(1): 75-83.

Pan, P. Y., Q. Cai, et al. (2005). "SNAP-29-mediated modulation of synaptic transmission in cultured hippocampal neurons." Journal of Biological Chemistry 280(27): 25769-25779.

Potter, S. M. and T. B. DeMarse (2001). "A new approach to neural cell culture for long-term studies." Journal of Neuroscience Methods 110(1-2): 17-24.

Ram, S., E. S. Ward, et al. (2006). "Beyond Rayleigh's criterion: A resolution measure with application to single-molecule microscopy." Proceedings of the National Academy of Sciences of the United States of America 103(12): 4457-4462.

Rasnik, I., S. A. McKinney, et al. (2006). "Nonblinking and longlasting single-molecule fluorescence imaging." Nature Methods 3(11): 891-893.

Ravichandran, V., A. Chawla, et al. (1996). "Identification of a novel syntaxin- and synaptobrevin/VAMP-binding protein, SNAP-23, expressed in non-neuronal tissues." Journal of Biological Chemistry 271(23): 13300-13303.

Rossi, G., A. Salminen, et al. (1997). "Analysis of a yeast SNARE complex reveals remarkable similarity to the neuronal SNARE complex and a novel function for the C terminus of the SNAP-25 homolog, Sec9." Journal of Biological Chemistry 272(26): 16610-16617.

Roy, R., S. Hohng, et al. (2008). "A practical guide to single-molecule FRET." Nature Methods 5(6): 507-516.

Rust, M. J., M. Bates, et al. (2006). "Sub-diffraction-limit imaging by stochastic optical reconstruction microscopy (STORM)." Nature Methods 3(10): 793-795.

Saito, T., F. Guan, et al. (2001). "Polymorphism in SNAP29 gene promoter region associated with schizophrenia." Molecular Psychiatry 6(2): 193-201.

Sako, Y., S. Minoghchi, et al. (2000). "Single-molecule imaging of EGFR signalling on the surface of living cells." Nature Cell Biology 2(3): 168-172.

Sako, Y. and T. Yanagida (2003). "Single-molecule visualization in cell biology." Nature Cell Biology: Ss1-Ss5.

Sambrook, J., E. F. Fritsch, et al. (1989). Molecular Cloning: A Laboratory Manual, 2nd Ed. Cold Spring Harbor, NY., Cold Spring Harbor Laboratory Press.

Sass, L. E., C. Lanyi, et al. (2010). "Single-Molecule FRET TACKLE Reveals Highly Dynamic Mismatched DNA-MutS Complexes." Biochemistry 49(14): 3174-3190.

Sato, M., K. Nagayama, et al. (2000). "Local mechanical properties measured by atomic force microscopy for cultured bovine endothelial cells exposed to shear stress." Journal of Biomechanics 33(1): 127-135.

Saxton, M. J. and K. Jacobson (1997). "Single-particle tracking: Applications to membrane dynamics." Annual Review of Biophysics and Biomolecular Structure 26: 373-399.

Scales, S. J., Y. A. Chen, et al. (2000). "SNAREs contribute to the specificity of membrane fusion." Neuron 26(2): 457-464.

Schiavo, G., C. C. Shone, et al. (1995). "Botulinum Neurotoxin Type-C Cleaves a Single Lys-Ala Bond within the Carboxyl-Terminal Region of Syntaxins." Journal of Biological Chemistry 270(18): 10566-10570.

Schmidt, T., G. J. Schutz, et al. (1996). "Imaging of single molecule diffusion." Proceedings of the National Academy of Sciences of the United States of America 93(7): 2926-2929.

Schmitt, J., H. Hess, et al. (1993). "Affinity Purification of Histidine-Tagged Proteins." Molecular Biology Reports 18(3): 223-230.

Seeley, P. J., C. H. Keith, et al. (1983). "Pressure Microinjection of Nerve Growth-Factor and Anti-Nerve Growth-Factor into the Nucleus and Cytoplasm - Lack of Effects on Neurite Outgrowth from Pheochromocytoma Cells." Journal of Neuroscience 3(7): 1488-1494.

Seisenberger, G., M. U. Ried, et al. (2001). "Real-time single-molecule imaging of the infection pathway of an adeno-associated virus." Science 294(5548): 1929-1932.

Selkoe, D. J. (2003). "Folding proteins in fatal ways." Nature 426(6968): 900-904.

Simon, S. M. (2009). "Partial internal reflections on total internal reflection fluorescent microscopy." Trends in Cell Biology 19(11): 661-668.

Sprecher, E., A. Ishida-Yamamoto, et al. (2005). "A mutation in SNAP29, coding for a SNARE protein involved in intracellular trafficking, causes a novel neurocutaneous syndrome characterized by cerebral dysgenesis, neuropathy,

ichthyosis, and palmoplantar keratoderma." American Journal of Human Genetics 77(2): 242-251.

Steegmaier, M., B. Yang, et al. (1998). "Three novel proteins of the syntaxin/SNAP-25 family." Journal of Biological Chemistry 273(51): 34171-34179.

Su, Q. N., S. Mochida, et al. (2001). "SNAP-29: A general SNARE protein that inhibits SNARE disassembly and is implicated in synaptic transmission." Proceedings of the National Academy of Sciences of the United States of America 98(24): 14038-14043.

Sutton, R. B., D. Fasshauer, et al. (1998). "Crystal structure of a SNARE complex involved in synaptic exocytosis at 2.4 angstrom resolution." Nature 395(6700): 347-353.

Tamm, L. K., J. Crane, et al. (2003). "Membrane fusion: a structural perspective on the interplay of lipids and proteins." Current Opinion in Structural Biology 13(4): 453-466.

Tokunaga, M., N. Imamoto, et al. (2008). "Highly inclined thin illumination enables clear single-molecule imaging in cells." Nature Methods 5(2): 159-161.

Ungar, D. and F. M. Hughson (2003). "SNARE protein structure and function." Annual Review of Cell and Developmental Biology 19: 493-517.

van den Berg, B., R. Wain, et al. (2000). "Macromolecular crowding perturbs protein refolding kinetics: implications for folding inside the cell." Embo Journal 19(15): 3870-3875.

Wang, Y. and B. L. Tang (2006). "SNAREs in neurons - beyond synaptic vesicle exocytosis (Review)." Molecular Membrane Biology 23(5): 377-384.

Weiss, S. (2000). "Measuring conformational dynamics of biomolecules by single molecule fluorescence spectroscopy." Nature Structural Biology 7(9): 724-729.

Weninger, K., M. E. Bowen, et al. (2008). "Accessory proteins stabilize the acceptor complex for synaptobrevin, the 1 : 1 syntaxin/SNAP-25 complex." Structure 16(2): 308-320.

Weninger, K., M. E. Bowen, et al. (2003). "Single-molecule studies of SNARE complex assembly reveal parallel and antiparallel configurations." Proceedings of the National Academy of Sciences of the United States of America 100(25): 14800-14805.

Wonodi, I., L. E. Hong, et al. (2005). "Association between polymorphism of the SNAP29 gene promoter region and schizophrenia." Schizophrenia Research 78(2-3): 339-341.

Xie, X. S. (1996). "Single-molecule spectroscopy and dynamics at room temperature." Accounts of Chemical Research 29(12): 598-606.

Xie, X. S., J. Yu, et al. (2006). "Perspective - Living cells as test tubes." Science 312(5771): 228-230.

Yang, B., L. Gonzalez, et al. (1999). "SNARE interactions are not selective - Implications for membrane fusion specificity." Journal of Biological Chemistry 274(9): 5649-5653.

Yildiz, A., J. N. Forkey, et al. (2003). "Myosin V walks hand-over-hand: Single fluorophore imaging with 1.5-nm localization." Science 300(5628): 2061-2065.

Zerby, S. E. and A. G. Ewing (1996). "Electrochemical monitoring of individual exocytotic events from the varicosities of differentiated PC12 cells." Brain Research 712(1): 1-10.

Zipfel, W. R., R. M. Williams, et al. (2003). "Live tissue intrinsic emission microscopy using multiphoton-excited native fluorescence and second harmonic generation." Proceedings of the National Academy of Sciences of the United States of America 100(12): 7075-7080.